Investigating the Role of *O*-GlcNAc Glycosylation in Neurodegeneration

Thesis by
Andrew C. Wang

In Partial Fulfillment of the Requirements
for the Degree of
Doctor of Philosophy in Chemistry

California Institute of Technology
Pasadena, CA
2015
(Defended May 27, 2015)

© 2015

Andrew C. Wang

All Rights Reserved

Acknowledgements

I have been extremely fortunate throughout my life, and it is only through the support of an amazing group of family and friends that I have been able to complete the dissertation that follows. It has been a privilege to conduct my graduate work at Caltech, and in the lab of Dr. Linda Hsieh-Wilson. Linda has been a wonderful mentor to me, by cultivating an unyielding desire to explore the most interesting science at the highest level. Her passion for always tackling tough questions continually inspires me and the training I've received will serve me for the rest of my professional career. I am truly thankful for her guidance and the opportunity to pursue important and exciting research.

I would also like to thank the rest of my thesis committee, Dennis Dougherty, Shu-ou Shan, and David Chan. It has been an incredible experience interacting with them and receiving their helpful input and guidance throughout my time at Caltech. It is truly a unique experience to have such talented and engaging mentors thinking about my project and providing essential feedback and one that I appreciate immensely.

I am also grateful for the Hsieh-Wilson lab members past and present, who have been incredibly supportive, providing a wonderful environment to spend my graduate school years. Dr. Jessica Rexach and Dr. Peter Clark taught me everything I needed to know, and were instrumental to my training and development. I want to thank them both for their tireless enthusiasm for science, and especially Jess for taking me under her wing when I first joined the lab. I'd also like to thank Dr. Chithra Krishnamurthy for her helpful insight and guidance

with everything in the lab. Her patience and willingness to help others is something I strive to emulate. I've also had the good fortune to work directly with Elizabeth Jensen, who is an incredibly talented scientist and has contributed tremendously to my research. Other members of the lab have made the daily grind enjoyable, and to them I owe my sanity. I also wanted to thank the amazing group of people that make Caltech great. Agnes Tong has been a wonderful friend, and I'll never forget the moment I received the email from her saying I was accepted to Caltech. Joe, Ron, and Memo at the Chemistry stock room have been great friends as well, supporting research on a daily basis. Jennifer Costanza, Gwen Williams, Jeff Cochrane, Scott Wang, and Syed Ahsan have supported my research as well, through their hard work supporting the animal facility. I also wanted to thank the friendly faces at the Rathskeller, Mike and Jorge in particular.

I have had a great group of friends at Caltech, who have made the past 6 years some of my best. A few names include Jeff, JJ, Greg, Myles, Jeanluc, Chithra, Keith, Garret, Young In, Abby, Alli, Ben, Nick, Matt, Elizabeth, Sheldon, Seth, Anna, Ariel, Tim, Alyson, and many others. We've all experienced many good and bad times in the past few years, and I am excited for what the future holds for all of us, albeit some more so than others. I've also had great friends outside of Caltech, who have reminded me of all the wonderful things that await in the real world. I want to thank Dan, Michelle, Richard, Peter, Chris C., Chris H., Sam, and Nick U. for their friendship, as I've known most of them for most of my life.

Finally I want to thank my family, who has supported me in every way. My successes are only possible because of their hard work, sacrifice, and determination. My parents, Alice and Vincent, have shown me how to be a good person and what it takes to find happiness and success in life. I love them very much, and work every day to make them proud. My sister Kathy has always supported me, and her success is a welcomed reminder of the things I hope to achieve one day. My new family, Ryan Doherty, Peter, Carol, and Russ Komor, have been so kind to me, and I am lucky to have such genuinely good people in my family. If I'm ever in their shoes one day, I hope to be as kind and loving as they have been to me, although this is highly unlikely.

To Alexis, I love you! As uncertainties of the future loom, and with the coming months assuredly stress-filled, the constant love that we have for each other is something that provides me with great optimism and courage. You are indeed my better half, and I can only imagine what the future holds for the two of us (Teslas and Sportfishers, to begin). I need nothing more than to spend the rest of my life with you.

Abstract

O-GlcNAc glycosylation of nuclear and cytosolic proteins is an essential post-translational modification implicated in many diseases, from cancer to diabetes. Importantly, many important neuronal proteins are also *O*-GlcNAc modified, and aberrant *O*-GlcNAcylation of these proteins may contribute to the pathology of neurodegenerative diseases although these mechanisms have not been well defined. Here we investigated the role of *O*-GlcNAc glycosylation in the brain, utilizing both chemistry and molecular biology to study *O*-GlcNAc transferase (OGT), the enzyme that adds the sugar modification. To evaluate the role of OGT in adult neurons, we generated a forebrain-specific conditional knockout of OGT (OGT cKO) in mice. Although indistinguishable from wild-type littermates at birth, after three weeks we observe progressive neurodegeneration in OGT cKO mice. Hallmarks of Alzheimer's disease, including neuronal loss, neuroinflammation, behavioral deficits, hyperphosphorylated tau, and amyloid beta peptide accumulation, are observed. Furthermore, decreases in OGT protein levels were found in human AD brain tissue, suggesting that altered *O*-GlcNAcylation likely contributes to neurodegenerative diseases in humans. This model is one of a few mouse models that recapitulate AD phenotypes without mutating and overexpressing human tau, amyloid precursor protein, or presenilin, highlighting the essential role of OGT in neurodegenerative pathways.

Given the importance of OGT in the brain, we further investigated the regulation of the OGT enzyme by phosphorylation. We found that phosphorylation of OGT near its C-terminus reduces its activity in cancer cells,

and have developed phosphorylation-specific antibodies to aid mechanistic studies. Furthermore, mutation of this phosphorylation site on OGT, followed by overexpression in neurons was shown to enhance neurite outgrowth, demonstrating a functional consequence for this site. Thus phosphorylation of OGT inhibits its activity and enhances neurite outgrowth, and current studies aim to characterize the signaling pathway that regulates OGT phosphorylation in neurons.

Table of Contents

List of Figures and Tables

Chapter 1

Chapter 2

Chapter 4

Chapter 1: Introduction

1.1 *O*-GlcNAc Glycosylation

O-linked N-acetylglucosamine (*O*-GlcNAc) glycosylation of proteins is an increasingly important post-translational modification, implicated in a multitude of disease processes. *O*-GlcNAc glycosylation is ubiquitous, present in all metazoans, and is essential for cellular proliferation. The *O*-GlcNAc transferase (OGT) enzyme is responsible for the addition of a single *O*-GlcNAc sugar to serine and threonine residues of proteins, and an *O*-GlcNAcase (OGA) enzyme removes it. Together, these two highly conserved proteins differentially modify over one thousand different substrates in a regulated manner, and dynamically in response to cellular signaling events. *O*-GlcNAc modifications have been identified on proteins that regulate fundamental cellular processes including protein synthesis (1), transcription (2), and cell cycle progression (3, 4).

Understanding the role of *O*-GlcNAc in these diverse pathways is of great interest, as many disease-relevant pathways are known to be *O*-GlcNAc regulated. Although *O*-GlcNAc is an essential post-translational modification, it was not discovered until the 1980's, due to its low stoichiometry and chemically labile nature. The *O*-linkage is readily disrupted in typical mass spectrometry procedures, which along with its low abundance makes it extremely challenging to detect and study. Much work has been done in the past few years to develop the tools necessary to study *O*-GlcNAc, and the most interesting insights into *O*-GlcNAc biology have yet to come, as the field matures and the broader scientific community begins to appreciate the importance of this unique form of

glycosylation. This introductory chapter will establish the key topics associated with understanding *O*-GlcNAc biology, with a focus on its role in the brain.

1.2 Tools to study *O*-GlcNAc glycosylation

To facilitate the identification and investigation of *O*-GlcNAcylated proteins, there has been a concerted effort in the field to develop strategies to selectively label them in complex lysates and in cells. One such method uses a chemoenzymatic approach, where *O*-GlcNAcylated proteins are tagged with a galactose sugar containing a bio-orthogonal tag (N-azidoacetylgalactosamine, or ketogalactose) (Figure 1.1) (5). This is accomplished with a mutant form of β-1,4-galactosyltransferase enzyme (Y289L GALT) that specifically adds a galactose sugar to terminal *O*-GlcNAc moieties. This strategy results in stoichiometric labeling and allows for the subsequent isolation of *O*-GlcNAc modified proteins which can be analyzed by mass spectrometry to identify amino acid residues containing *O*-GlcNAc modifications. The utility of this method is further extended with the addition of a polyethylene glycol (PEG) group to *O*-GlcNAcylated proteins, which results in a shift in apparent molecular weight of a protein of interest (6). This allows for the direct quantification of protein *O*-GlcNAc glycosylation, and the use of phosphorylation-specific antibodies further elucidates the relationship between *O*-GlcNAcylation and protein phosphorylation.

Methods to metabolically label *O*-GlcNAcylated proteins have also been developed, and were shown to label *O*-GlcNAc-modified proteins in living cells. In one study, N-azidoacetylgalactosamine (GalNAz) was shown to be converted to

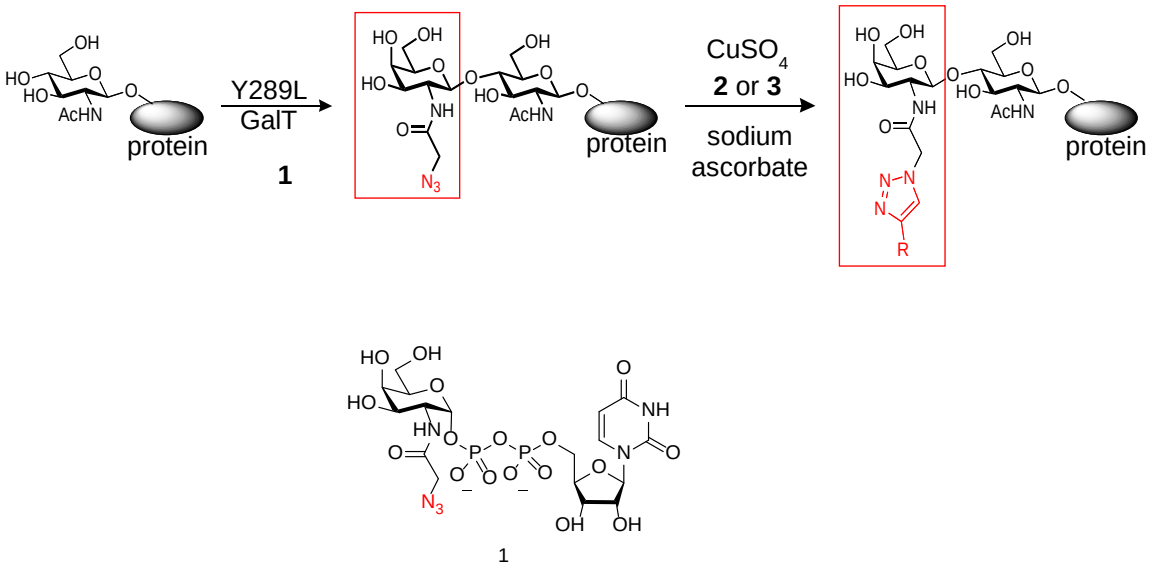

Figure 1.1: Overview of the chemoenzymatic labeling strategy. *O*-GlcNAcylated proteins in complex lysates are selectively labeled with a mutant GalT enzyme (Y289L) that adds GalNAz (or ketogalactose) to *O*-GlcNAc moieties. After reaction of the bio-orthogonal azido group with an alkyne tag via 3+2 cycloaddition chemistry, labeled *O*-GlcNacylated proteins can be isolated and subjected to downstream applications. This method allows for stoichiometric labeling of *O*-GlcNAcylated proteins. Quantification of *O*-GlcNAc stoichiometries of specific proteins is achieved by appending a polyethylene glycol (PEG) mass tag, which results in a shift in apparent molecular weight upon SDS-PAGE.

UDP-GalNAz, which was further epimerized to N-azidoacetylglucosamine (GlcNAz) (7). This substrate was accepted by OGT in cells to label protein substrates. Metabolic labeling allows for the labeling of *O*-GlcNAcylated proteins in live cells, which has the potential to facilitate labeling in whole animals as well as labeling in a time resolved manner. However, metabolic labeling is substoichiometric, as endogenous UDP-GlcNAc is much more abundant in the cell. Thus, labeling of *O*-GlcNAcylated proteins is incomplete and may suffer from significantly lower efficiency.

The development of these new strategies to monitor *O*-GlcNAc glycosylation greatly facilitates our ability to investigate the roles of *O*-GlcNAc in the cell. The continued development of tools such as more potent and selective inhibitors of OGT or OGA, and model cellular or animal systems to study the effects of perturbations in *O*-GlcNAc levels, will drive future insights.

1.3 *O*-GlcNAc Transferase

Full-length *O*-GlcNAc transferase contains 1035 amino acids, with an apparent molecular weight of 110 kDa. Through complex splicing of its mRNA (8, 9), OGT exists as three distinct isoforms, which include nuclear/cytoplasmic, mitochondrial-targeted, and short forms. These isoforms differ by truncations at their N-termini, with mitochondrial and short form OGT having truncations of their first 2 and 9 TPR domains, respectively.

As OGT is responsible for the addition of *O*-GlcNac onto hundreds of different proteins, understanding the regulation of this process represents a significant challenge. Whereas over four hundred different genetically encoded

kinases are responsible for phosphorylating specific substrates, a single OGT enzyme must modify all substrates selectively and in response to cellular signaling events. Current strategies to understand OGT's substrate specificity focus on characterizing its protein-protein interaction domain, the tetratricopeptide repeats (TPR) (10). OGT has a series of 11.5 TPR domains at its N-terminus that have been shown to mediate its substrate interactions. A crystal structure of OGT is shown in Figure 1.2 (11).

Each TPR domain is 34-residues long and consists of two anti-parallel α-helices, which stack in a parallel fashion to form a super-helix that mediates binding of different protein partners (12). The sequence of each TPR is unique and has the potential to mediate unique interactions. TPR motifs have been identified in other proteins, including protein phosphatase 5 (13), anaphase promoting complex, and STI1, a co-chaperone protein that forms a complex with heat shock proteins (12). It represents a highly conserved protein-protein interaction motif, and the presence of different TPR-like structures suggests convergent evolution and thus the importance of this structural motif.

Several studies have investigated the importance of the TPR domains in mediating OGT-substrate interactions. Specifically, nucleoporin 62 (Nup62) (14), casein kinase II (CKII) (14), Milton (10, 15), and *O*-GlcNAcase (16) have all been shown to interact with a particular part of OGT's TPR domains. For example, Milton, a protein responsible for mitochondrial trafficking, was shown to be *O*-GlcNAc modified, and to associate with TPRs 2-6 of OGT (10). *O*-GlcNAcylation of Milton was shown to inhibit mitochondrial trafficking in axons which potentially

Figure 1.2: Cartoon representation of a crystal structure of OGT. N to C-terminus spans blue to red color range. TPR domains are arranged in a superhelical orientation and mediate OGT-substrate interactions. The C-terminal catalytic domain is shown with a casein kinase II peptide bound (red).

plays a role in the localization of mitochondria to regions of the neuron that require increased ATP or have an abundance of glucose. OGA was also shown to interact with the N-terminus of OGT, through TPR domains 1-6 (16). A specific domain of OGA was also shown to be sufficient for interaction with OGT (aa 336-548), and this OGT/OGA complex possibly would allow for rapid addition or removal of *O*-GlcNAc in response to stimuli. Indeed, an OGT/OGA complex was shown to associate with Aurora B and may regulate cell cycle progression (17). Tab1, an activator in TGF-β signaling was shown to interact near the catalytic domain of OGT, with TPRs 9-13 (18). Although a handful of these interactions have been identified, most OGT-substrate interactions remain undefined.

In addition to regulation of OGT activity by substrate interactions, other forms of regulation include controlling subcellular localization or post-translational modification of the enzyme, by phosphorylation or self *O*-GlcNAcylation. Exploring the role of phosphorylation in OGT regulation is of tremendous interest, and the subject of a following chapter.

As the regulation of OGT and its substrate interactions become more defined, improved control over OGT activity towards its substrates will be possible by either modulating OGT activation by PTM's, or targeting specific OGT-substrate interactions. Modulation of OGT activity will serve as a powerful tool to understand the function of *O*-GlcNAc on specific substrates, and holds great promise for therapeutic development, by targeting *O*-GlcNAcylation of specific substrates.

1.4 *O*-GlcNAcase

OGA (previously referred to as MGEA5 or NCOAT) is a 916 amino acid protein with an apparent molecular weight of 103 kDa. OGA exists in two isoforms, a short and long form, that differs by a C-terminal truncation (8, 9). OGA is subjected to complex mRNA splicing events and is potentially expressed from more than one promoter (19). The enzyme consists of an N terminal catalytic domain, and a C-terminal histone acetyltransferase (HAT) domain, and contains a caspase 3 cleavage site between the two (20). It is unclear how cleavage regulates OGA; however, there is evidence that OGA is catalytically active in the absence of its HAT domain (short form) (21). HAT domain of OGA is considered to be important for epigenetic regulation, as OGA and OGT exist in a complex together at histones. It has been proposed that this complex regulates epigenetic factors by dynamically *O*-GlcNAc glycosylating, or de-glycosylating and acetylating histones in response to signaling events (22).

1.5 *O*-GlcNAc in metabolism and stress

The substrate of OGT, UDP-GlcNAc is a metabolic byproduct of glycolysis, through the hexosamine biosynthetic pathway (HBP). An estimated 2-5% of all glucose is diverted to the HBP to produce UDP-GlcNAc. The synthesis of the UDP-GlcNAc substrate thus ties together several different metabolic and nutrient dependent pathways, including glucose availability, nucleotide biosynthesis, and amino acid metabolism. Thus, *O*-GlcNAc is intimately related to cellular metabolism, and affects diseases that involve metabolic dysfunction such as cancer (23) and diabetes (24).

For example, *O*-GlcNAc was shown to regulate insulin signaling through its modification of IRS1/2, and AKT in 3T3-L1 adipocytes (25). Specifically, increased *O*-GlcNAcylation on IRS1 correlates with reduced binding with PI3K. This in turn decreases the activation of AKT in response to insulin signaling, which ultimately reduces glucose uptake (Figure 1.3). Furthermore, phosphofructokinase-1 (PFK1) was shown to be inhibited by *O*-GlcNAc glycosylation (23). PFK1 glycosylation increases in cancer cells and shunts glycolytic flux from glycolysis to the pentose phosphate pathway, providing a selective advantage to cancer cells by producing NADH to combat oxidative stress and by producing pentose sugars to support nucleic acid biosynthesis (Figure 1.3).

O-GlcNAc has also been studied extensively in the context of the stress response, and has been shown to have a protective role. Increasing *O*-GlcNAc levels in cardiomyocytes significantly reduced ER stress-induced cell death by attenuating the unfolded protein response (26). Furthermore, *O*-GlcNAcylation was also shown to confer cytoprotection in the heart by attenuating mitochondrial permeability transition pore (mPTP) after ischemia injury (27). Specifically, calcium overload and reactive oxygen species generation were significantly reduced in cardiomyocytes with enhanced *O*-GlcNAcylation. These studies suggest that regulation of OGT and *O*-GlcNAc is a complex and multifaceted system. Thus, this represents a challenging therapeutic target as increased *O*-GlcNAcylation in the context of adipocytes contributes to insulin resistance, and in cardiomyocytes contributes to cytoprotection.

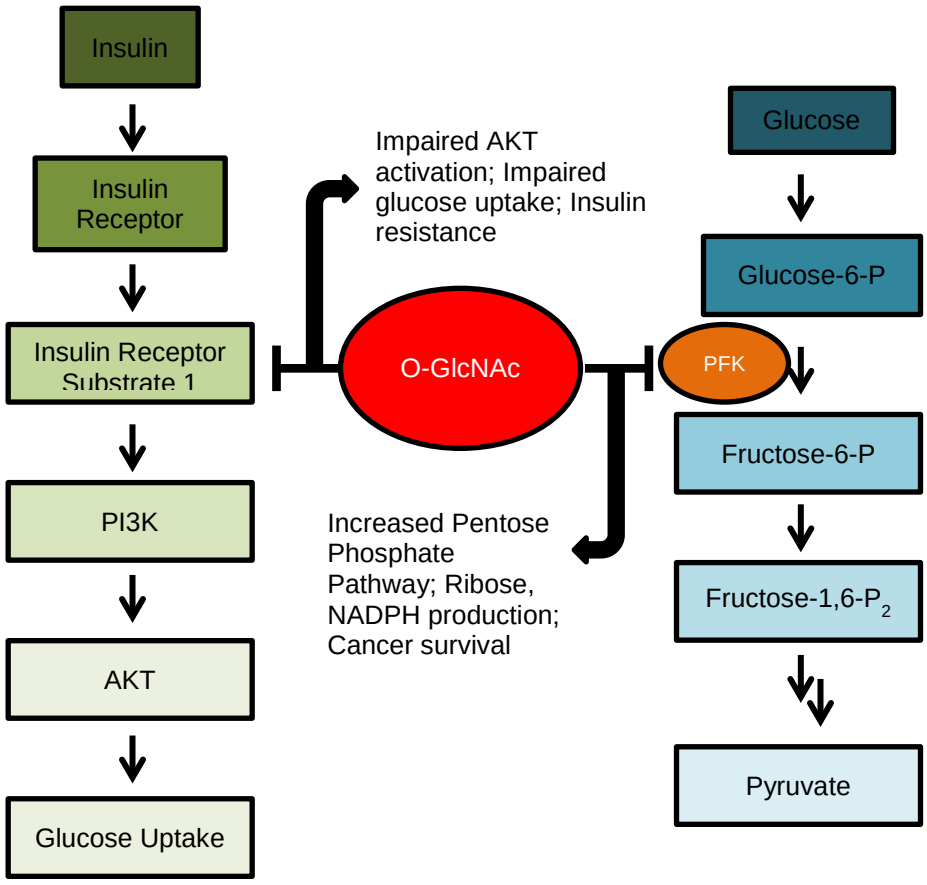

Figure 1.3: *O*-GlcNAc modification of key proteins regulates disease pathways. *O*-GlcNAc modification of insulin receptor substrate 1 was shown to reduce its binding to PI3K, leading to reduced AKT activation and downstream glucose uptake. Furthermore, *O*-GlcNAc modification of PFK inhibits its activity, reducing glycolytic flux. Metabolic products are shunted to the pentose phosphate pathway, an alternative metabolic pathway that produces Ribose, NADPH, and other molecules essential for cellular proliferation and combating oxidative stress. The production of these molecules that support cell growth provides a selective growth advantage for cancer cells that upregulate their *O*-GlcNAc modification of PFK.

1.6 *O*-GlcNAc in Neurons

Although *O*-GlcNAc is found in all cell types, it is highly enriched in the brain. The OGT gene is located in a region of the X chromosome (Xq13) linked to Parkinson's dystonia (28). The gene that encodes OGA is located in a region of the chromosome (10q24.1) linked to increased risk of late-onset AD (29). It remains to be seen whether mutations or alterations to these chromosome regions alter *O*-GlcNAc cycling in disease; however, the fact that OGT and OGA are associated with neurodegeneration-sensitive regions suggests their importance in degenerative processes.

Furthermore, many key neuronal proteins are *O*-GlcNAc modified, including CREB (30), synapsin 1 (31, 32), axonal transport protein Milton (15), and AMPA receptor subunit GluA2 (33). Recently, cAMP response element-binding protein (CREB) was shown to be *O*-GlcNAc modified. As a key regulator of genes responsible for learning and memory in mice, the regulation of CREB has been studied extensively in the context of phosphorylation and binding with co-activators (34). This recent study identified a new form of CREB regulation via *O*-GlcNAc glycosylation, which was shown to repress CREB activity and affect consolidation of short-term memory in mice (30).

Several studies have suggested that *O*-GlcNAcylation may play a critical role in neurodegenerative processes. Many neurodegeneration-related proteins are *O*-GlcNAc modified, including amyloid precursor protein (APP) (35), clathrin assembly protein AP-180 (36), neurofilament M (37), and tau (38). Although the precise roles of the modification in regulating these proteins are not well

understood, *O*-GlcNAcylation of nicastrin, a component of the γ-secretase complex that cleaves APP, was shown to decrease γ-secretase activity (39). Furthermore, increasing *O*-GlcNAc levels was shown to increase non-amyloidogenic processing of APP (40), suggesting a neuroprotective role for *O*-GlcNAc in neurons. Similarly, *O*-GlcNAcylation of tau has been proposed to be reciprocally related to its phosphorylation at disease-associated sites (38).

An increasingly recurrent theme in *O*-GlcNAc biology is the importance maintaining *O*-GlcNAc levels within an appropriate range. For example, several studies have investigated the significance of the modification on synaptic activity and long term potentiation/depression. Conflicting results have shown that an increase in *O*-GlcNAc in hippocampal slices increased long-term potentiation (LTP) (32), and also increased long-term depression (LTD) (33). Although there are differences in the studies (acute (induced LTD) vs. long term (induced LTP) treatment with an OGA inhibitor, rat vs. mouse slices, etc), these discrepancies illustrate the importance of maintaining a correct balance between OGT and OGA activity. Furthermore, characterization of *O*-GlcNAc levels in Alzheimer's disease (AD) brains has shown a reduction in *O*-GlcNAc modifications (41). However, a recent paper reported increases in *O*-GlcNAc levels in the brainstem of AD patients (42), again providing conflicting results. Collectively, these findings suggest that targeting OGT or OGA with general inhibitors to treat diseases may lead to unwanted consequences, and motivates the development of complementary strategies to carefully spatially control OGT and OGA activity.

1.7 Challenges to Studying *O*-GlcNAc Glycosylation

As previously stated, *O*-GlcNAc glycosylation has been challenging to study for a variety of reasons. First, the modification is substoichiometric and chemically labile, which makes detection quite difficult (6, 43, 44). As a result, new methods and strategies for reliably detecting *O*-GlcNAc modifications have been recently developed (5, 7, 44). Another significant challenge to studying *O*-GlcNAc modifications is that single OGT and OGA enzymes are responsible for cycling the modification on and off hundreds of different substrates (20, 45). Thus, studies with small-molecule inhibitors or RNAi that are typically employed to study protein function provide results that are difficult to interpret. Inhibition of OGT activity for instance, generally decreases *O*-GlcNAc modification of over one thousand substrates all at once, and convolutes phenotypic analysis.

Furthermore, as *O*-GlcNAc modification is required for cell-cycle progression, complete knockout of OGT in dividing cells is not possible (3, 4). Indeed, our studies have shown that knockdown of OGT with RNAi is often incomplete, and more importantly, selected against after several passages because of the selective growth advantage conferred by OGT (46). Work in the following sections describes our efforts to study *O*-GlcNAc glycosylation by utilizing conditional knockout strategies, characterizing the regulation of the OGT enzyme, and developing better tools to manipulate *O*-GlcNAc *in vitro*. Through this work, some of these challenges have been addressed while others await ongoing and future studies.

1.8 Conclusions

After its discovery over thirty years ago, *O*-GlcNAc glycosylation has proven to be a tremendously interesting regulator of cellular biology. Significant challenges to studying the modification due to its low abundance and chemically labile *O*-linkage have been addressed through the development of new strategies. By specifically tagging *O*-GlcNAc modifications, modified proteins can be enriched and facilitate downstream molecular biology studies. Furthermore, advancements in mass spectrometry technologies have greatly improved our ability to identify sites of *O*-GlcNAcylation and have facilitated functional studies of *O*-GlcNAc-modified proteins.

Both OGT and OGA are complex proteins responsible for acting on many hundreds of proteins. As a result they require extensive regulation that is only beginning to be understood. As more proteins involved in fundamental cellular and disease processes are found to contain *O*-GlcNAc modifications, it will become increasingly important to understand the regulation of the OGT and OGA enzymes, and to modulate their activity.

Developing better inhibitors of *O*-GlcNAc glycosylation, possibly at the level of substrate-OGT interactions may provide viable strategies for targeted disruption of *O*-GlcNAcylation. Studies that currently seek to modulate OGT activity often rely on small molecule OGT active-site inhibitors, many of which suffer from poor specificity and significant off-target effects. Furthermore, specific and potent inhibition of OGT, even when possible, leads to a global decrease of *all O*-GlcNAc modified proteins, complicating phenotypic or mechanistic analysis.

Given the modular nature of TPR domains, it is expected that specific inactivation of one or a few TPR domains at a time would provide significantly improved control over OGT activity by inhibiting small sets of substrates at a time. Both understanding *O*-GlcNAc biology and finding ways to augment the modification will be important areas of focus for future therapeutic development.

1.9 References

1. Xu J WS, Viollet B, Zou MH. (2012) Regulation of the proteasome by AMPK in endothelial cells: the role of O-GlcNAc transferase (OGT). *PLoS One.* 7(5):36717.
2. Ranuncolo SM, Ghosh S, Hanover JA, Hart GW, & Lewis BA (2012) Evidence of the involvement of O-GlcNAc-modified human RNA polymerase II CTD in transcription in vitro and in vivo. *The Journal of biological chemistry* 287(28):23549-23561.
3. O'Donnell N ZN, Hart GW, Marth JD. (2004) Ogt-dependent X-chromosome-linked protein glycosylation is a requisite modification in somatic cell function and embryo viability. *Mol Cell Biol.* 24(4):1680-1690.
4. Slawson C*, et al.* (2005) Perturbations in O-linked β-N-acetylglucosamine protein modification cause severe defects in mitotic progression and cytokinesis. *Journal of Biological Chemistry* 280(38):32944-32956.
5. Clark PM DJ, Mason DE, Hart CR, Buck SB, Peters EC, Agnew BJ, Hsieh-Wilson LC. (2008) Direct in-gel fluorescence detection and cellular imaging of O-GlcNAc-modified proteins. *J Am Chem Soc.* 130(35):11576-11577.
6. Rexach JE*, et al.* (2010) Quantification of O-glycosylation stoichiometry and dynamics using resolvable mass tags. *Nature chemical biology* 6(9):645-651.
7. Boyce M*, et al.* (2011) Metabolic cross-talk allows labeling of O-linked beta-N-acetylglucosamine-modified proteins via the N-

acetylgalactosamine salvage pathway. *Proceedings of the National Academy of Sciences of the United States of America* 108(8):3141-3146.

8. Hanover JA*, et al.* (2003) Mitochondrial and nucleocytoplasmic isoforms of O-linked GlcNAc transferase encoded by a single mammalian gene. *Archives of biochemistry and biophysics* 409(2):287-297.
9. Comtesse N, Maldener E, & Meese E (2001) Identification of a nuclear variant of MGEA5, a cytoplasmic hyaluronidase and a beta-N-acetylglucosaminidase. *Biochemical and biophysical research communications* 283(3):634-640.
10. Iyer SP & Hart GW (2003) Roles of the tetratricopeptide repeat domain in O-GlcNAc transferase targeting and protein substrate specificity. *The Journal of biological chemistry* 278(27):24608-24616.
11. Lazarus MB, Nam Y, Jiang J, Sliz P, & Walker S (2011) Structure of human O-GlcNAc transferase and its complex with a peptide substrate. *Nature* 469(7331):564-567.
12. Blatch GL & Lassle M (1999) The tetratricopeptide repeat: a structural motif mediating protein-protein interactions. *BioEssays : news and reviews in molecular, cellular and developmental biology* 21(11):932-939.
13. Das AK, Cohen PW, & Barford D (1998) The structure of the tetratricopeptide repeats of protein phosphatase 5: implications for TPR-mediated protein-protein interactions. *The EMBO journal* 17(5):1192-1199.

14. Lazarus BD, Love DC, & Hanover JA (2006) Recombinant O-GlcNAc transferase isoforms: identification of O-GlcNAcase, yes tyrosine kinase, and tau as isoform-specific substrates. *Glycobiology* 16(5):415-421.

15. Pekkurnaz G, Trinidad JC, Wang X, Kong D, & Schwarz TL (2014) Glucose regulates mitochondrial motility via Milton modification by O-GlcNAc transferase. *Cell* 158(1):54-68.

16. Whisenhunt TR*, et al.* (2006) Disrupting the enzyme complex regulating O-GlcNAcylation blocks signaling and development. *Glycobiology* 16(6):551-563.

17. Slawson C, Lakshmanan T, Knapp S, & Hart GW (2008) A mitotic GlcNAcylation/phosphorylation signaling complex alters the posttranslational state of the cytoskeletal protein vimentin. *Mol Biol Cell* 19(10):4130-4140.

18. Clarke AJ*, et al.* (2008) Structural insights into mechanism and specificity of O-GlcNAc transferase. *The EMBO journal* 27(20):2780-2788.

19. Twine NA, Janitz K, Wilkins MR, & Janitz M (2011) Whole transcriptome sequencing reveals gene expression and splicing differences in brain regions affected by Alzheimer's disease. *PloS one* 6(1):e16266.

20. Toleman C, Paterson AJ, Whisenhunt TR, & Kudlow JE (2004) Characterization of the histone acetyltransferase (HAT) domain of a bifunctional protein with activable O-GlcNAcase and HAT activities. *The Journal of biological chemistry* 279(51):53665-53673.

21. Butkinaree C, Park K, & Hart GW (2010) O-linked beta-N-acetylglucosamine (O-GlcNAc): Extensive crosstalk with phosphorylation to regulate signaling and transcription in response to nutrients and stress. *Biochimica et biophysica acta* 1800(2):96-106.

22. Sakabe K, Wang Z, & Hart GW (2010) Beta-N-acetylglucosamine (O-GlcNAc) is part of the histone code. *Proceedings of the National Academy of Sciences of the United States of America* 107(46):19915-19920.

23. Yi W CP, Mason DE, Keenan MC, Hill C, Goddard WA 3rd, Peters EC, Driggers EM, Hsieh-Wilson LC. (2012) Phosphofructokinase 1 glycosylation regulates cell growth and metabolism. *Science.* 337(6097):975-980.

24. Park K, Saudek CD, & Hart GW (2010) Increased expression of beta-N-acetylglucosaminidase in erythrocytes from individuals with pre-diabetes and diabetes. *Diabetes* 59(7):1845-1850.

25. Whelan SA, Dias WB, Thiruneelakantapillai L, Lane MD, & Hart GW (2010) Regulation of insulin receptor substrate 1 (IRS-1)/AKT kinase-mediated insulin signaling by O-Linked beta-N-acetylglucosamine in 3T3-L1 adipocytes. *The Journal of biological chemistry* 285(8):5204-5211.

26. Ngoh GA, Hamid T, Prabhu SD, & Jones SP (2009) O-GlcNAc signaling attenuates ER stress-induced cardiomyocyte death. *Am J Physiol Heart Circ Physiol* 297(5):H1711-1719.

27. Ngoh GA, Watson LJ, Facundo HT, & Jones SP (2011) Augmented O-GlcNAc signaling attenuates oxidative stress and calcium overload in cardiomyocytes. *Amino acids* 40(3):895-911.

28. Nolte D & Muller U (2002) Human O-GlcNAc transferase (OGT): genomic structure, analysis of splice variants, fine mapping in Xq13.1. *Mamm Genome* 13(1):62-64.

29. Farook VS, Bogardus C, & Prochazka M (2002) Analysis of MGEA5 on 10q24.1-q24.3 encoding the beta-O-linked N-acetylglucosaminidase as a candidate gene for type 2 diabetes mellitus in Pima Indians. *Mol Genet Metab* 77(1-2):189-193.

30. Rexach JE*, et al.* (2012) Dynamic O-GlcNAc modification regulates CREB-mediated gene expression and memory formation. *Nature chemical biology* 8(3):253-261.

31. Skorobogatko Y*, et al.* (2014) O-linked beta-N-acetylglucosamine (O-GlcNAc) site thr-87 regulates synapsin I localization to synapses and size of the reserve pool of synaptic vesicles. *The Journal of biological chemistry* 289(6):3602-3612.

32. Tallent MK*, et al.* (2009) In vivo modulation of O-GlcNAc levels regulates hippocampal synaptic plasticity through interplay with phosphorylation. *The Journal of biological chemistry* 284(1):174-181.

33. Taylor EW*, et al.* (2014) O-GlcNAcylation of AMPA receptor GluA2 is associated with a novel form of long-term depression at hippocampal

synapses. *The Journal of neuroscience : the official journal of the Society for Neuroscience* 34(1):10-21.

34. Silva AJ, Kogan JH, Frankland PW, & Kida S (1998) CREB and memory. *Annual review of neuroscience* 21:127-148.

35. Griffith LS, Mathes M, & Schmitz B (1995) Beta-amyloid precursor protein is modified with O-linked N-acetylglucosamine. *J Neurosci Res* 41(2):270-278.

36. Yao PJ & Coleman PD (1998) Reduced O-glycosylated clathrin assembly protein AP180: implication for synaptic vesicle recycling dysfunction in Alzheimer's disease. *Neuroscience letters* 252(1):33-36.

37. Ludemann N*, et al.* (2005) O-glycosylation of the tail domain of neurofilament protein M in human neurons and in spinal cord tissue of a rat model of amyotrophic lateral sclerosis (ALS). *The Journal of biological chemistry* 280(36):31648-31658.

38. Arnold CS*, et al.* (1996) The microtubule-associated protein tau is extensively modified with O-linked N-acetylglucosamine. *The Journal of biological chemistry* 271(46):28741-28744.

39. Kim C*, et al.* (2013) O-linked beta-N-acetylglucosaminidase inhibitor attenuates beta-amyloid plaque and rescues memory impairment. *Neurobiology of aging* 34(1):275-285.

40. Jacobsen KT & Iverfeldt K (2011) O-GlcNAcylation increases non-amyloidogenic processing of the amyloid-beta precursor protein (APP). *Biochemical and biophysical research communications* 404(3):882-886.

41. Liu F SJ, Tanimukai H, Gu J, Gu J, Grundke-Iqbal I, Iqbal K, Gong CX. (2009) Reduced O-GlcNAcylation links lower brain glucose metabolism and tau pathology in Alzheimer's disease. *Brain.* 132(7):1820-1832.

42. Forster S*, et al.* (2014) Increased O-GlcNAc levels correlate with decreased O-GlcNAcase levels in Alzheimer disease brain. *Biochimica et biophysica acta* 1842(9):1333-1339.

43. Khidekel N, Ficarro SB, Peters EC, & Hsieh-Wilson LC (2004) Exploring the O-GlcNAc proteome: direct identification of O-GlcNAc-modified proteins from the brain. *Proceedings of the National Academy of Sciences of the United States of America* 101(36):13132-13137.

44. Khidekel N*, et al.* (2007) Probing the dynamics of O-GlcNAc glycosylation in the brain using quantitative proteomics. *Nature chemical biology* 3(6):339-348.

45. Shafi R IS, Ellies LG, O'Donnell N, Marek KW, Chui D, Hart GW, Marth JD. (2000) The O-GlcNAc transferase gene resides on the X chromosome and is essential for embryonic stem cell viability and mouse ontogeny. *Proc Natl Acad Sci U S A.* 97(11):5735-5739.

46. Yi W (2010) Unpublished.

Chapter 2: Generation and characterization of a conditional forebrain-specific OGT knockout to understand the role of *O*-GlcNAc in the brain

2.1 Introduction

Alzheimer's disease (AD) is the sixth leading cause of death in the United States, and is characterized by the accumulation of extracellular senile plaques, intracellular neurofibrillary tangles, and progressive cognitive decline. There are currently no effective treatments for AD and current efforts to combat disease progression focus on reducing amyloid beta peptide and hyperphosphorylated tau protein levels. It is unclear how AD pathology proceeds in humans, but mouse models have provided significant insight. Through these studies, key disease-relevant pathways have been identified, including protein homeostasis, cell-cycle progression, and metabolism. It remains to be seen whether these diverse pathways are related and how they contribute to neurodegeneration.

O-GlcNAc glycosylation is a dynamic, inducible post-translational modification that regulates many critical biological processes, including insulin signaling (1), transcription (2), cell cycle regulation (3), stress responses (4)and proteosomal degradation (5-7). In mammalian cells, a single *O*-GlcNAc transferase (OGT) enzyme catalyzes addition of the sugar *N*-acetylglucosamine to serine or threonine residues of proteins (8), and a single glycosidase enzyme, *O*-GlcNAcase (OGA) (9), removes it. Together, these enzymes cycle the modification on and off proteins in response to nutrient availability, various cellular stresses, neuronal depolarization, and other stimuli.

Emerging evidence suggests that *O*-GlcNAcylation plays essential roles in the brain and may contribute to the regulation of learning and memory. For example, the transcription factor cAMP-response element binding protein (CREB) is highly *O*-GlcNAcylated in neurons and its glycosylation is dynamically induced by neuronal activity (10). CREB glycosylation at a single site disrupts its interaction with the coactivator TORC and thereby represses both basal and inducible CREB-dependent transcription. Notably, blocking glycosylation at this site leads to accelerated formation of long-term fear memories in mice suggesting that *O*-GlcNAc can contribute to higher order brain functions. The *O*-GlcNAc modification has also been identified on numerous synaptic proteins, including synapsin I (11), the axonal transport protein Milton (12), and the AMPA receptor subunit GluA2 (13). Glycosylation of synapsin I at Thr87 affects its targeting to synaptic vesicles, and overexpression of a glycosylation-deficient synapsin mutant increases the density of synaptic vesicle clusters along axons (14). On the other hand, induced *O*-GlcNAcylation of Milton significantly reduces mitochondrial motility in axons (12). Local increases in glucose levels or neuronal activity, both of which are known to upregulate OGT activity, are thought to dynamically increase Milton *O*-GlcNAcylation, thereby increasing the local concentration of mitochondria. This potentially serves as a mechanism by which mitochondria are targeted to regions of abundant glucose, or regions of high neuronal activity to efficiently produce ATP where it is needed. Global increases in *O*-GlcNAcylation have also been shown modulate long-term depression (LTD)

in rat hippocampal slices through GluA2 (13), although the exact mechanisms are unknown.

In addition to its effects on fundamental neuronal processes, *O*-GlcNAcylation may play a critical role in neurodegenerative diseases such as Alzheimer's disease, amyotrophic lateral sclerosis (ALS), and Huntington's disease. Several key proteins involved in neurodegeneration are *O*-GlcNAc modified, including amyloid precursor protein (APP) (15), clathrin assembly protein AP-180 (16), neurofilament M (17), and tau (18). Although the precise roles of the modification are not well understood, *O*-GlcNAcylation appears to be reciprocally related to phosphorylation on neurofilament M and tau at disease-associated sites (18). Decreased *O*-GlcNAcylated neurofilament M (NFM) was associated with increased phosphorylation of NFM in the spinal cord of a transgenic rat model of ALS (10). Similarly, increased tau *O*-GlcNAcylation at serine-400 led to a decrease in tau phosphorylation at serine-404 *in vitro* (19), while increasing global *O*-GlcNAcylation reduced tau phosphorylation at threonine-212, threonine-217, serine-396, and serine-422 in mouse brain slices (20). Consistent with a neuroprotective role for *O*-GlcNAc, glycosylation of nicastrin, a component of the γ-secretase complex that cleaves APP, was shown to decrease γ-secretase activity (21), and globally increasing *O*-GlcNAc levels enhanced the non-amyloidogenic processing of APP (22). In addition, treatment of certain AD mouse models (5XFAD, JNPL3, and Tau.P301L) with small molecule inhibitors of OGA attenuated amyloid-β deposition (21), tau phosphorylation (23), motor deficits (24), and memory impairment (21).

On the other hand, studies show that decreasing O-GlcNAc levels can also rescue certain neurodegenerative phenotypes, which suggests that a delicate homeostatic balance in *O*-GlcNAc levels may be required. For example, elevating *O*-GlcNAc glycosylation levels inhibited the 26S proteasome (7) and autophagic flux (25), which may impair the degradation of toxic protein aggregates. Indeed, a recent report demonstrated that in *C. elegans*, genetic deletion of OGT reduced the ubiquitinylated protein load and altered autophagic flux, which alleviated neurodegenerative phenotypes in transgenic models of tauopathy, amyloid β-peptide, and polyglutamine expansion (26). In addition, global reduction in *O*-GlcNAcylation increased the survival of Neuro2A cells expressing mutant huntingtin I (mHtt) by increasing autophagic flux (27). Thus, *O*-GlcNAc glycosylation appears to play a complex role in neurodegeneration, and whether decreased *O*-GlcNAcylation contributes to neuroprotection or neurodegeneration is presently unclear. Moreover, it is unclear whether aberrant *O*-GlcNAc signaling merely correlates with neurodegenerative phenotypes or whether it can cause neurodegeneration *in vivo*.

OGT is ubiquitously expressed and essential for cell cycle progression and proliferation (28, 29), complicating efforts to study its function. For instance, deletion of OGT in multiple mammalian cell types leads to cell death (28, 29). Previous efforts to generate a constitutive OGT knockout mouse resulted in embryonic lethality, and a later study that generated a brain-specific OGT knockout mouse produced early postnatal lethality (28, 29). This conditional knockout was accomplished by using a Cre-loxP system, in which exon 1 of OGT

was flanked by two loxP sequences (floxed). LoxP sequences consist of 34 base pairs that are recognized by the Cre recombinase enzyme (30). Upon binding loxP sequences, Cre recombinase catalyzes the excision of the stretch of DNA between the two loxP sites. Thus, by restricting expression of Cre recombinase with a brain-specific promoter (synapsin), OGT knockout was limited to the brain (31). Despite the early postnatal lethal phenotype, these mice displayed increases in phosphorylated tau and provided initial evidence that OGT may play an important role in degenerative processes (31).

In this study, we generated a forebrain-specific conditional OGT knockout mouse to assess the effects of global loss of *O*-GlcNAcylation on learning, memory, and neurodegeneration in adult mice. The mice were healthy at birth, but starting at 2 months, they developed signs of progressive neurodegeneration, including loss of neurons, neuroinflammation, memory deficits, and increased hyperphosphorylated tau and pathogenic amyloid β-peptide. Microarray analysis of gene expression revealed an upregulation of networks associated with inflammation and cell cycle arrest, suggesting possible roles for gliosis and aberrant cell cycle regulation in *O*-GlcNAc-dependent neurodegeneration. Finally, our analysis of cortical tissue from human AD patients indicated a significant reduction in OGT protein levels compared to healthy individuals, suggesting that altered *O*-GlcNAcylation likely contributes to neurodegenerative diseases in humans. Together, our studies directly link reduced *O*-GlcNAcylation to the induction of several neurodegenerative phenotypes, suggesting a viable strategy for the amelioration of such diseases.

2.2 Results

2.2.1 Generation of a conditional OGT knockout mouse

In order to circumvent the requirement for OGT during neuronal development, we restricted knockout to the forebrain and beginning after birth. We utilized an αCaMKII promoter driven Cre recombinase mouse (αCamKII – Cre) that expresses Cre recombinase in the forebrain beginning after postnatal day 14 (32). Validation of the expression profile of αCamKII -Cre was performed by crossing this line with a floxed YFP mouse and characteristic forebrain specific expression of YFP was confirmed (Figure 2.1). We then crossed the αCamKII -Cre mouse with a previously characterized floxed OGT (OGTfl) mouse (28), and obtained a conditional knockout of OGT (OGT cKO). OGT cKO mice did not breed and necessitated maintaining OGTfl and αCaMKII -CRE mouse lines separately. By breeding homozygous OGTfl females (OGTfl-/-) with heterozygous αCaMKII-CRE males (CamKIICRE+/-) we were able to produce OGT cKO mice along with wild-type littermates (Figure 2.2). Additionally, only male mice were considered in this study due to random X inactivation of the OGT gene in females, which would complicate phenotypic analysis. Genotyping was conducted with previously established protocols for CRE and OGTfl genes and OGT cKO mice were produced at the expected frequencies and were indistinguishable from wild type littermates at birth.

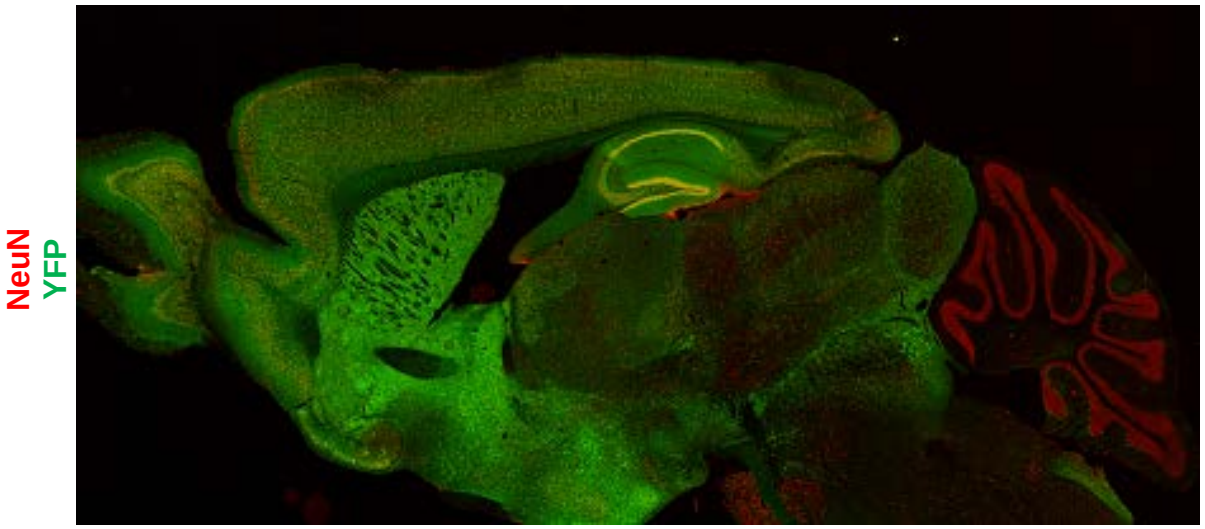

Figure 2.1: CaMKII-CRE expression is forebrain specific. CaMKII-CRE mice were crossed with floxed ROSA YFP mice to characterize the expression pattern of CaMKII-CRE. 6 month old animals were stained for YFP (green) and imaged with a NeuN (red) counterstain, and show largely forebrain specific expression with no signal in the cerebellum, in a pattern similar to previous reports.

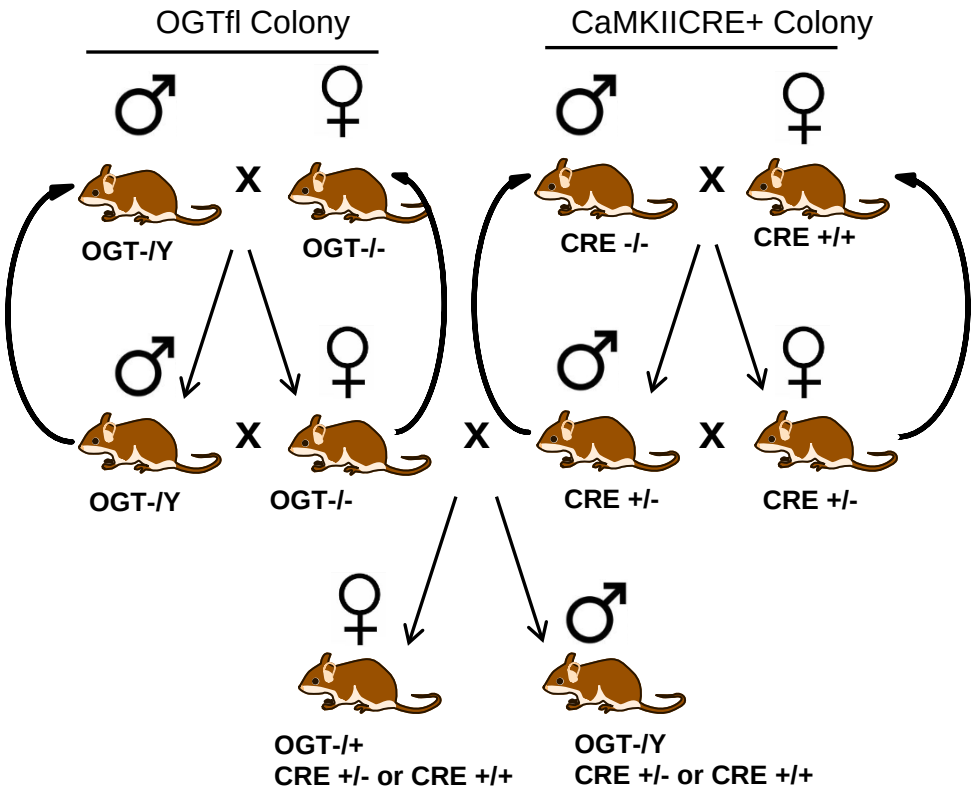

Figure 2.2: Breeding strategy to generate OGT cKO mice. CaMKII-CRE mice were bred separately from the floxed OGT (OGTfl) mouse line, because OGT cKO mice did not breed. Homozygous OGTfl females were bred with heterozygous CaMKII-CRE studs to produce male offspring that were OGTfl/Y, CRE wt/- or CRE wt/wt. Thus, OGT cKO mice were generated with wild type littermates for control studies. Female offspring were culled to avoid any complications with phenotypic analysis due to random X-inactivation. – denotes carrier, + denotes wild type.

2.2.2 Loss of *O*-GlcNAcylation is accompanied by progressive neuronal loss

OGT cKO mice were indistinguishable from their WT littermates until 7 weeks of age, after which they began to show a significant reduction in weight (10.9% reduction at 7 weeks; 32% at 16 weeks; Figure 2.3A, B). Along with this weight reduction, the brains of OGT cKO mice were significantly smaller overall, by 4 months (Figure 2.3C). We observed global changes in brain morphology by Nissl staining, which revealed a striking loss of neurons in the hippocampus by 16 weeks of age and a 56% reduction in cortical thickness at 6 months (Figure 2.3C, D). Although OGT cKO mice did not have decreased survival rates before 6 months, they exhibited excessive grooming by 5 months of age, which resulted in hair-loss, skin lesions and necessitated culling of the mice after 7 months.

Golgi stain was used to examine the morphology of hippocampal and cortical neurons. At 6 months, hippocampal neurons showed dramatic reductions in dendritic arborization, and pyramidal cortical neurons showed significant loss of dendrites (Figure 2.4). Reduction in brain volume was more accurately quantified by MRI and tensor-based morphometry, and demonstrated a 20% reduction in brain volume (Figure 2.5). Regions of decreased brain volume are denoted with red shading, whereas regions with increases are denoted with blue shading. Significant decreases in hippocampal and cortical volume are observed, as well as a reduction in the volume of thalamus/midbrain regions. Some decreases are also observed in the cerebellar region, but these changes are not seen in histological experiments.

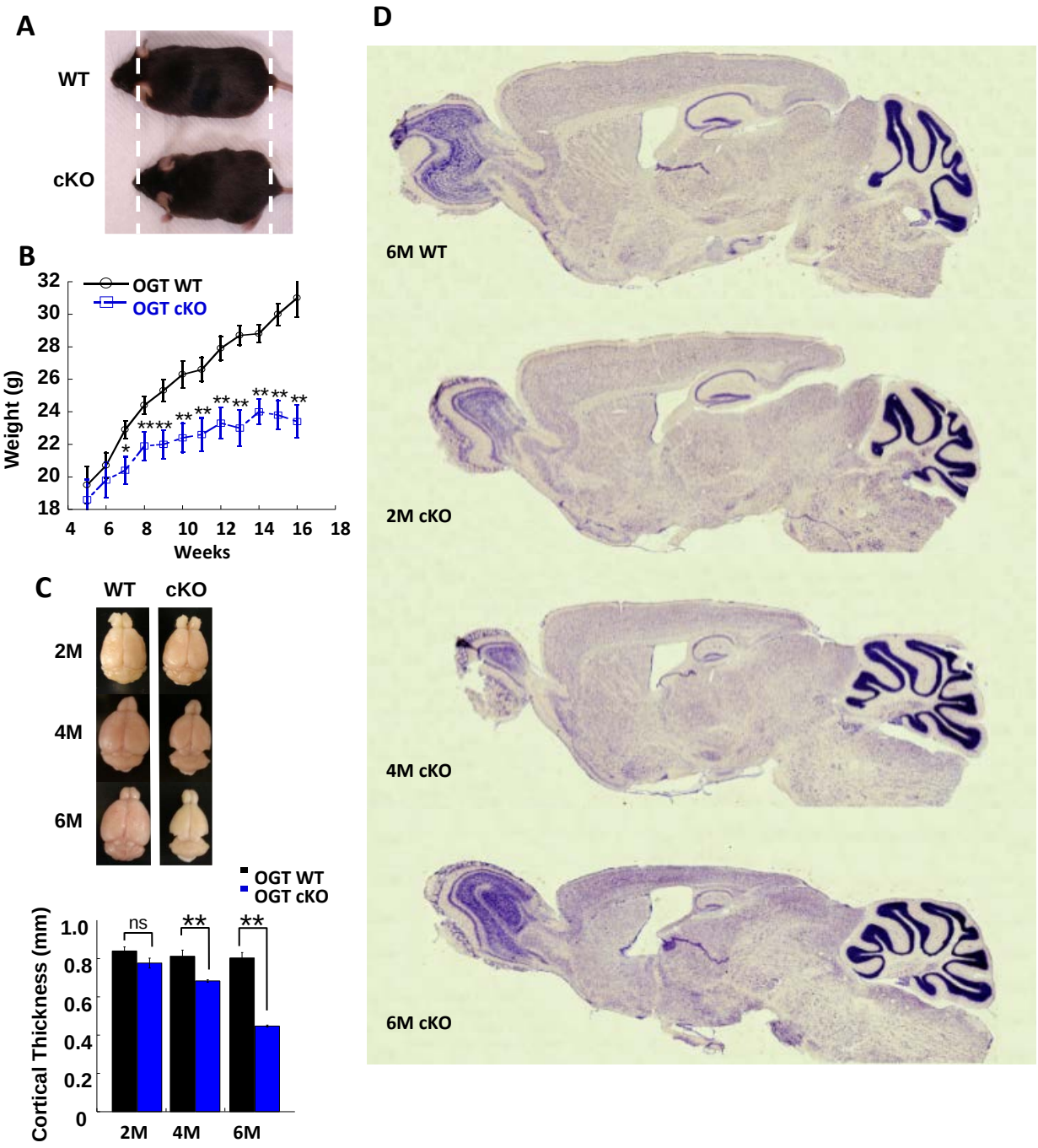

Figure 2.3: OGT cKO mice display reduced weight and brain size beginning at 2 months. (A) OGT cKO mice were significantly smaller by 6 months of age. (B) A decrease in weight is observed in OGT cKO mice beginning at 7 weeks. (C) Overall brain size and cortical thickness are reduced at 4 and 6 months in OGT cKO mice. (D) Nissl stain shows shrinking cortical and hippocampal structures in OGT cKO mice. *P<0.005, **-P<0.0005.

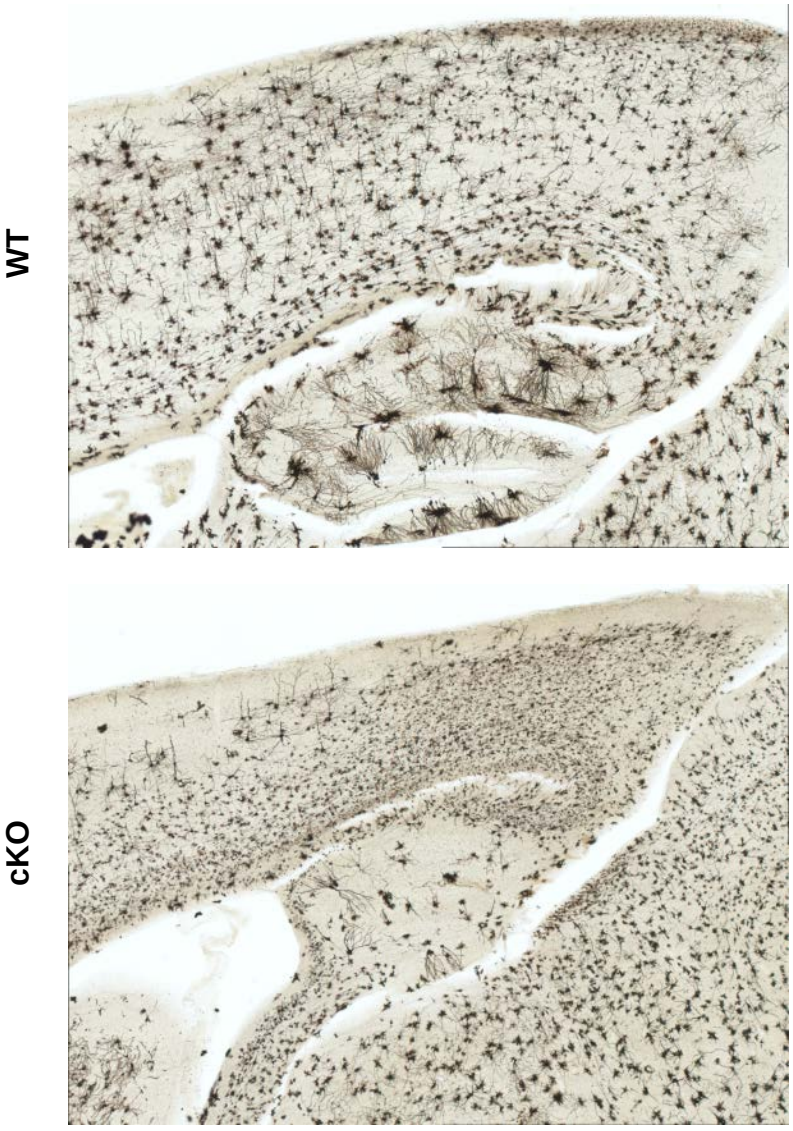

Figure 2.4: Golgi stain reveals dramatic degeneration of neuronal processes. Neurons in the hippocampus and cortex have fewer processes in 6 month old cKO mice. In addition, cortical and hippocampal structures are significantly reduced in size.

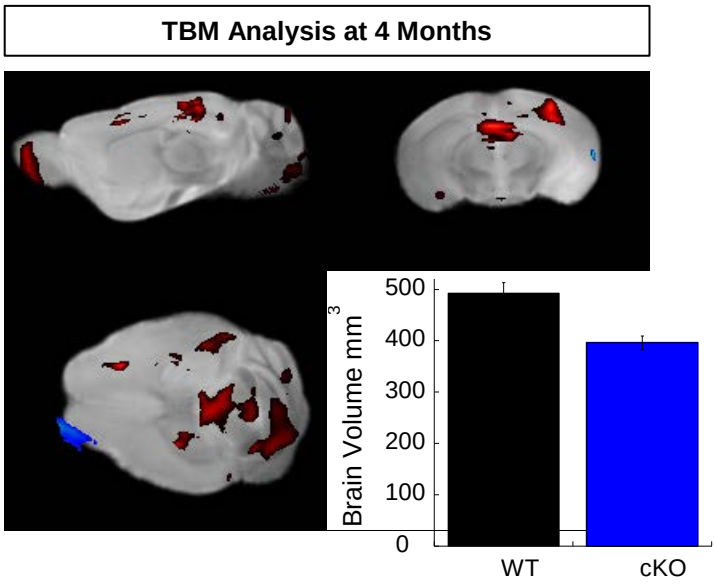

Figure 2.5: MRI analysis identifies reduction in cortical, hippocampal, and thalamic brain volume. Tensor-based morphometry analysis of MRI scans shows regions of cKO brains that are significantly reduced in size compared to wild-type controls (red). Regions affected include the cortex, hippocampus, and part of the thalamus.

Immunohistochemistry using a pan-specific anti-*O*-GlcNAc antibody (RL2) confirmed progressive loss of *O*-GlcNAcylation in the cortex and hippocampus (Figure 2.6A). Beginning at 1 month, 5-10% of CA1, dentate gyrus (DG), and cortical neurons lacked O-GlcNAc, and by 2-4 months, the loss of *O*-GlcNAc peaked in approximately 40% of the neurons (Figure 2.6B). By 6 months, fewer O-GlcNAc-depleted neurons remained. The pattern of *O*-GlcNAc loss was similar in the cortex, with knockout beginning at 2 months (Figure 2.7A, B). The specificity of the anti-*O*-GlcNAc antibody was confirmed by competition experiments using free GlcNAc sugar (Figure 2.8A). As an internal control, we measured OGT immunoreactivity in the cerebellum (which lacks αCaMKII expression) and detected levels comparable to those of WT mice (Figure 2.8B). Western analysis confirmed loss of O-GlcNAc modified proteins in the cortex, hippocampus, but not cerebellum (Figure 2.9A). Furthermore, OGT and OGA levels were both significantly reduced in the hippocampus of OGT cKO mice (Figure 2.9B, C).

OGT antibodies (DM17, AL25) were used to confirm the progressive loss of OGT in the cortex and hippocampus, and agree with the results obtained with RL2 immunohistochemistry (Figure 2.10). OGT protein levels are significantly reduced in the hippocampus at 1 month, consistent with the 5-12% reduction in RL2-positive neurons at 1 month (Figure 2.6B). This result suggests that loss of OGT begins around 1 month of age, while significant reduction in RL2-positive neurons is observed at 2 months. RL2 staining was much more robust than OGT

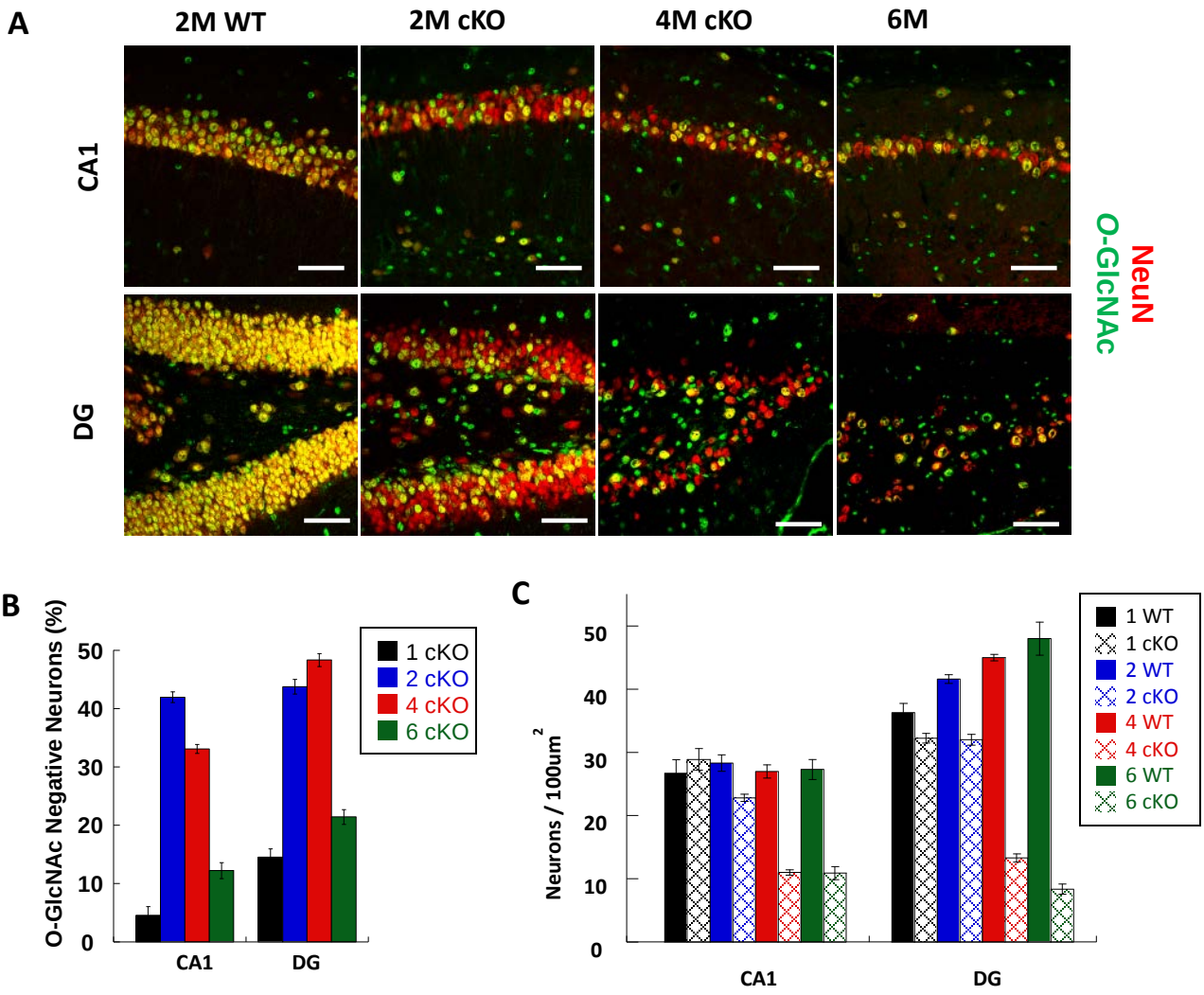

Figure 2.6: Characterization of OGT knockout, neuronal loss, and degeneration. (A) Knockout of OGT as well as neuronal loss occurs in the CA1, dentate gyrus, and cortex. (B) O-GlcNAc-negative (knockout) neurons in OGT cKO mice. (C) Quantification of neuronal loss in OGT cKO mice Scale bar = 50um.

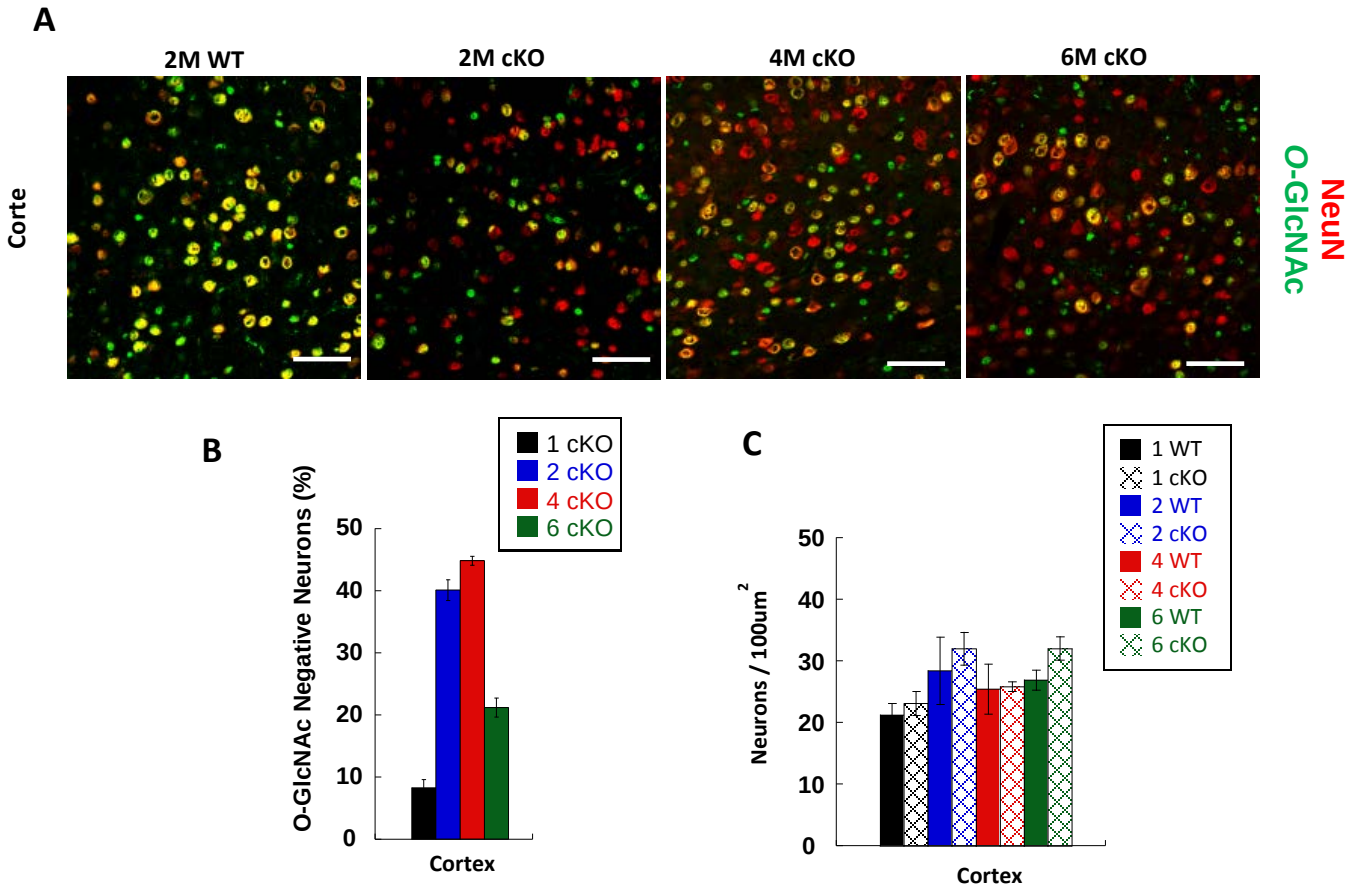

Figure 2.7: Characterization of OGT knockout, neuronal loss, and degeneration in the cortex. (A) Knockout of OGT as well as neuronal loss occurs in cortex. (B) O-GlcNAc-negative (knockout) neurons in OGT cKO mice. (C) Quantification of neuronal loss in OGT cKO mice. Scale bar = 50um.

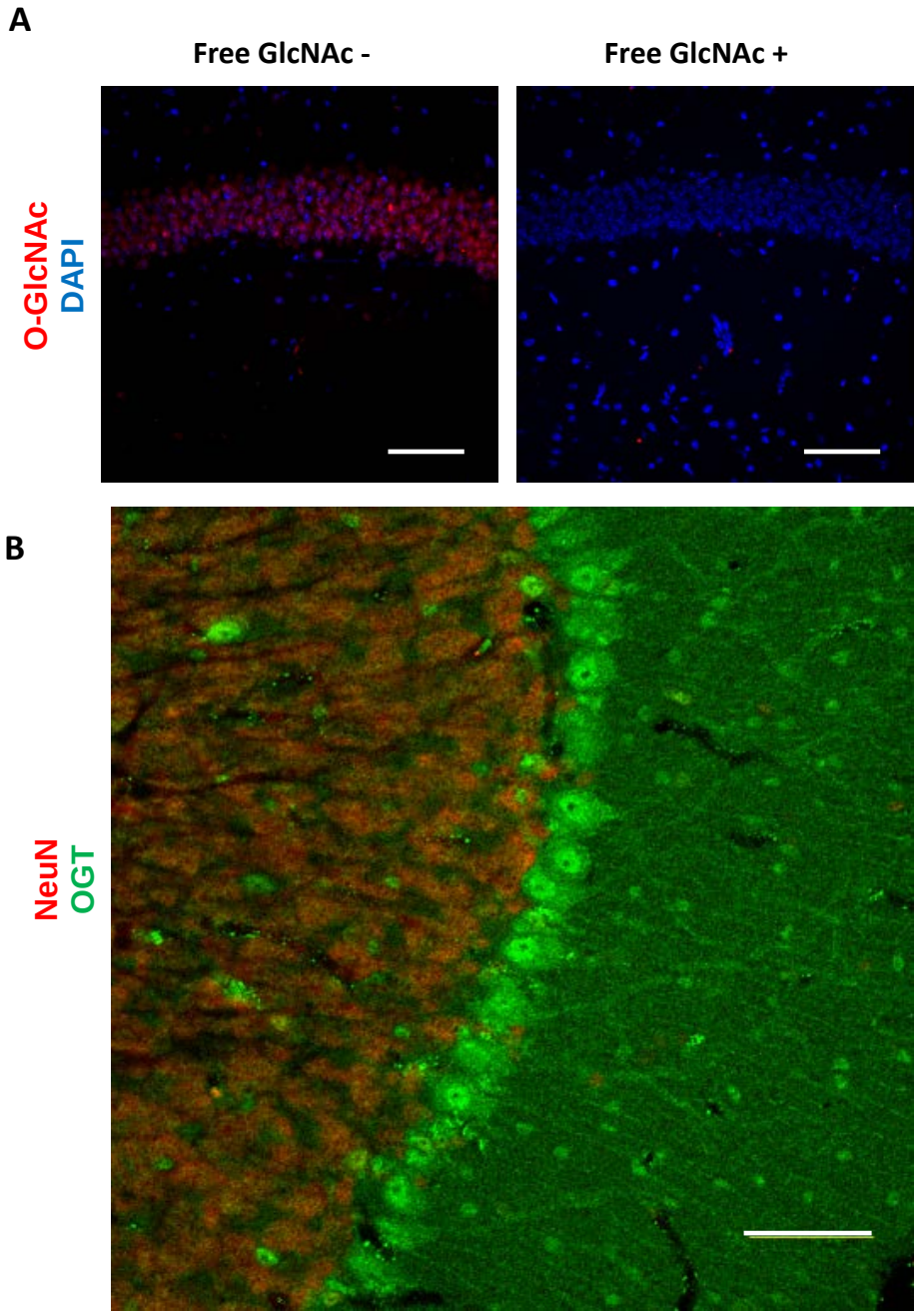

Figure 2.8: *O*-GlcNAc antibody is specific and OGT protein is present in the cerebellum. (A) *O*-GlcNAc antibody (RL2) signal is eliminated by competition with the addition of free GlcNAc sugar (1M) during incubation with primary antibody . (B) OGT (AL25) protein is present in purkinge neurons of the cerebellum (green) in 2 month OGT cKO mice, demonstrating forebrain-specific knockout of OGT. Neurons are stained with NeuN (red). Scale bar = 50um.

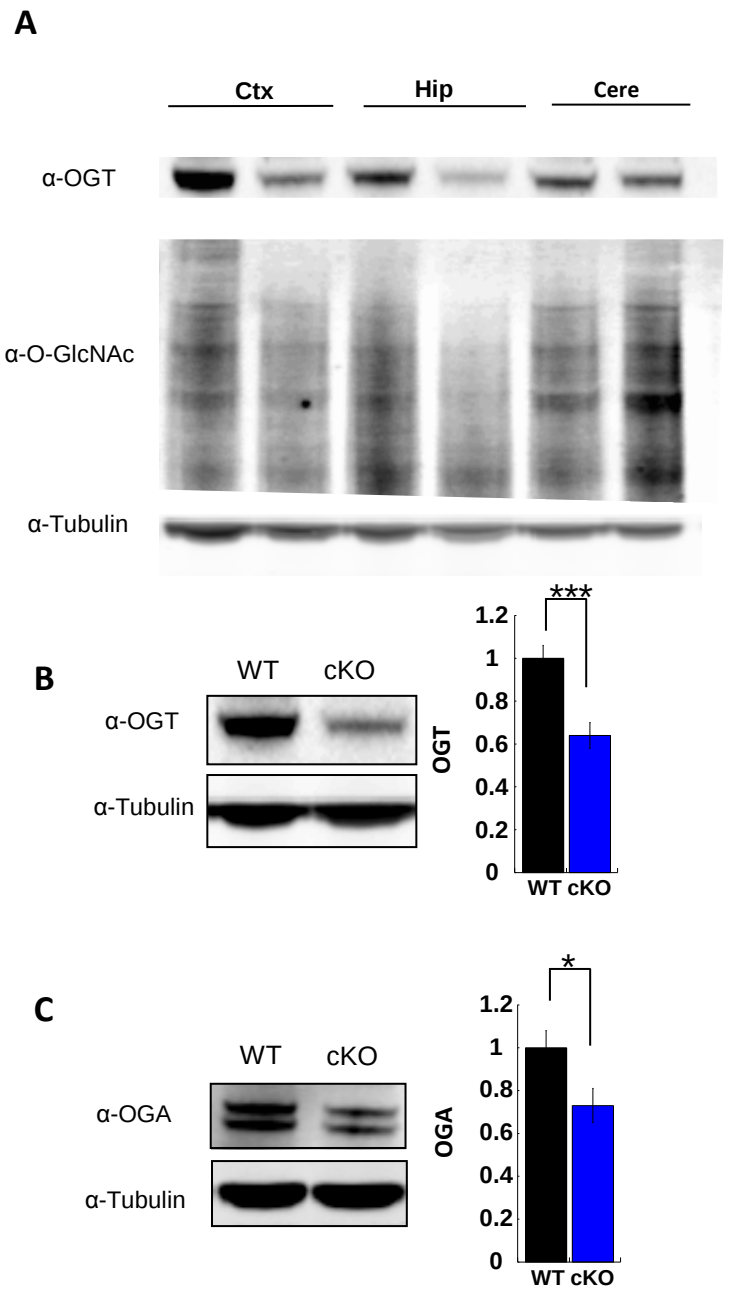

Figure 2.9: Conditional knockout of OGT in the forebrain. (A) *O*-GlcNAc-modified proteins (RL-2) are significantly decreased in OGT cKO mouse hippocampi and cortex but not cerebellum at 2 months. (B) OGT protein levels are significantly reduced in cKO mice at 2 months. (C) OGA protein levels are significantly reduced by 2 months. *-P<0.05, ***-P<0.0005.

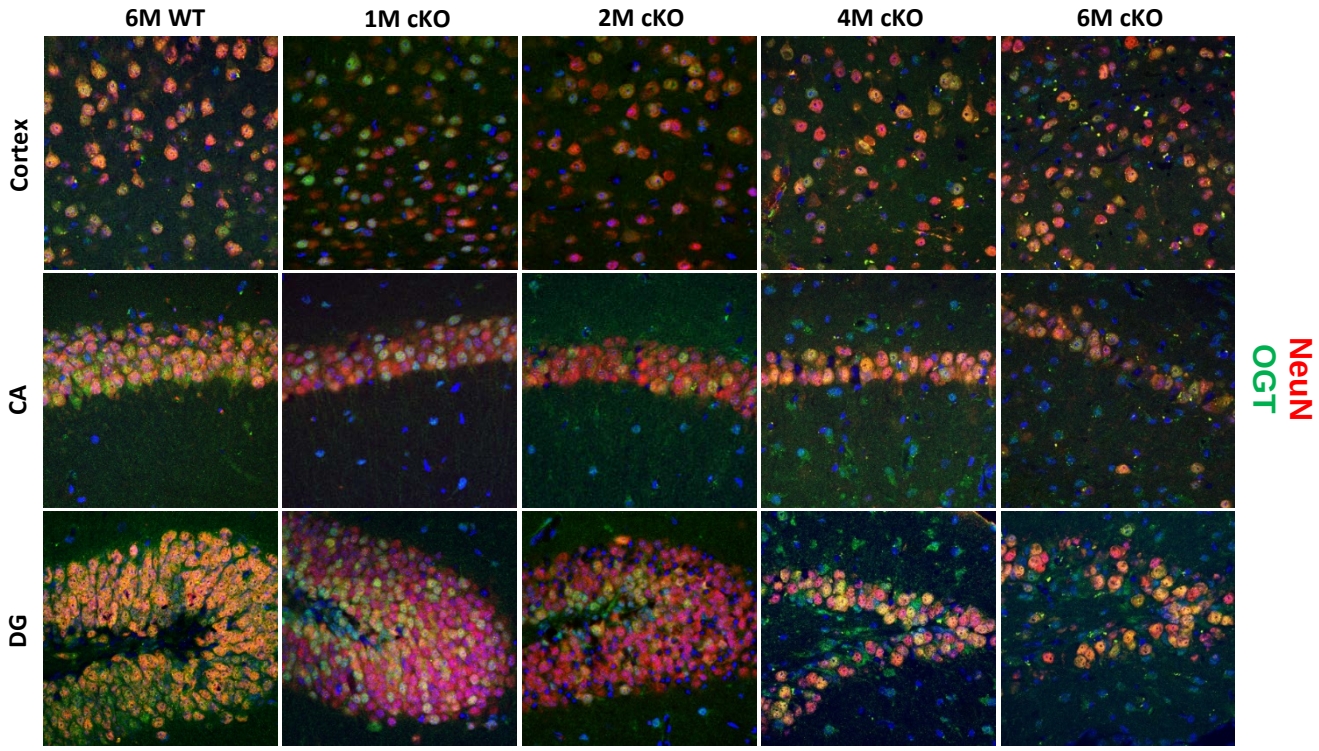

Figure 2.10 : Loss of OGT Begins at 1 Month and Continues to 6 Months. OGT antibody (AL-25, green) was used to stain for OGT in the cortex, CA1, and dentage gyrus of OGT cKO mice. NeuN (red) was used to stain neuronal nuclei, and DAPI (blue) was used to stain DNA. Loss of OGT signal begins at 1 month but by 4 months most OGT-null neurons are absent. Progressive loss of neurons is also apparent at 4 and 6 months.

staining, and thus RL2 immunohistochemistry was used to quantify the time course of OGT knockout.

OGT cKO mice displayed a profound and progressive loss of neurons by 2 months. Quantification of CA1 neurons by NeuN staining revealed a 19.4% reduction in neuronal number at 2 months (Figure 2.6C) and a 23.1% reduction in the dentate gyrus. At 4 months, there was a 52.6% reduction in neuronal number, and at 6 months, the value progressed to 60.0%. A similar trend in neuronal loss was observed in the DG region of the hippocampus (23.1%, 70.7% and 82.6%, at 2, 4, and 6 months, respectively; Figure 2.6C). The cortex showed no appreciable change in neuronal density (Figure 2.7C), however the significant reduction in cortical thickness illustrates the overall loss of cortical neurons (Figure 2.3C).

Neuronal loss was also quantified by Nissl and TUNEL staining. At 2 months, Nissl stained slices showed a significant amount of condensed pyknotic nuclei, which are indicative of cells undergoing apoptosis (Figure 2.11A). Furthermore, 56.6% (16.7 neurons / 100 μm^2) of DG neurons were positive for TUNEL labeling (Figure 2.11B), confirming extensive apoptosis in the hippocampus of OGT cKO mice. To identify degenerating neurons, we used Fluorojade-C (FJC), which revealed that 33.2% (19.4 neurons /100 μm^2) of DG neurons were FJC-positive (Figure 2.11C). Interestingly, while most FJC-positive neurons lacked *O*-GlcNAcylation, some neurons were positive for both FJC and O-GlcNAc (Figure 2.11C, arrowheads). This suggests that loss of OGT can lead

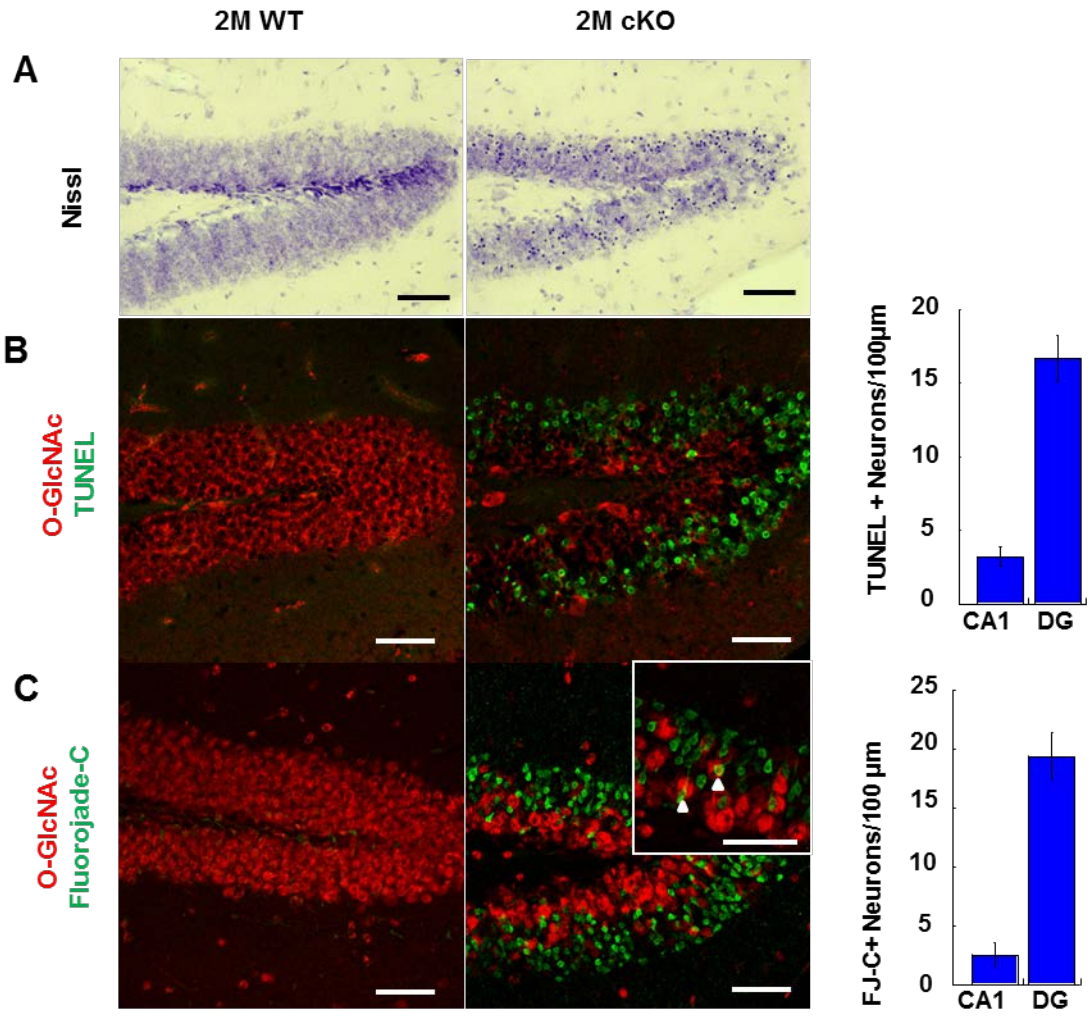

Figure 2.11: Characterization of neuronal death and degeneration in OGT cKO mice. (A) Nissl stain, showing cellular morphology and appearance of condensed neuclei characteristic of apoptosis. (B) Co-stain for O-GlcNAc (red) and TUNEL (green) identify apoptotic neurons. (C) Co-stain for O-GlcNAc (red) and FJC (green) identify degenerating neurons. O-GlcNAc postive, FJC positive neurons (C, arrowheads). Scale bar = 50um

to degeneration of neighboring OGT-positive neurons. In contrast, no TUNEL or FJC labeling of DG neurons from WT mice was observed.

2.2.3 Changes in anxiety and deficits in fear conditioning accompany OGT cKO

To assess the functional consequences of conditional OGT knockout, we evaluated OGT cKO mice in a series of behavioral tasks. Initially, we observed that OGT cKO mice exhibit deficits in nest making abilities, as well as an excessive grooming phenotype at 4 months, both of which have been observed in neurodegenerative mouse models of OCD and schizophrenia (33, 34). To assess basic motor ability, we used a rotarod exercise and determined that OGT cKO mice retain normal motor function, at both 2 and 4 months compared to wild-type littermates (Figure 2.12A). Subsequently, an open field test was used to determine basal anxiety levels. OGT cKO mice demonstrated significant increases in anxiety, with a 27.8 and 95.3% decrease at 2 and 4 months, respectively, in the duration spent exploring the exposed quadrant of an open field (Figure 2.12B). Additionally OGT cKO mice exhibited a 45.4% decrease in total distance traveled during the open field task (Figure 2.12B), suggesting an increase in basal anxiety through reduced exploration of an exposed environment.

We used a fear conditioning task to evaluate changes in the ability of OGT cKO mice to learn new associations. OGT cKO mice displayed a small but significant 10.9% deficit in cued-auditory (amygdala dependent) freezing at 2 months, but no change in contextual (hippocampus dependent) freezing (Figure

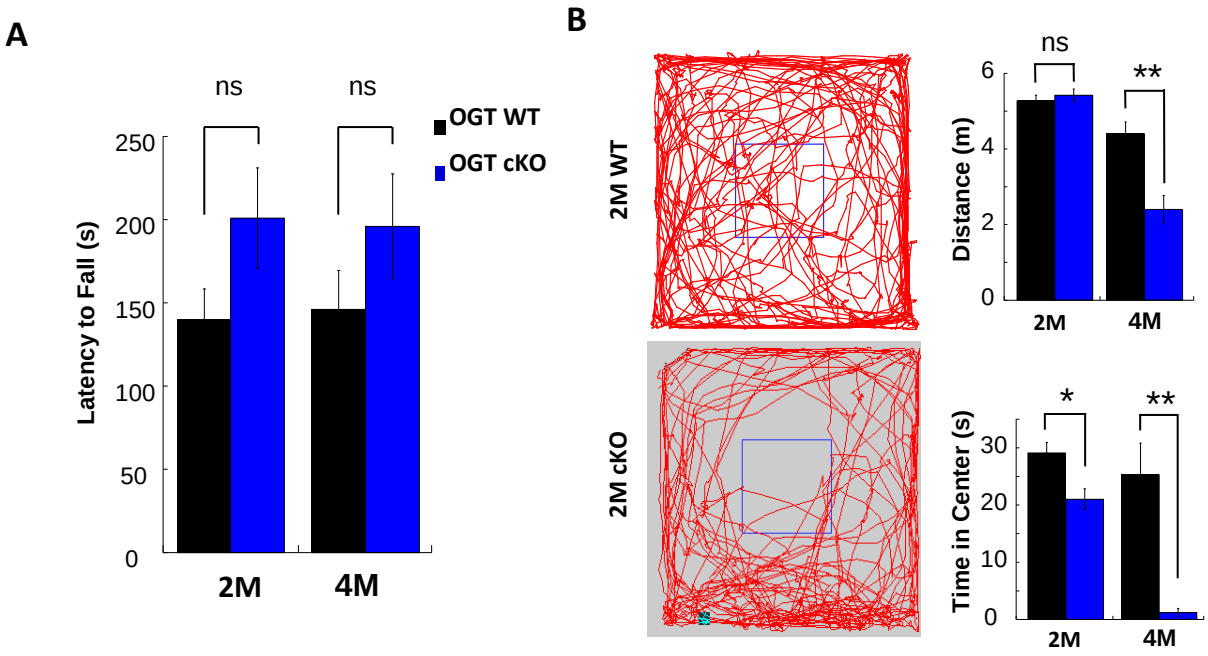

Figure 2.12: OGT cKO mice have normal locomotor function but show increases in anxiety. (A) Mice were subjected to a rotarod test, and cKO mice show no deficits in locomotion. (B) OGT cKO mice show increased anxiety in an open field test with significant reductions in time spent in the middle (exposed) quadrant of the box as well as in total distance traveled, as illustrated by a representative trace of movement. *-*P*<0.05, **-*P*<0.005. n= 12 for each genotype.

2.13). By 4 months, however, significant deficits in both cued (31.1%) and contextual (24.4%) fear-related freezing were observed. These results are consistent with the observed neurodegeneration by histology, and demonstrate significant progression of memory impairments in OGT cKO mice.

2.2.4 Deficits in additional memory tests suggest short-term memory impairments

The Y-maze was used to assess short-term memory, as mice with good short-term memory are able to recall which arm of the maze they were previously exploring, and will alternate their arm entries. OGT cKO mice showed no significant changes in alternation of arm entries compared to wild-type mice (Figure 2.14). Furthermore, they explored the maze with a similar number of arm entries when compared to wild-type mice, which eliminates complicating factors such as a reduced activity or increased anxiety.

A place preference test was the performed to assess whether the mice are able to recall the context or location of a particular object. Mice were allowed to explore an environment containing two objects, and then removed from the environment. While absent, one of the objects was relocated. Mice were then replaced in the environment, and exploration of each object was quantified. If the mice recalled the context of the objects, they would generally identify that one object had been moved, and would have a preference for exploring that relocated object. OGT cKO mice showed a small decrease in place preference, but because the preference of wild type mice was quite low, this experiment was not pursued further (Figure 2.15). Thus it is possible that OGT cKO mice have

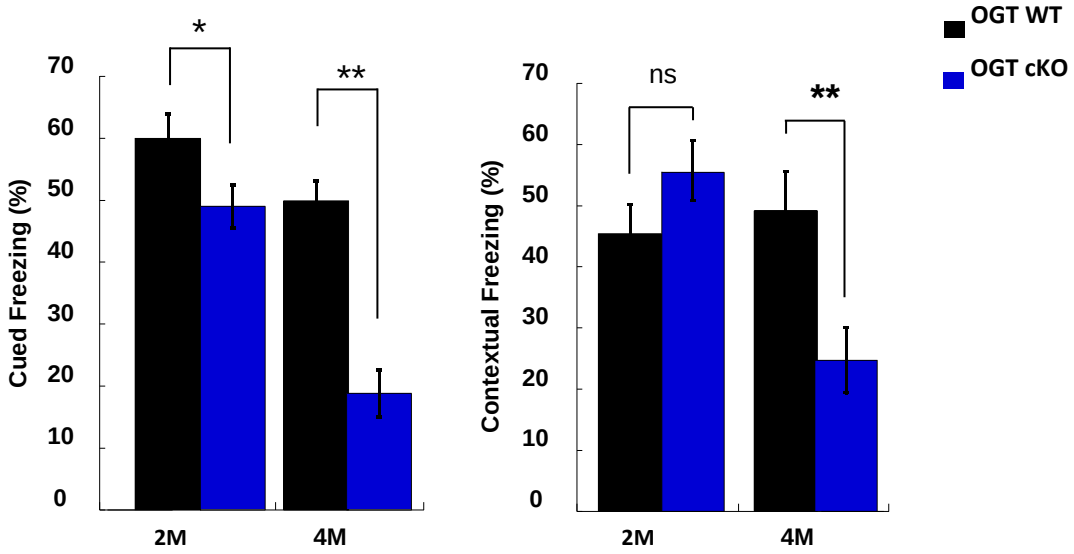

Figure 2.13: Behavioral changes in OGT cKO mice include impaired fear-related related learning. Significant deficits in cued (amygdala-dependent) fear conditioning is observed at 2 months in OGT cKO mice, and deficits in both cued (amygdala-dependent) and contextual (hippocampus-dependent) are observed by 4 months of age (C). *-*P*<0.05, **-*P*<0.005. n=12 for each genotype.

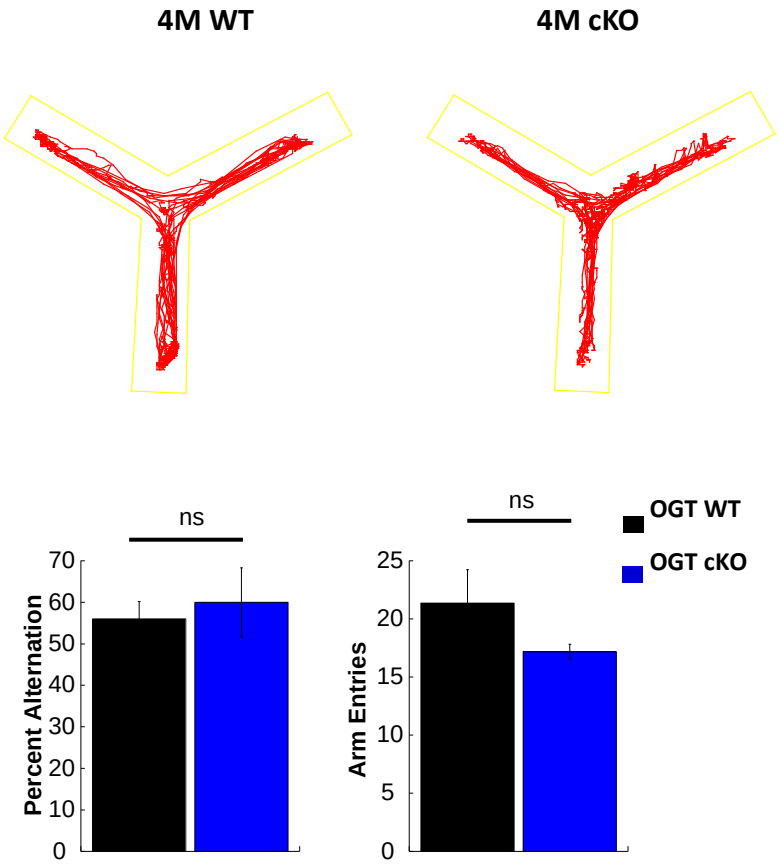

Figure 2.14: Y-maze shows no significant change in short term memory of OGT cKO mice. Total arm entries were counted to evaluate changes in exploratory activity and no changes were observed. Entries into each arm of the Y-maze were noted and used to evaluate short-term memory, by quantifying the percentage of alternating arm entries. Deficits in short-term memory would present as decreased alternation, as animals would not recall the arm they immediately vacated, and would have no preference for entering a less recently explored arm. N=8 for each genotype. 4 month time point.

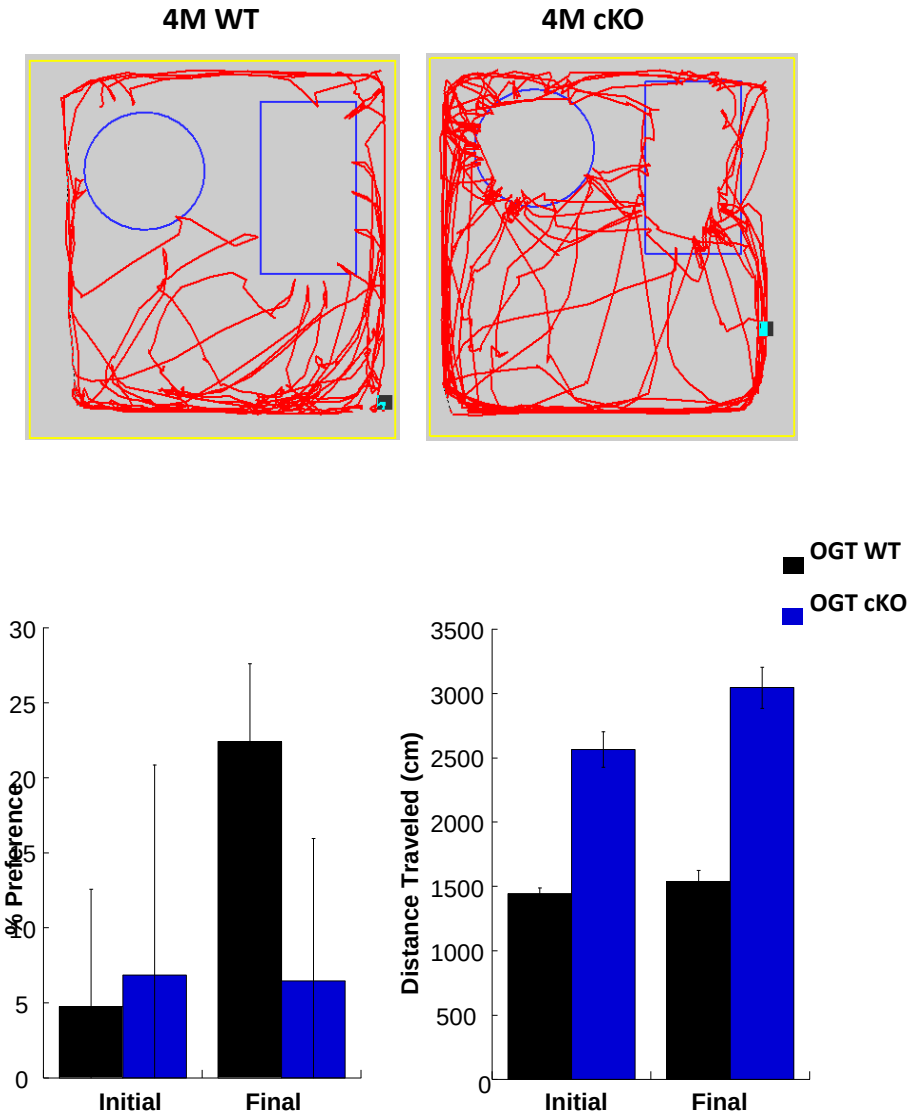

Figure 2.15: Place preference study suggests a deficit in short-term memory and identifies a possible hyperactive phenotype. Preference for exploring an object that was moved between an initial and final exploration period was assessed. Animals that recall the original location of the moved object would preferentially explore the moved object. OGT WT mice seemed to have a preference for exploring the moved object, and OGT cKO mice appeared to have no preference, but more replicates are needed as the changes are not significant. Furthermore, total distance traveled while exploring the objects was quantified, and demonstrates increased activity of OGT cKO mice as they explore the objects. This increased exploration is interesting to consider in light of the increased anxiety observed in the open field test, and may suggest a hyperactive phenotype. N=4 for each genotype, 2 month time point.

impaired short-term memory, but more replicates are required to draw meaningful conclusions. Interestingly, OGT cKO mice displayed a significant increase in total distance traveled while exploring the environment, compared to wild-type mice. This was in stark contrast to the open field test, where OGT cKO mice were shown to have increased anxiety and lower overall distance traveled. OGT cKO mice not only traveled longer distances to explore each object more thoroughly, they routinely made contact with the objects and were much less inhibited in their exploration of the object compared to wild-type mice (Figure 2.15).

2.2.5 Microarray analysis of OGT cKO mRNA suggests changes in immune and cell cycle related genes

OGT modifies and regulates many different intracellular substrates including many different transcription factors. We sought to better understand the specific transcriptional changes in OGT cKO mice using microarray technology. Messenger RNA from the hippocampi of 3-week and 2-month old cKO mice and their wild-type littermates were isolated and run on microarray chips. At 3 weeks of age, there were only 10 differentially-expressed genes in the hippocampi when comparing OGT cKO mice to wild-type mice (Table 2.1). In contrast, at two months, there were over 900 differentially-expressed genes in cKO hippocampus compared to their wild-type littermates (Table 2.2). Immune response genes expressed by microglia and astrocytes were among the most highly upregulated genes (Table 2.2). Markers such as GFAP and C1q were significantly upregulated and confirmed by qRT-PCR. Furthermore, many of these genes

	log2 (Ratio)	Ratio	P-value (Differentially expressed)	P-value (Bonferroni)	Annotation			
ID	cKO/WT	cKO/WT	cKO/WT	cKO/WT	Gene_symbol	Description	Group	Entrez
mMC024723	0.844064	1.7951	5.24E-24	0.	Pfkfb3	6-phosphofructo-2-kinase/fructose-2,6-biphosphatase 3	1	170768
PH_mM_0007183	0.703678	1.628652	6.89E-16	0.	Prrt1	proline-rich transmembrane protein 1	1	260297
PH_mM_0001626	-0.689742	0.619965	2.20E-13	0.	Cdh6	cadherin 6	1	12563
PH_mM_0011619	1.173475	2.255543	7.48E-13	0.	NA	NA	5	NA
PH_mM_0013209	0.66419	1.584678	3.97E-12	0.	Pabpc6	poly(A) binding protein, cytoplasmic 6	1	67543
mMC013038	0.637743	1.555893	1.87E-11	0.	Lgals3bp	lectin, galactoside-binding, soluble, 3 binding protein	1	19039
PH_mM_0009722	0.580355	1.495217	7.09E-10	0.000019	Abhd11	abhydrolase domain containing 11	1	68758
PH_mM_0008432	1.600014	3.031462	9.97E-10	0.000026	Slx4	SLX4 structure-specific endonuclease subunit homolog (S. cerevisiae)	1	52864
mMC018137	0.399368	1.31893	9.94E-09	0.000263	C1qc	complement component 1, q subcomponent, C chain	1	12262
mMC010198	0.42828	1.345628	2.17E-08	0.000573	1810062O18Rik	RIKEN cDNA 1810062O18 gene	1	75602
PH_mM_0010274	-0.483226	0.715376	2.17E-08	0.000574	4930597O21Rik	RIKEN cDNA 4930597O21 gene	1	75373

Table 2.1: Differentially Expressed Genes in OGT cKO Mice at 3 weeks. Few genes are differentially expressed at 3 weeks of age, when conditional knockout of OGT is just beginning. Elizabeth Jensen

		OGT cKO/WT Microarray		qRT-PCR		Mouse Model Microarray Studies[1]			qRT-PCR[2]	
Genes	**Description**	**Fold change**	**p values**	**Fold Change**	**p values**	**A**	**B**	**C**	**B**	**SEM**
Gfap	glial fibrillary acidic protein	6.05	1.00E-37	11.747	4.58E-02	1.3	6.3	7.3	4.83	0.64
C1qb	complement component 1 q subcomponent beta polypeptide	4.03	1.00E-37	6.752	4.58E-02	1.6	2.5	2.8	2	0.16
Tyrobp	TYRO protein tyrosine kinase binding protein	3.97	1.00E-37	6.089	4.58E-02	2	3.6	4.8	2.54	0.06
Cd14	CD14 antigen	3.94	1.00E-37	5.438	4.58E-02	1.4	1.8	2.3	-	-
C1qc	complement component 1, q subcomponent, C chain	3.50	1.00E-37	6.151	4.58E-02	2	3.6	4.8	-	-
Gusb	glucuronidase beta	2.67	1.00E-37	3.59	4.58E-02	1.4	2.3	2.4	-	-
Ctsd	cathepsin D	2.28	5.34E-14	3.747	0.1107	1.4	1.8	2.1	2.53	0.32
B2m	beta-2 microglobulin	2.14	1.80E-29	4.422	4.58E-02	-	-	-	2.03	0.09
C3	complement component 3	2.07	2.57E-21	8.105	4.58E-02	-	-	-	-	-
Vim	vimentin	1.91	5.25E-04	3.104	4.58E-02	-	-	-	1.81	0.14
Man2b1	mannosidase 2, alpha B1	1.67	6.39E-34	2.316	4.58E-02	1.3	1.9	2.1	1.62	0.07

[1] Fold expression changes of regulated genes in 18-month old $APP^{NLh/NLh}$/$PS\text{-}1^{P264L/P264L}$ mice (A); 12-month old Tg2576/$PS\text{-}1^{P264L/+}$ mice(B); and 12-month old Tg2576/$PS\text{-}1^{P264L/P264L}$ mice (C) (Wu, et al. *Neurobiology of Aging*. 27 (2006) 377-386)

[2] Fold expression changes of regulated genes in the 17-18-month old Tg2576/$PS\text{-}1^{P264L/P264L}$ mouse (Dickey, et al. *The Journal of Neuroscience*. 23 (12) 2003. 5219-5226)

Table 2.2: Differentially Expressed Genes in OGT cKO Mice at 8 weeks. Immune response related genes are upregulated in our flOGT cKO mouse as well as in several mouse models of AD. In all of these mouse models of AD, the mice express a familial Alzheimer's disease mutant amyloid precursor protein as well as a familial Alzheimer's disease mutant presenilin-1. The upregulation of immune response genes is observed at 2 months while the other mouse models observe upregulation at 12 or 18 months of age. The p-values are Bonferroni corrected p-values. Elizabeth Jensen

were found to also be upregulated in other established models of AD (Table 2.2). Interestingly, these transcriptional changes are observed at 2 months of age, while similar immune response gene upregulation is observed in other mouse models at 12 or 18 months of age (35-37).

In order to determine other networks of genes that were deregulated in the OGT cKO, a weighted gene co-expression network analysis (WGCNA) was performed on the microarray data (38, 39). Our WGCNA identified two gene modules (green and magenta), which were significantly correlated with Cre expression and OGT knock-out (Figure 2.16). Using DAVID and gene ontology analysis, the green module was shown to be enriched with genes involved with immune response ($p < 3.4 \times 10^{-4}$) (40). VisANT was used to visualize the green module network (41-43).

Interestingly, the magenta module was enriched for genes involved with cell cycle arrest ($p < 3.75 \times 10^{-5}$) (Figure 2.16). The WGCNA data implicates cell cycle deregulation as an important mechanism that underlies the physiological and behavioral changes observed in the OGT cKO mice.

To explore this further, we probed our model for changes in CDK5, a key regulator of neuronal cell cycle. CDK5 protein levels were decreased by 26% in 2 month old cKO mice by western blot, and IHC staining showed a significant decrease in CDK5 levels in *O*-GlcNAc null neurons in the hippocampus (Figure 2.17A, B). Interestingly, CDK5 was also found to be *O*-GlcNAc modified in mouse brain after chemoenzymatic labeling (Figure 2.17C). CDK5 has many functions in addition to suppressing cell cycle progression, including phosphorylation of tau

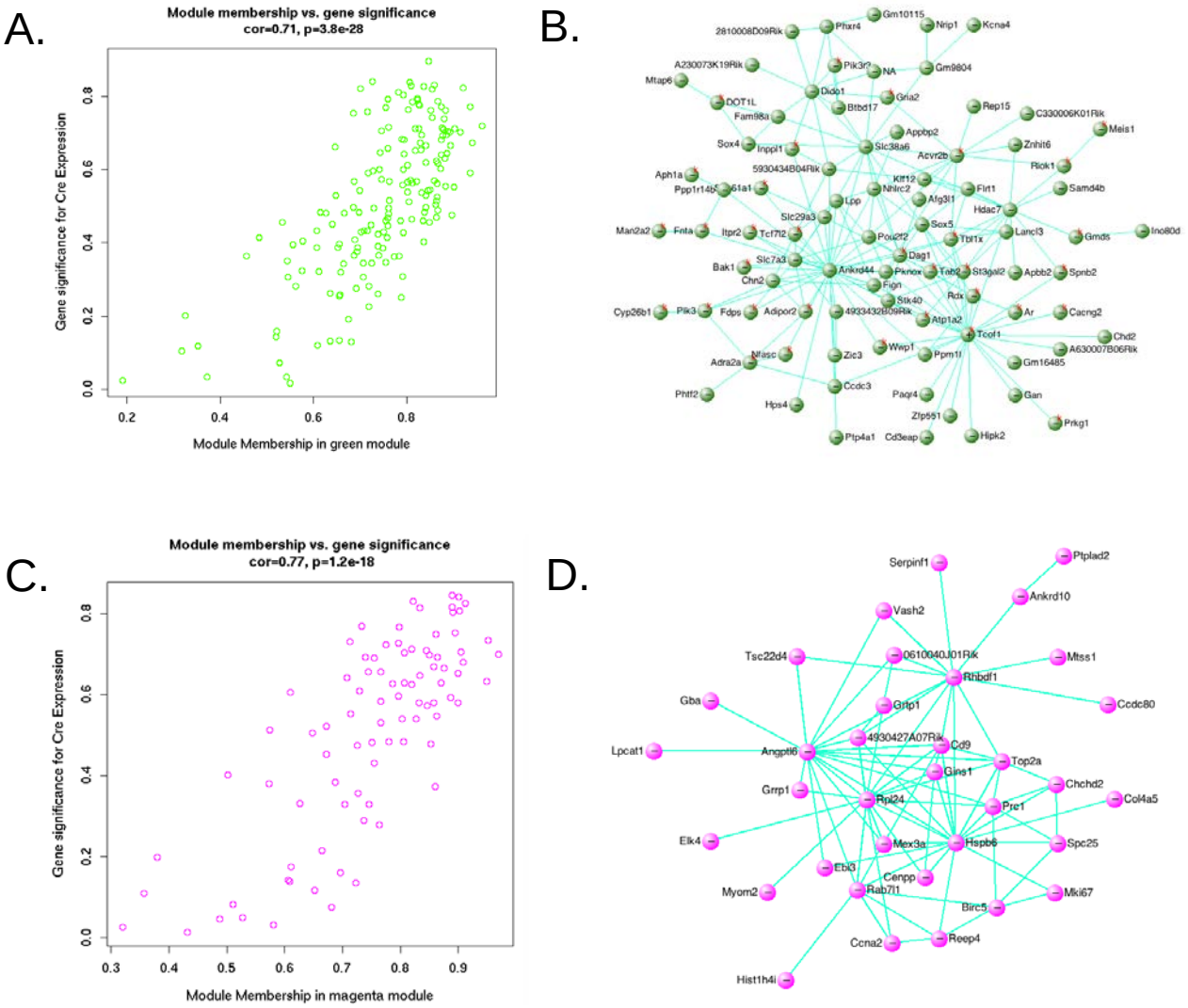

Figure 2.16: WGCNA Results indicate increases in immune and cell cycle arrest genes. A. Cre expression and OGT knock-out is significantly and highly correlated with the green module membership (cor = 0.71, p = 3.8 x 10^{-28}). B. Displayed is the Visant green module network (cutoff > 0.1). Gene ontology analysis reveals that these genes are overwhelmingly related to immune response (enrichment p < 3.75 x 10^{-5}). C. Cre expression is highly correlated with the magenta module (cor = 0.77, p = 1.2 x 10^{-18}). D. Shown here is the Visant green module network (cutoff > 0.1). Gene ontology analysis reveals that these genes are overwhelmingly related to immune response (enrichment p < 3.4 x 10^{-4}).

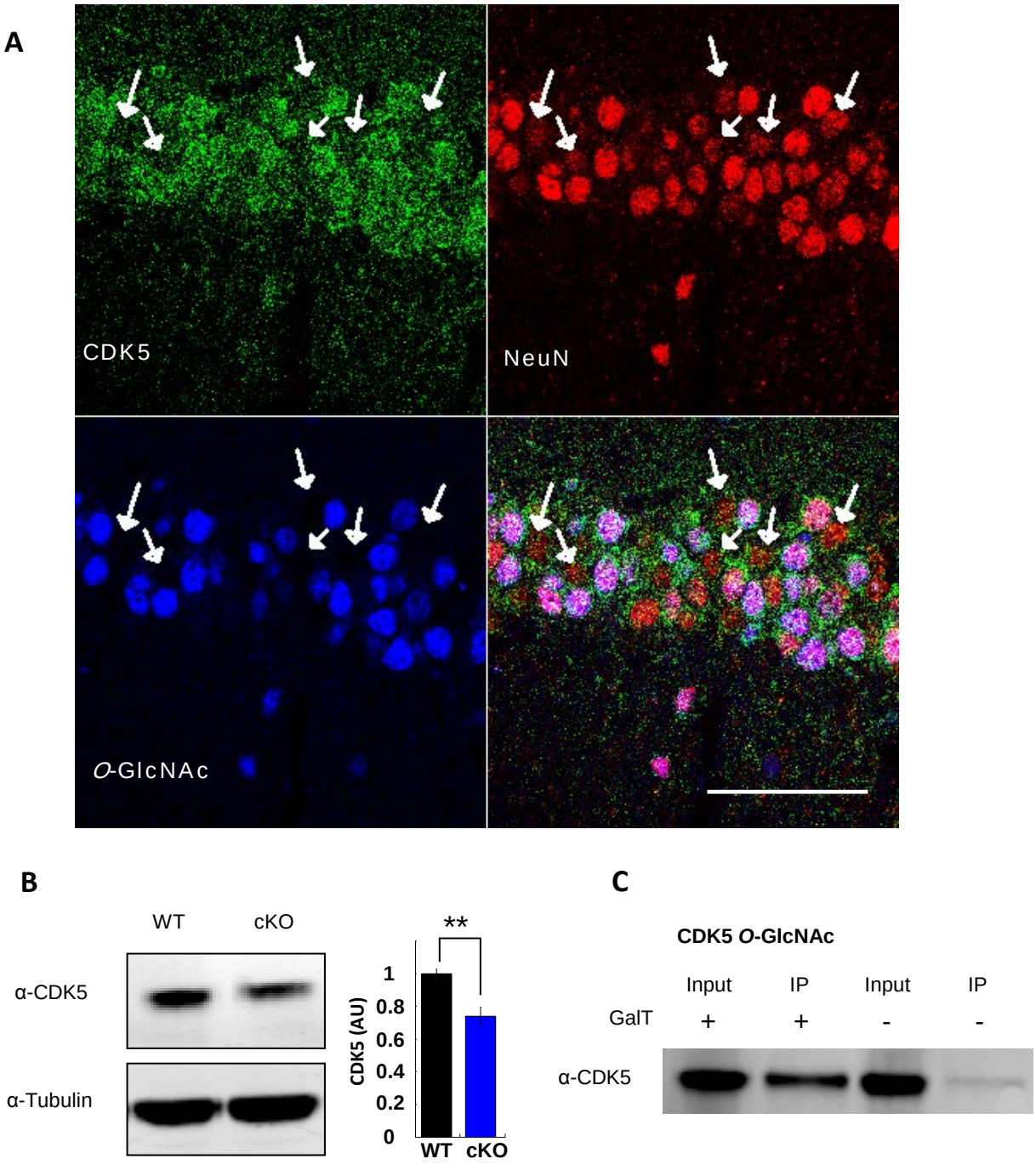

Figure 2.17: CDK5 is decreased in O-GlcNAc negative neurons and is *O*-GlcNAc glycosylated. (A) Immunohistochemistry shows O-GlcNAc negative neurons have decreased CDK5 staining (A, arrowheads) in the hippocampus at 2 months. OGT cKO mice show a 26% decrease in global CDK5 levels by western blot. (C) CDK5 is O-GlcNAc modified in mouse brains after chemoenzymatic labeling with biotin and streptavidin pull down (C). Scale bar = 50um.

and regulating MEK1 signaling. Thus it is possible that the reduction in CDK5 levels in OGT cKO mice could contribute to our observed neurodegeneration.

2.2.6 OGT cKO recapitulates AD phenotypes including neuroinflammation, phosphorylated tau, and increases in amyloid β peptide

As *O*-GlcNAc modifications have been shown to affect several AD-related proteins, including tau and APP, we explored whether our mouse displayed changes in these hallmarks of neurodegeneration. We began by evaluating changes in microglia and astrocytes, as both play an important role in supporting neuronal health. Beginning at 2 months, a 6.48-fold increase in astrocyte and 14.9-fold increase in microglia markers was observed in the hippocampus of OGT cKO mice (Figure 2.18). This striking gliosis spreads to the cortex by 6 months and persisted throughout the life of the animal.

O-GlcNAc modification of tau was shown to reduce tau aggregation and phosphorylation in other AD mouse models (44). Using immunohistochemistry, we evaluated several epitopes of phosphorylated tau that have been shown to be characteristic of paired-helical filamentous (PHF) tau oligomers, which aggregate to form neurofibrillary tangles (NFTs) in AD (45, 46). We observed an increase in phosphorylation of tau at T205 (1.8 fold), S396 (2.9 fold), and T231 (1.4 fold) beginning at 2 months in the mossy fibers and cell bodies of neurons in the dentate gyrus in a pattern similar to NFTs (Figure 2.19, arrowheads). These results were confirmed by western blot analysis, using additional tau antibodies AT8 (T202/T205, 1.4 fold) and AT180 (T231, 1.4 fold) (Figure 2.20). A 3D

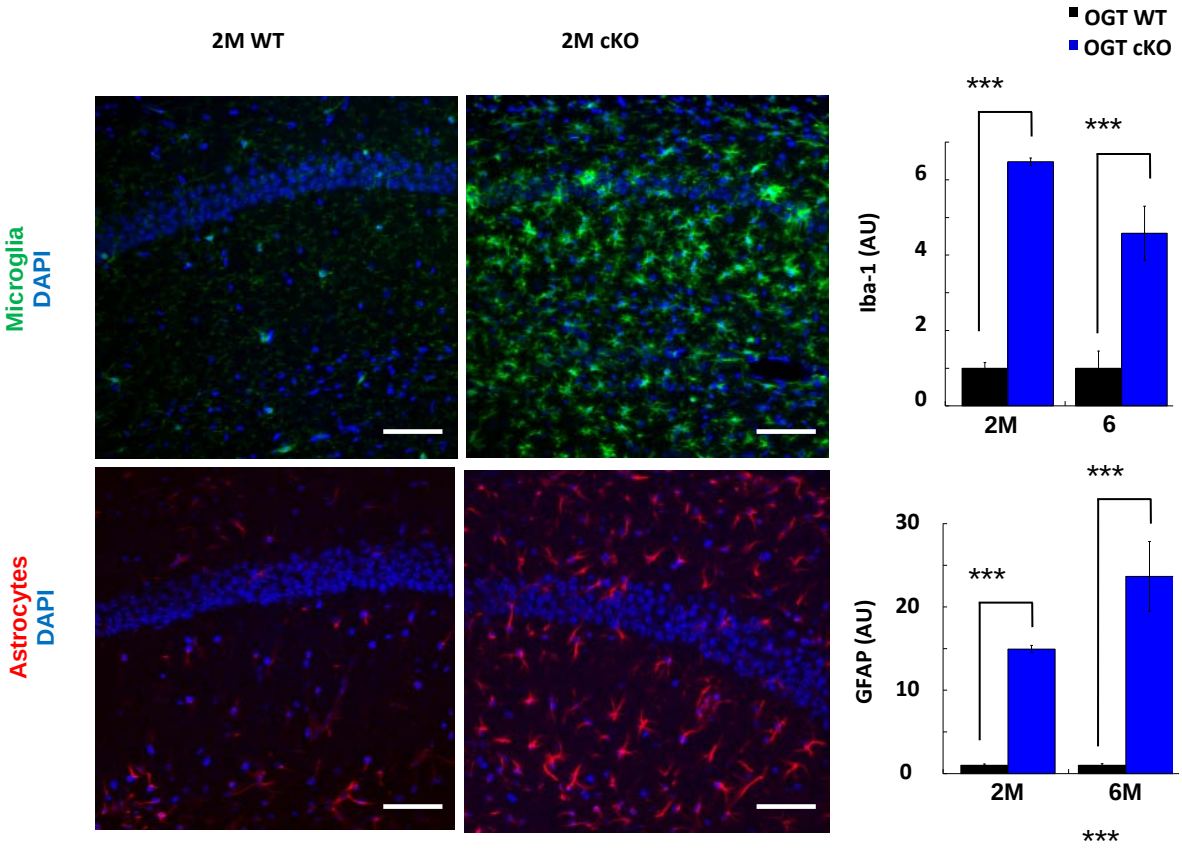

Figure 2.18: OGT cKO mice exhibit Gliosis. Microglia and astrocyte proliferation in CA1 region of the hippocampus ***-*P*<0.0005. Scale bar = 50um.

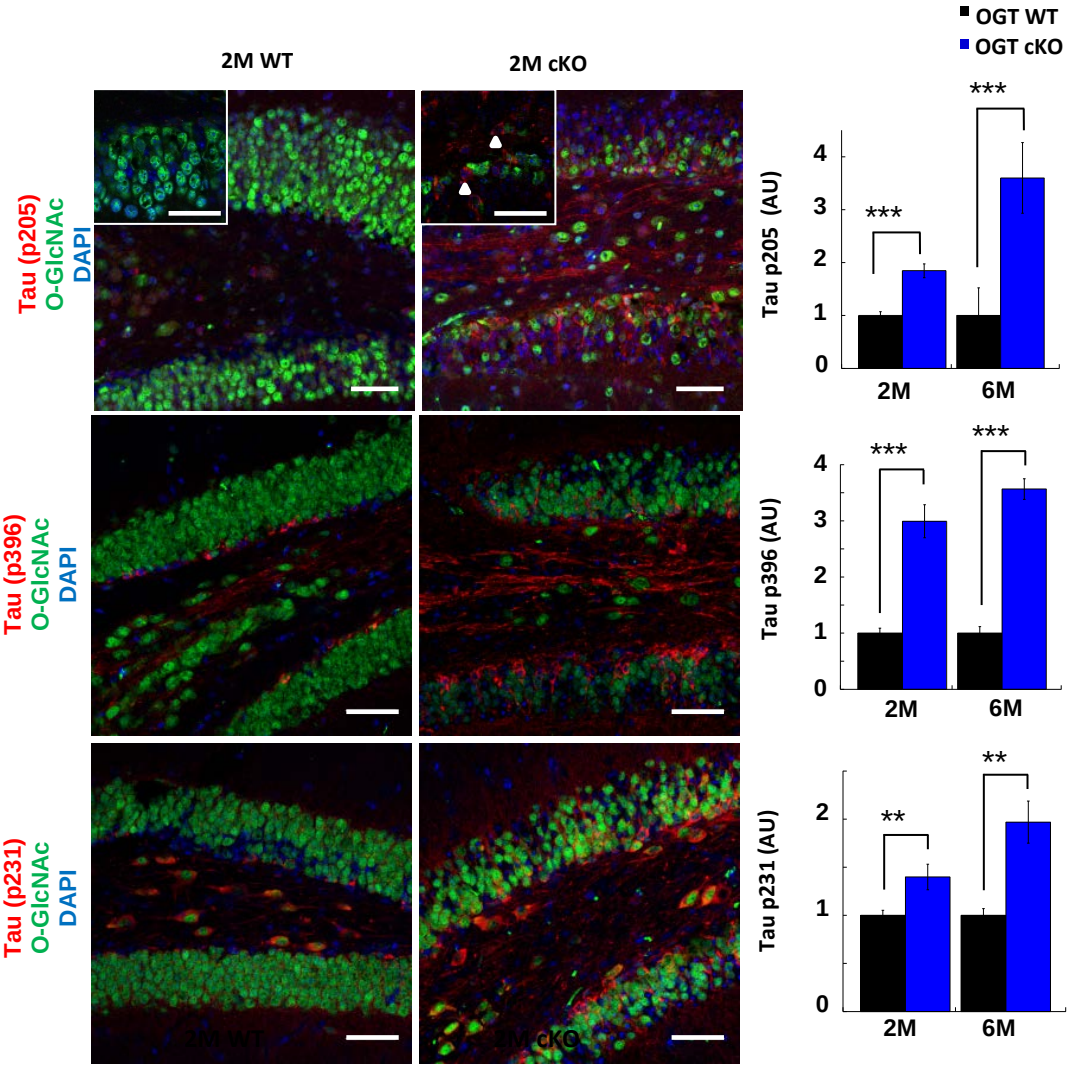

Figure 2.19: OGT cKO mice accumulate hyperphosphorylated tau. Increases in several pathological phosphorylation sites on tau and can be seen accumulating in both soma and axons of dentate gyrus neuron by immunohistochemistry (A, arrowheads). **-*P*<0.005, ***-*P*<0.0005. Scale bar = 50um.

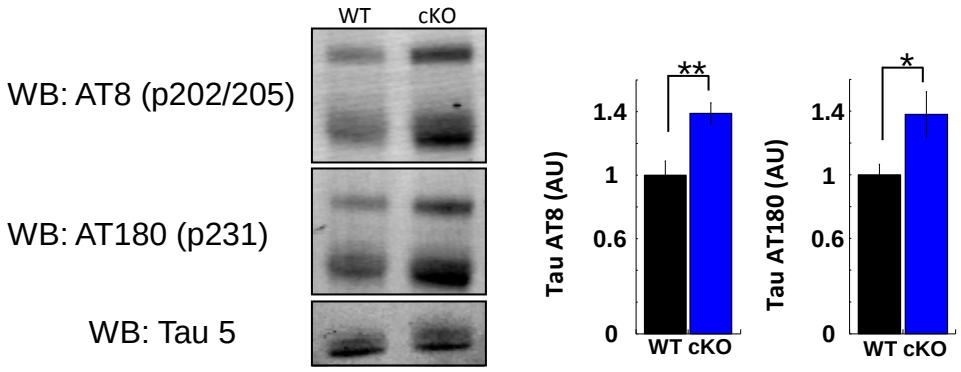

Figure 2.20: OGT cKO mice accumulate hyperphosphorylated tau. (western blot) Increases in several pathological phosphorylation sites on tau by western blot at 6 months. *-P<0.05, **-*P*<0.005.

rendering of hyperphosphorylated tau in the mossy fibers of the dentate gyrus illustrates the accumulation of pathogenic tau (Figure 2.21).

As hyperphosphorylation of tau has been shown to affect tau solubility (47, 48), we isolated tau from OGT cKO mice and assessed whether changes in solubility were detectable compared to wild-type mice. Lysates were solubilized in sarkosyl detergent, and evaluated by ultracentrifugation. Total tau and phospho-S396 tau were probed on a western blot, and showed no significant changes in solubility between OGT cKO and wild-type mice (Figure 2.22). A majority of tau was soluble in detergent-free lysis buffer, and there was no change in the percentage of tau that was insoluble in sarkosyl.

Tau is expressed as different isoforms, and changes in isoform expression have been previously associated with diseased states (49-51). Tau can be expressed with 3 or 4 repeat domains depending on splicing events, and these species have different apparent molecular weights. We initially observed that OGT cKO mouse tau would often display an increase in the ‘upper band’ compared to wild-type mouse tau, and we hypothesized that this could be due to changes in tau isoform expression (Figure 2.23, bold arrow). Tau phosphorylation has previously been shown to affect tau migration on SDS-PAGE, and we sought to identify the cause of the changes in the abundance of the ‘upper band’ from OGT cKO mice. Protein phosphatase lambda (PPL) was added to lysates, and samples were compared to untreated lysates. After PPL treatment, changes in apparent molecular weight between OGT cKO and wild-

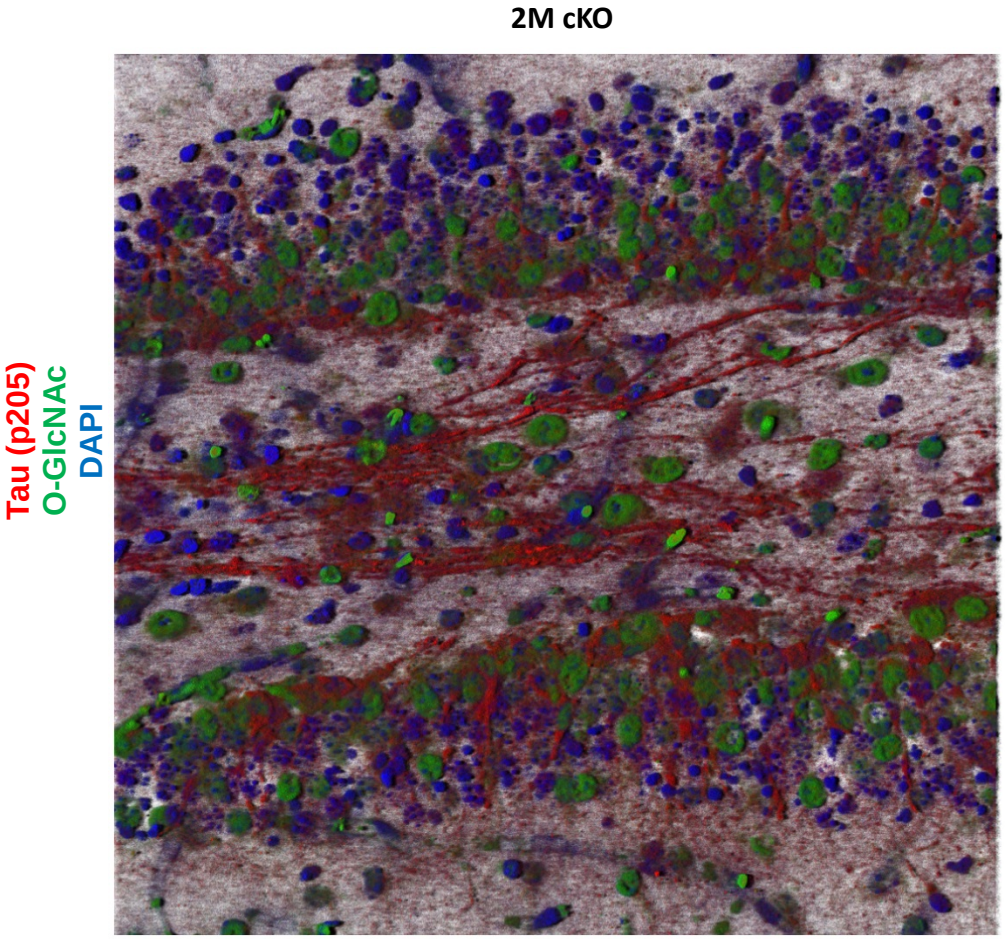

Figure 2.21: 3D rendering of hyperphosphorylated tau in dentate gyrus of OGT cKO mice. 3D rendering of a z-stack of the dentate gyrus illustrate accumulation of tau phosphorylated at T205 in the mossy fibers and cell bodies of DG neurons.

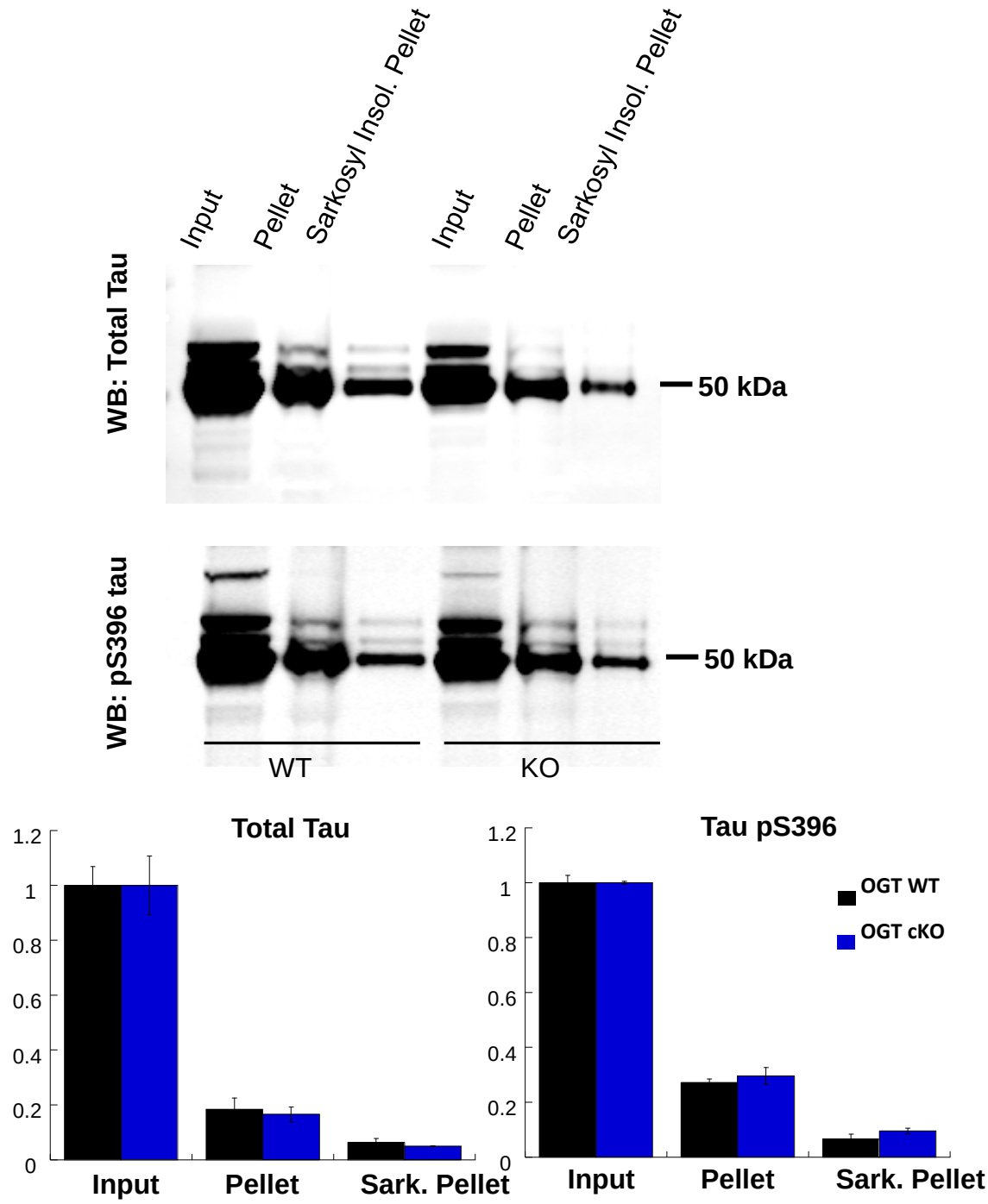

Figure 2.22: Tau sedementation assay shows no changes in solubility in OGT cKO mice. Insoluble tau was isolated by ultracentrifugation with and without sarkosyl detergent, and there were no apparent changes in the solubility of both total tau or pS396 tau levels in OGT cKO mice. N=2 for each genotype, and values are normalized to total tau in the input.

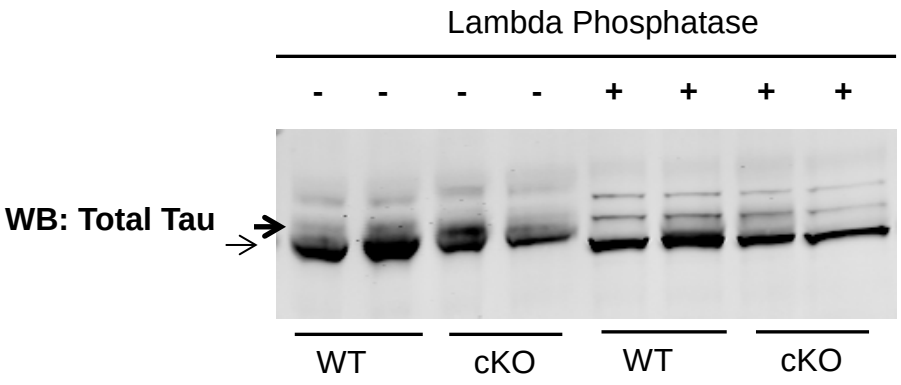

Figure 2.23: Protein phosphatase lambda treatment demonstrates that changes in apparent molecular weight in tau result from phosphorylation state and not alternative 3R vs. 4R splicing. The 50kDa band that represents tau shows a higher abundance of the upper band (bold arrow) in OGT cKO mice. After treatment with protein phosphatase lambda, the changes in the distribution of tau between the upper and lower bands is eliminated, suggesting that apparent changes in molecular weight are due to phosphorylation and not changes in the expression of 3R vs 4R isoforms.

type mouse tau were eliminated, suggesting that these changes were due to tau phosphorylation, and not changes in the regulation of tau splicing (Figure 2.23).

As *O*-GlcNAc has also been shown to modulate APP processing (52), an ELISA was used to quantify changes in amyloid beta peptide levels in 6 month old OGT cKO animals. Amyloid precursor protein can be proteolytically cleaved to form both 42 and 40-mer peptides, and both peptides are increased in OGT cKO mice (6.8 fold and 2.7 fold, respectively; Figure 2.24A). Importantly, the ratio of 42/40 peptide also increased 2.5 fold and represents an accumulation of the more amyloidogenic 42-mer peptide (53) (Figure 2.24A). Furthermore, at 6 months, the appearance of plaque-like aggregates was observed by Thioflavine-S staining (6.9 fold increase) (Figure 2.24B).

2.2.7 OGT is decreased in human AD brain

A previous study demonstrated a significant reduction in O-GlcNAcylated proteins in the frontal cerebral cortex of AD brains compared to healthy individuals (54). A more recent study, suggested that AD brains showed significant increases in O-GlcNAcylated proteins in the inferior parietal lobule and the cerebellar cortex (55). In light of these conflicting studies, and the dramatic neurodegenerative phenotype of the OGT cKO mice, we evaluated whether changes in OGT protein levels were evident in human AD tissue. Using immunohistochemistry, we quantified OGT protein levels in AD brains with an anti-OGT antibody (AL28). Remarkably, a 1.6 fold decrease in OGT protein levels was observed in cortical AD neurons (Braak VI) compared to healthy control individuals (Figure 2.25). This result suggests that our model of reduced

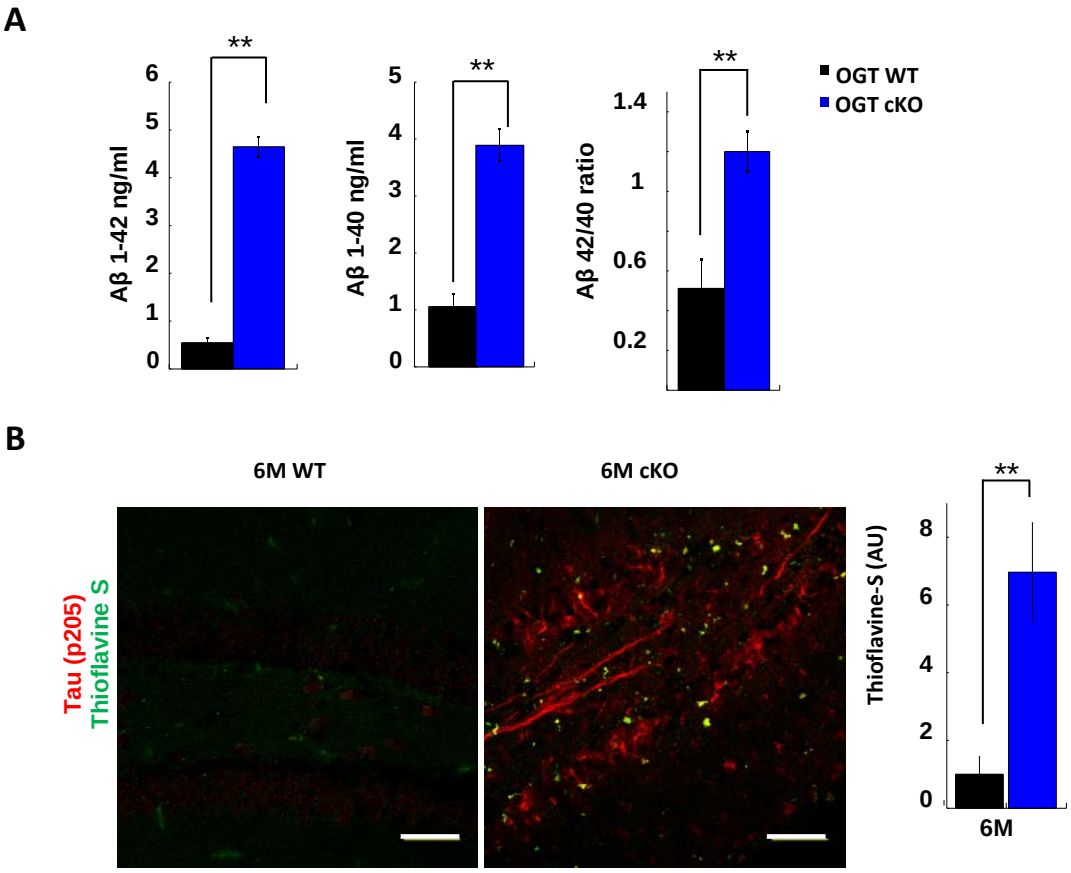

Figure 2.24: OGT cKO mice have increases in amyloid beta peptide and protein aggregates. (A) Increases in both amyloid beta 42 and 40-mer peptides are quantified by ELISA in 6 month OGT cKO mice, with accompanying increase in the 42/40-mer peptide ratio. (B) Thioflavine-S positive aggregates appear in 6 month old OGT cKO mice. **-*P*<0.005. Scale bar = 50um.

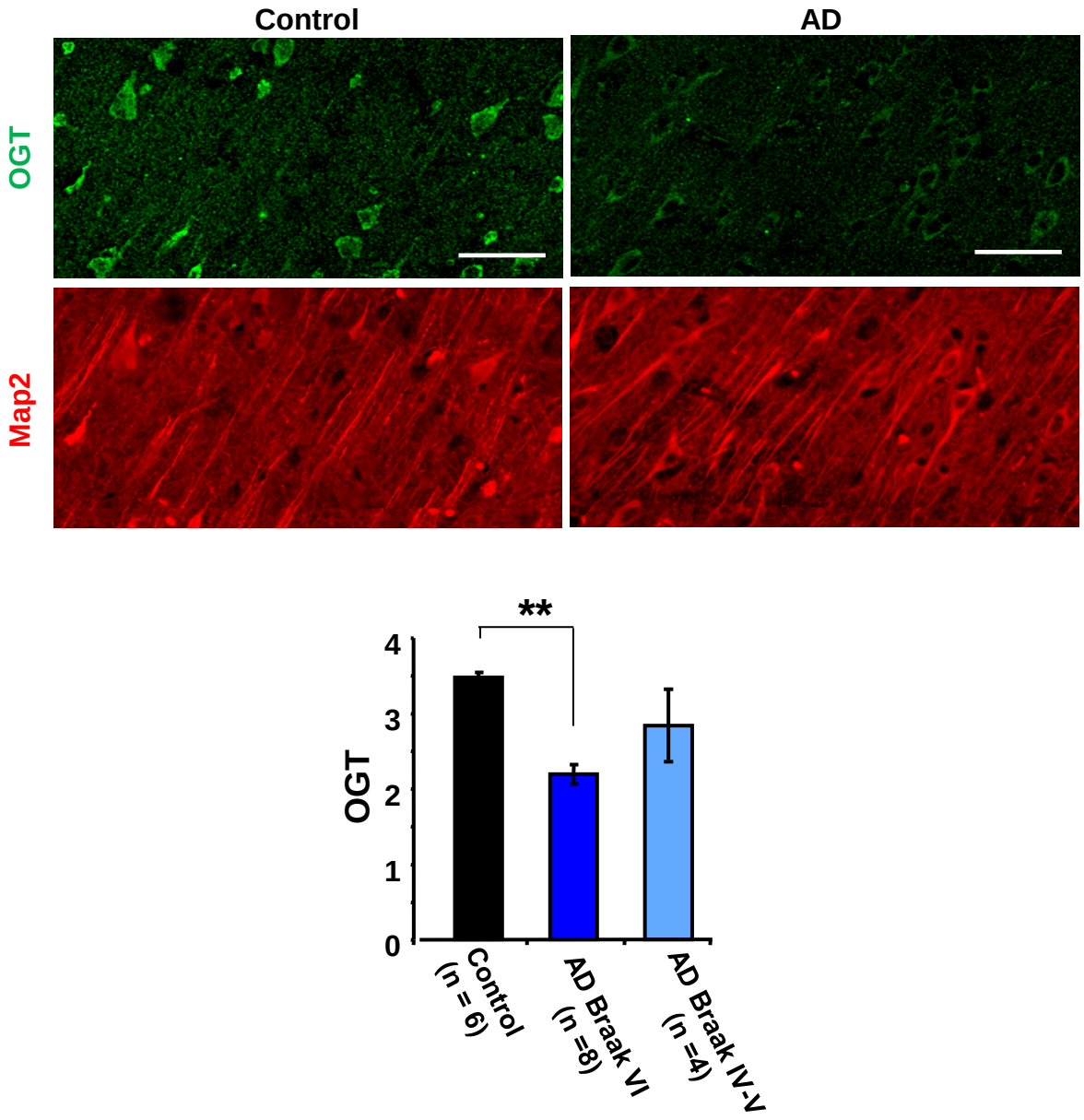

Figure 2.25: AD brain tissues show significant reductions in OGT protein levels. AD brain tissues were stained for OGT protein levels with immunohistochemistry. A 1.6 fold reduction in OGT protein levels was observed between AD Braak stage VI patients and control healthy individuals. Although not statistically significant, Braak IV-V tissues showed a reduction in OGT between normal and stage VI levels. Map2 was used as a control to quantify neuronal numbers in different slides. **-P<0.005, n=6.

OGT represents a disease-relevant pathway. Although not statistically significant, Braak IV-V demonstrated a level of OGT that was intermediate, between healthy control and advanced stage Braak VI patients.

2.2.8 The role of Excitotoxicity in Neuronal Death after loss of OGT

O-GlcNAc glycosylation has been shown to have a significant neuroprotective role in ischemia-reperfusion injuries (4, 56-58). We hypothesized that after loss of OGT, stress responses may be impaired and neurons may be especially vulnerable to excitotoxicity. To test this hypothesis, we cultured floxed OGT cortical neurons, and compared CRE treated (OGT knockout) neurons with Cherry control treated neurons (wild-type). After 24 hour glutamate treatments, cell viability was assessed with an MTT assay (Figure 2.26). Although the experiment was repeated many times, it yielded irreproducible results. Several times, OGT KO neurons were significantly more sensitive to glutamate treatment compared to wild-type neurons. However, in other experiments, there was no difference in excitotoxicity. Many parameters were varied, such as plating density, glutamate treatment time, and excitotoxic stimulus (NMDA vs. glutamate). Control wild-type neurons (non floxed OGT) were treated with CRE or Cherry virus, and showed no change in excitotoxicity.

2.2.9 Changes in AKT and GSK3β phosphorylation in OGT cKO mice

As we had characterized increases in hyperphosphorylated tau, we sought to investigate whether key cellular kinases were altered in OGT cKO mice. An activating phosphorylation of AKT at S473 was significantly increased in OGT cKO mice at 4 months (Figure 2.27A). AKT phosphorylates GSK3β at S9, and

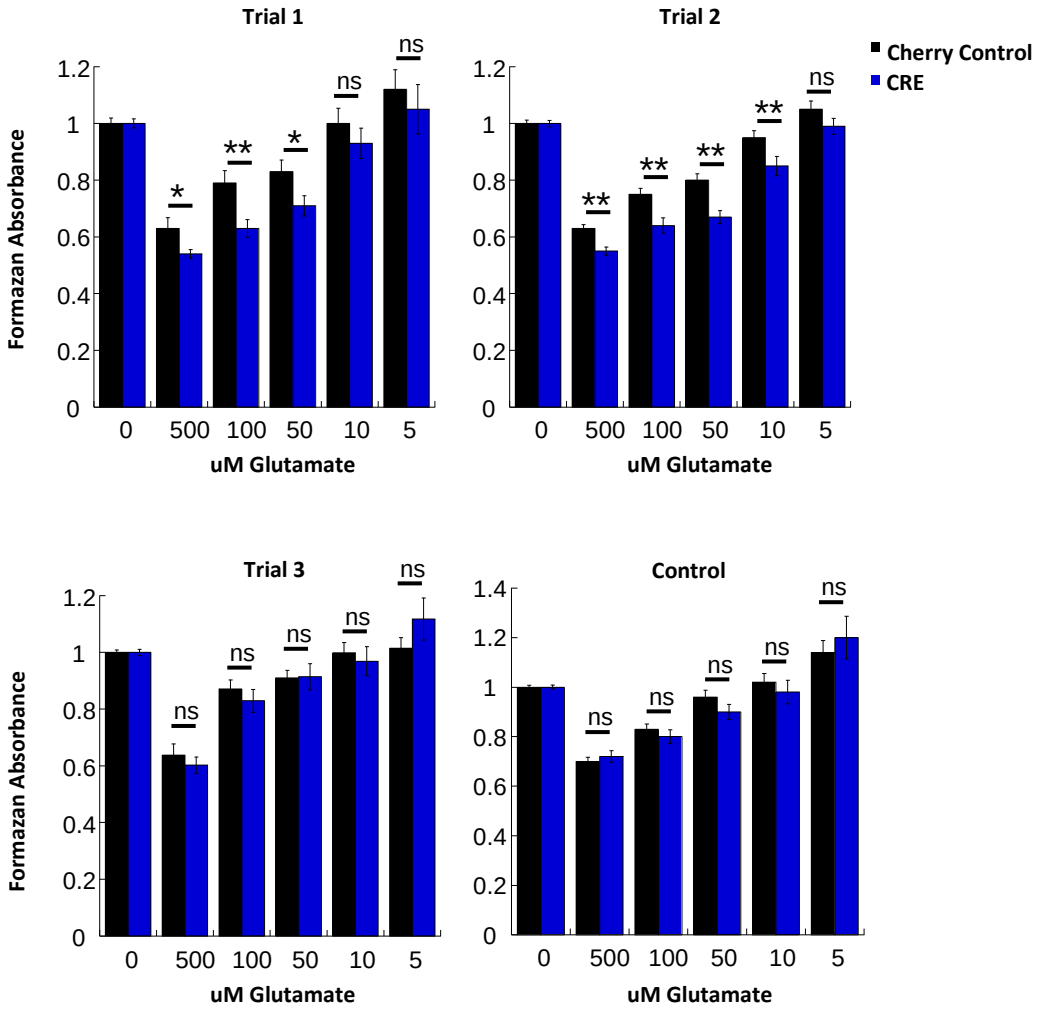

Figure 2.26: MTT assays are inconclusive as to whether OGT loss potentiates neuronal excitotoxicity to glutamate. Dissociated floxed OGT neurons were treated with cherry control or CRE virus on 1DIV, followed by 24 hour glutamate treatment on 6DIV at the indicated concentrations. An MTT assay was used to quantify cell death at 7DIV, and representative results of several experiments are presented here. A small but significant change in the susceptibility of OGT KO neurons (CRE treated) to death after glutamate was detected in several experiments (Trial 1 & 2), but not in others (Trial 3). Three and 12 hour treatments with glutamate were also tried and showed no significant changes in excitotoxicity (data not shown). Control neurons (wild-type) were treated with cherry control and CRE virus and showed no change in cell death.

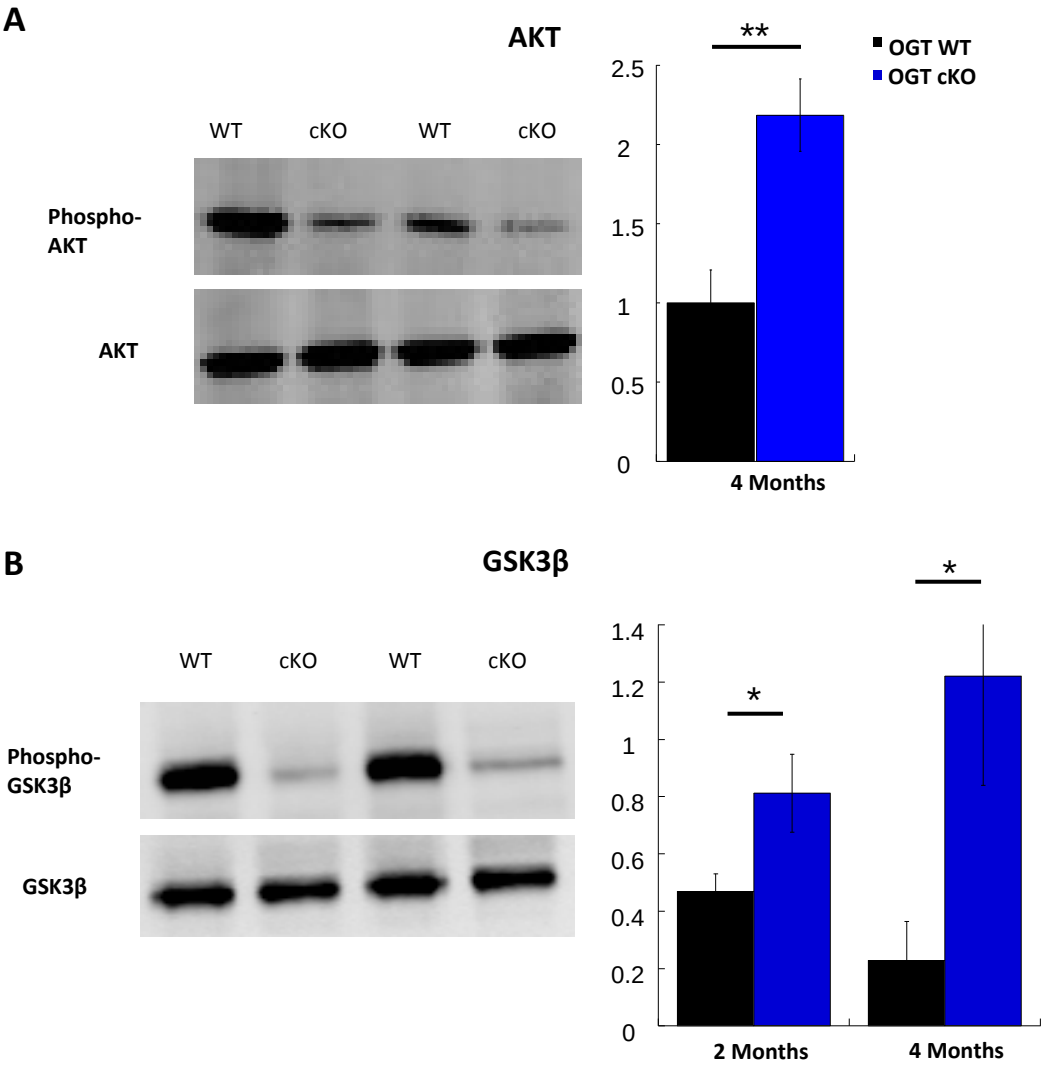

Figure 2.27: OGT cKO mice have activated AKT and inhibited GSK3β. (A) OGT ckO mice have increased activation of AKT by phosphorylation at S473 at 4 months. (B) Inactivation of GSK3β by phosphorylation at S9 is also increased in OGT cKO mice, at both 2 and 4 months. *-P<0.05, **-P<0.005.

accordingly, GSK3β was found to have increased phosphorylated S9 in OGT cKO mice at both 2 and 4 months (Figure 2.27B). This modification represses GSK3β activity, and it is unclear how these changes contribute to OGT cKO neurodegeneration.

2.3 Discussion:

Previously characterized mouse models of OGT knockout were limited by an embryonic or early postnatal lethal phenotype, but demonstrated an increase in tau phosphorylation. As OGT is clearly necessary for neuronal development and regulates key neuronal proteins, we sought to better characterize its role in the mature mouse brain. Our αCamKII-Cre mouse produced a gradual knockout of OGT in which a subset of hippocampal and cortical neurons were continually knocked out from 1 to 6 months. This progressive knockout of forebrain neurons led to neuronal loss, beginning at 2 months at about 20%, increasing to over 50% by 4 months. Hippocampal neurons were shown to be TUNEL positive, and thus undergo apoptosis. In addition, FJ-C was used to quantify degenerating neurons, and demonstrated that over 30% of hippocampal neurons were degenerating in 2 month old OGT cKO mice.

Although neuronal degeneration and death is observed shortly after loss of OGT, we observed degeneration in *O*-GlcNAc positive neurons as well. When examining FJ-C staining, some neurons were positive for both *O*-GlcNAc and FJC. This suggests that neuronal dysfunction observed in OGT knockout neurons can spread to nearby wild-type cells. It is likely that the extensive neuroinflammation observed and release of cellular contents after apoptosis may

contribute to degeneration of OGT positive neurons. The spreading of degeneration is thought to play an integral role in the pathology of neurodegenerative diseases and is seen in other mouse models (59, 60).

OGT cKO mice survived well past 6 months even after a ~70% reduction in forebrain neurons. During this time several behavioral abnormalities were observed. Most mice exhibited an excessive grooming phenotype beginning at 5 months, which resulted in hair loss and development of skin lesions. This phenotype has been observed in mouse models of OCD and schizophrenia (33, 34). The cause for this phenotype is unclear, although other models suggest that cortico-striatal networks and microglia may be involved. Certainly both severe cortical degeneration and microglial activation are observed in OGT cKO mice.

Despite this progressive loss of neurons in the forebrain, 4 month old OGT cKO mice retain good motor function, as assessed by a rotarod assay. Increases in anxiety are observed at 2 months, and changes in amygdala-dependent fear memory are apparent at 2 months before overt loss of neurons. By four months, there are significant deficits in both cued and contextual fear-related memory, but despite significant reductions in the total number of forebrain neurons (60%), OGT cKO mice are still able to make new associations. Furthermore, although not statistically significant, place preference tests suggest that short-term memory is impaired in OGT cKO mice. These behavioral studies demonstrate significant memory impairments that are seen in other AD mouse models.

Although OGT has been implicated in the regulation of both tau and APP, it was not clear whether altering *O*-GlcNAc signaling in healthy neurons could

induce tau and APP pathology. Of great significance is that the observed changes in tau phosphorylation and amyloid beta peptide levels in OGT cKO mice are produced from endogenous mouse proteins. This is in contrast to most AD mouse models that utilize overexpression of mutant human proteins to recapitulate disease phenotypes (61, 62). Furthermore, unlike several established AD mouse models which require 12 months to generate pathological phenotypes, OGT cKO mice display AD phenotypes beginning at 2 months.

One of the most immediate and striking phenotypes observed in OGT cKO mice is gliosis. Both microglia and astrocytes are massively upregulated in the entire hippocampal region at 2 months of age, spreading to the cortex by 6 months. As neurons are clearly undergoing apoptosis, it is likely that glial cells are responding directly to degeneration and neuronal loss.

It has been shown that *O*-GlcNAc modifies nicastrin, a component of the γ-secretase complex that proteolytically cleaves APP (63), and APP itself has been shown to be *O*-GlcNAc modified, although the significance of these modifications is not understood (64). We observed increases in the levels of both 42 and 40-mer amyloid beta peptide, as well as the ratio of 42/40-mer Aβ peptide. As the 42-mer peptide is more amyloidogenic, this ratio is a biomarker for AD diagnosis (65) and our finding suggests that the changes in APP processing that occur in the human disease also occur in OGT cKO mice.

We observe increases in phosphorylated tau in both axons and soma of dentate gyrus neurons, which form neurofibrillary tangle-like inclusions. The increases in tau phosphorylation are observed at epitopes (T205, S396, T231)

that are associated with paired-helical filamentous tau, which is the major component of neurofibrillary tangles. *O*-GlcNAc modifications have been shown previously to regulate tau phosphorylation both by directly competing for phosphorylation sites, as well as regulating kinases involved in tau phosphorylation (66-68). Importantly, we observe significant AKT activation and GSK3β inactivation in OGT cKO mice. This pathway likely plays a role in neurodegeneration, although the significance of these changes in our model remains to be elucidated. Ongoing studies seek to identify other kinases that are responsible for the observed increases in phosphorylated tau after OGT knockout.

Hyperphosphorylation of tau has been shown to affect its solubility, and we evaluated this property of tau in OGT cKO mice. Using a tau sedimentation assay, no changes in tau solubility were apparent, but we did observe an increased amount of a higher molecular weight tau species in OGT cKO mice. We hypothesized that this could be due to altered tau isoform expression (3R vs. 4R) but upon phosphatase treatment, the changes were no longer present and thus are likely the result of altered phosphorylation of tau.

We also observe an increase in Thioflavine-S staining in OGT cKO mice at 6 months. These aggregates co-stain with a phospho-tau antibody (T205) although they appear to be extracellular. Such Thioflavine-s stained species are observed in other AD mouse models and likely represent insoluble protein aggregates in OGT cKO mice.

As OGT cKO mice display such striking degeneration, we sought to better characterize the transcriptional changes that underlie the observed pathology. After identifying changes in gene expression by microarray, subsequent WGCNA analysis revealed that genes involved in the immune response as well as cell cycle arrest were significantly increased in OGT cKO mice at 2 months. While immune response activation was expected given the level of gliosis observed, the increase in cell cycle arrest gene expression was quite surprising and suggests that *O*-GlcNAc may regulate the pathology of AD through a mechanism involving inappropriate cell cycle advancement. Several studies have shown that manipulation of *O*-GlcNAc glycosylation has been shown to perturb cell cycle progression (69-71), and inappropriate cell cycle advancement has been shown to occur in neurons from the brains of Alzheimer's disease patients and in neurons of various mouse models of AD (72-76).

We investigated CDK5, which is essential for repressing neuronal cell cycle advancement. A reduction in CDK5 protein was observed in *O*-GlcNAc negative neurons of OGT cKO mice and suggests that neuronal cell cycle re-entry may be occurring in OGT cKO mice. Future studies are required to understand how *O*-GlcNAc might regulate this process. Furthermore, we demonstrate that CDK5 itself is *O*-GlcNAc glycosylated, although the significance of this modification remains to be elucidated.

Another interesting possible mechanism for the neurodegeneration in OGT cKO mice is increased susceptibility to excitotoxicity. OGT has been shown to play an important role in modulating the stress response, and O-GlcNAc

modifications have been shown to be neuroprotective in ischemia-reperfusion injury models. Our assessment of the effects of OGT knockout on excitotoxicity in cultured neurons was inconclusive, with experiments yielding mixed results. Future studies could focus on finding other ways to perturb *O*-GlcNAc levels in neurons and evaluate their effects on excitotoxic insults.

2.4 Conclusion

Previous studies investigating the role of *O*-GlcNAcylation in neurodegeneration have provided conflicting results, with studies in mice suggesting that increasing *O*-GlcNAc levels can be neuroprotective, while studies in *C. elegans* suggest the opposite (26, 77, 78). To better define the role of OGT in adult neurons, we generated a conditional knockout of OGT in the postnatal forebrain. Our OGT cKO mouse model demonstrates that a loss of OGT in adult neurons directly results in neurodegenerative phenotypes which include neuronal loss, inflammation, behavioral deficits, and increases in hyperphosphorylated tau and amyloid beta peptide. Furthermore, we find that neurons in human AD tissue have significantly reduced levels of OGT, suggesting that our model of OGT knockout is representative of the pathology found in the human disease. Future insights into the mechanisms that contribute to the observed degeneration in OGT cKO mice will facilitate the development of new therapeutic strategies for AD. Specifically, understanding the role of *O*-GlcNAcylation in regulating CDK5 and cell-cycle progression in neurons is of great interest, as is understanding how *O*-GlcNAc regulates the biology of tau and APP.

2.5 Materials and Methods:

2.5.1 Reagents:

Histoclear (Electron Microscopy Sciences, 641101-01), Tissue-Tek OCT (Fisher, 14-373-65), Vectashield (Vector labs, H-1200), Fluoro-Jade C (Millipore, AG325), ApopTag Fluorescein Kit (Millipore, S7110), Primary Antibodies: anti-OGT: DM-17 (Sigma O6264), AL-25/28 (Dr. Gerald Hart, Johns Hopkins), anti-O-GlcNAc: RL-2 (Pierce, MA1-072), anti-tau: p205 (Invitrogen 44738G), p231 (EMD Millipore, AB9668), AT180 (Pierce, MN1040), p396 (Abcam, 32057), tau-5 (Millipore, MAB361), AT8 (Pierce, MN1020), anti-Microglia: Iba-1 (WakoUSA, 019-19741), anti-astrocytes: GFAP (Cell Signaling, 3670P), anti-neuronal nuclei: NeuN (Millipore, MAB377), anti-CDK5: CDK5 (Santa Cruz, SC-173), anti-PCNA: PCNA (Abcam, 18197), anti-GFP: GFP (Life Technologies, G10362), anti-tubulin: a-Tubulin (Sigma, T9026). Secondary Antibodies: Alexafluor 405, 488, 546 goat anti-mouse (Invitrogen), Amyloid beta ELISA 1-40, 1-42 (Covance, SIG-38954, 38956)

2.5.2 Mice

C57/Bl6 backcrossed CamKIIa-Cre mice were a kind gift from Dr. Mary Kennedy, and were maintained and genotyped using established procedures (32). OGT floxed mice (B6.129-Ogttm1Gwh/J) were purchased from Jackson Labs (004860) and backcrossed into the C57/Bl6 background. Genotyping was done following JAX protocols. Mice were group housed whenever possible, and all experiments were approved by the IACUC protocols at Caltech.

2.5.3 Immunohistochemistry

Perfusion: Mice were trans-cardially perfused with 4% paraformaldehyde (PFA) fixative. Brains were dissected and fixed in 4% PFA overnight at 4 C, followed by cryoprotection with 15-30 % sucrose overnight. Hemispheres were embedded in OCT medium and snap frozen in dry ice/methanol. Sagittal sections at 20 um were collected with a cryostat and stored free floating in an ethylene glycol solution stored at -20 C. Slices were stained with primary antibody in 2% normal goat serum with 0.1% Triton-X 100 in PBS over night at 4C. After washing 3 x 5 min in PBS, slices were incubated with secondary antibodies at 1:400 dilution for 1 hr at room temperature. Slices were washed as before and mounted onto slides, allowed to dry, and coverslipped with vectashield. Tissue sections were coded and imaged with a Zeiss 700 confocal microscope. Images were collected for each region of interest from slices spaced 100 um apart through the region. A minimum of 12 slices were quantified for each animal.

Nissl staining: Slices were incubated in 100% EtOH for 2 min, Histoclear for 2 min, followed by re-hydrating in 100, 70, 50% EtOH for 2 min each. Slices were then stained with 0.1% Cresyl Violet solution for 10 min, rinsed in distilled water, and differentiated in 95% EtOH with 10% acetic acid for 10 seconds, rinsed in 100% EtOH, and cleared for 2m in in Histoclear. Slices were then mounted and imaged.

Fluorojade-C and Thioflavine-S staining: Slices were incubated in 0.06% potassium permanganate solution for 10 min, followed by a water rinse, and then transferred to a 0.0001% solution of Fluorojade-C in 0.1% acetic acid, or a 0.05%

Thioflavine-S solution in 50% EtOH for 10 min, rinsed in water (or 50% EtOh for Thioflavine-S), then mounted and imaged.

AD human tissue: samples from control (n=6) and Braak VI (n=8) were acquired from Dr. Harry Vinters, UCLA Medical School. Slices were pre-treated with heat antigen retrieval in citrate buffer pH 6, followed by treatment with sudan black and staining as described above. Four representative regions were imaged in each slice, and at least 4 slices were imaged per individual. Images were coded and researchers were blind to sample ID while qualitatively scoring OGT protein signal with a scale from 1-5. Non-specific signal from autofluorescent particles necessitated a qualitative approach.

Golgi Stain: Golgi stain was performed following manufacturers protocol (FD Neurotech). Fresh brains were submerged into a mixture of equal volumes of solutions A and B, stored at RT for 2 weeks in the dark. Solution was replaced after 6 hours. Tissue was transferred to solution C, for 72 hours in the dark, again with one replacement of solution after 24 hours. 200um sections were cut on a vibratome, and mounted on gelatin-coated slides. After drying, slides were rinsed in ddH2O and stained by submerging in a mixture of 1 part solution D, 1 part solution E, and 2 parts dd H2O for 10 min. Sections were rinsed in ddH2O twice for 4 min each, dehydrated with successive ethanol solutions, and finally in absolute ethanol 4 times, 4 min each. Slices were cleared in Histoclear and coverslipped with permount.

2.5.4 Behavioral Studies

Rotarod: Rotarod test was performed as described previously (79). Briefly, latency to fall from an accelerating rotarod (Ugo Basile) beginning at 5 rpm to 40 rpm over 240 s was scored. Mice were allowed to stay on the rotarod for a maximum of 300 s. Mice were trained for two consecutive days, with two trails per day with a 10 min intertribal interval. On testing days, two trials were performed and averaged.

Open Field: Open field tests were performed as described previously (79). Briefly, mice were placed in the lower left corner of a 50 x 50 cm white box and activity was recorded for 10 min by a ceiling-mounted video camera. Total distance traveled and center entries were scored.

Fear Conditioning: Fear conditioning was performed as described previously (80). Briefly, mice were placed in the chamber (Med Associates) for the first time and allowed to explore for 120 s after which an audible tone was played for 30 s. During the last 2 seconds of tone, a 0.7 mA foot shock was applied. Another tone was played at 180 s again for 30 s with another foot shock applied for the last 2 s of the tone. Mice were placed back into their cages. After 24 h, mice were placed in the same chamber and monitored for 5 min to quantify context dependent memory. Mice were placed into home cages for 1 hour, and then placed into an altered context chamber (altered scent, shape, lighting) for 5 min, with a tone playing for the last 180 seconds. All freezing quantification was done by Med Associates software, and freezing was normalized to pre-tone freezing % for cued tests.

Y-Maze: Animals were introduced to the Y-Maze and recorded for 5 min. Arms entries were noted and sequential overlapping triplets were analyzed to determine whether mice entered new arms each time, or revisited the same arm twice within each triplet of arm entries. Percent alternation was quantified by the number of alternating triplets, divided by the total number of triplets.

Place Preference: Mice were introduced to an open field with two objects (children's plastic toys), one in each of the upper quadrants of the box. Objects were placed at least 6 inches from the wall of the box, to allow room for mice to walk around the object without investigating. Investigations were classified as distinct head pointing or sniffing within 1 inch of the object. Animals were recorded for 5 min and removed. During a 5 min interphase period, one of the objects was moved from the upper right quadrant to the lower right quadrant. Mice were replaced and recorded for another 5 min, and investigations were quantified. Increases in the number of investigation events represented an increase in interest in the object. The experiment was conducted with normal fluorescent lighting, and in the future using the red light or dimmed lighting may provide a more suitable environment.

2.5.5 Microarray

Hippocampal tissue was isolated from 3-week or 2-month old mice and flash frozen in nuclease-free tubes. The hippocampal samples were stored in the -80^{o}C until RNA extraction. Total RNA was extracted using RNeasy kit with DNase treatment. Following RNA extraction, the samples were either sent to Phalanx Biotech Group for microarray analysis or reverse transcribed using the

iScript cDNA Synthesis Kit for qRT-PCR. Following reverse transcription, the cDNA was used for qPCR using Perfecta SYBR Green Fastmix with ROX on the AB7300 Real Time System. The qRT-PCR primers used for this study are listed in the supplemental Table 4. Statistical significance of qRT-PCR results was determined using an unpaired t-test. Reported p values for the microarray results from this study are Bonferroni-corrected (81).

2.5.6 Chemoenzymatic Labeling

Chemoenzymatic labeling of mouse brain lysate was performed as described previously (82). Briefly, 200 ug mouse cortical lysate labeled with UDP-GalNAz with GalT enzyme as described, and reacted with alkynyl-biotin. Biotinylated proteins were pulled down with streptavidin-conjugated agarose beads, washed, eluted, and subjected to SDS-PAGE electrophoresis followed by western blotting with CDK5 antibody. Specificity of the reaction was confirmed by omitting GalT enzyme.

2.5.7 TUNEL Labeling

TUNEL labeling was performed using manufacturer's protocols with one modification. Briefly, slices were treated with proteinase-k for 15 min, washed, and microwaved for 30 s in 10mM citrate buffer pH 3. Slices were then incubated with TdT enzyme for 1 h at 37 C. After subsequent wash steps, anti-digoxigenin conjugate was applied for 1 h at room temperature. Slides were then washed and mounted. Co-staining with another primary antibody was done after anti-digoxigenin incubation.

2.5.8 Tau Sedementation Assay

Whole brains were homogenized in 600 uL tissue homogenization buffer (THB) with PIC and PMSF using glass teflon douncer (about 10 dounces). 50mM Tris HCl pH 8, 274 mM NaCl, 5 mM KCl, 2 mM EDTA, 2 mM EGTA, 30 mM NaF, 1x protein phosphatase inhibitor cocktail containing sodium vanadate, beta glycerophosphate, and sodium fluoride, add fresh 1mM PMSF, protease inhibitor cocktail (Roche) with EDTA. Lysates were then spun down at 13000 x g at 4C for 20 minutes. Supernatant was collected, and the pellet was re-extracted with another 600 uL of THB as before (10 dounces with teflon douncer). After spinning down at 13000 xg at 4C for 20 minutes, supernatants from extraction 1 and 2 were combined. 25 uL was saved for the “input”. The remaining sample was divided into 2 equal portions for a high speed sup and high speed post sarcosyl sup. To the sarkosyl portion, add N-lauryl sarcosyl (20% stock solution) to a final 1%, and then shake in 37C incubator for 1h. The two fractions were then ultracentrifuged as follows: The volumes were brought up in their respective buffers (THB +/- 1% sarcosyl) to almost fill the ultracentrifuge tubes. They were then spun down at 100,000 x g for 45 min (34,163 rpm on swing rotor). A portion of the sup was collected and the rest discarded (be careful not to displace the pellet which is small and hard to see). The pellets were resuspended in 2x loading dye, and run on a gel. Blot with tau 5 overnight and p-tau.

2.5.9 Tensor Based Morphometry Analysis

MRI scan of fixed brains in skull was carried out with the assistance of Joe Gallagher and Dr. Russell Jacobs, at the Biological Imaging Facility of the

Beckman Institute. Briefly, scanned images were processed by stripping the skull from the brain. MIPAV software was used to visualize the MRI data. MRIcro was used to analyze the changes in volume.

2.5.10 MTT Excitotoxicity Assays

Dissociated floxed OGT neurons were plated at 15-30,000 cells per well of a 96-well plate. Neurons were treated with cherry control or CRE virus on 1DIV, followed by 24 hour glutamate treatment on 6DIV (0-500uM). After 24 hours, MTT at 0.125mg/mL final concentration was added to the wells for 1 hour. Wells were aspirated, and 100uL of DMSO was added to solubilize formazan. Wells were read at 550 nm.

2.6 References

1. Whelan SA, Dias WB, Thiruneelakantapillai L, Lane MD, & Hart GW (2010) Regulation of insulin receptor substrate 1 (IRS-1)/AKT kinase-mediated insulin signaling by O-Linked beta-N-acetylglucosamine in 3T3-L1 adipocytes. *The Journal of biological chemistry* 285(8):5204-5211.
2. Ranuncolo SM, Ghosh S, Hanover JA, Hart GW, & Lewis BA (2012) Evidence of the involvement of O-GlcNAc-modified human RNA polymerase II CTD in transcription in vitro and in vivo. *The Journal of biological chemistry* 287(28):23549-23561.
3. Slawson C*, et al.* (2005) Perturbations in O-linked β-N-acetylglucosamine protein modification cause severe defects in mitotic progression and cytokinesis. *Journal of Biological Chemistry* 280(38):32944-32956.
4. Ngoh GA, Hamid T, Prabhu SD, & Jones SP (2009) O-GlcNAc signaling attenuates ER stress-induced cardiomyocyte death. *Am J Physiol Heart Circ Physiol* 297(5):H1711-1719.
5. Liu K PA, Zhang F, McAndrew J, Fukuchi K, Wyss JM, Peng L, Hu Y, Kudlow JE. (2004) Accumulation of protein O-GlcNAc modification inhibits proteasomes in the brain and coincides with neuronal apoptosis in brain areas with high O-GlcNAc metabolism. *J Neurochem.* 89(4):1044-1055.
6. Xu J WS, Viollet B, Zou MH. (2012) Regulation of the proteasome by AMPK in endothelial cells: the role of O-GlcNAc transferase (OGT). *PLoS One.* 7(5):36717.

7. Zhang F*, et al.* (2003) O-GlcNAc modification is an endogenous inhibitor of the proteasome. *Cell* 115(6):715-725.

8. Kreppel LK, Blomberg MA, & Hart GW (1997) Dynamic glycosylation of nuclear and cytosolic proteins. Cloning and characterization of a unique O-GlcNAc transferase with multiple tetratricopeptide repeats. *The Journal of biological chemistry* 272(14):9308-9315.

9. Dong DL & Hart GW (1994) Purification and characterization of an O-GlcNAc selective N-acetyl-beta-D-glucosaminidase from rat spleen cytosol. *The Journal of biological chemistry* 269(30):19321-19330.

10. Rexach JE*, et al.* (2012) Dynamic O-GlcNAc modification regulates CREB-mediated gene expression and memory formation. *Nature chemical biology* 8(3):253-261.

11. Tallent MK*, et al.* (2009) In vivo modulation of O-GlcNAc levels regulates hippocampal synaptic plasticity through interplay with phosphorylation. *The Journal of biological chemistry* 284(1):174-181.

12. Pekkurnaz G, Trinidad JC, Wang X, Kong D, & Schwarz TL (2014) Glucose regulates mitochondrial motility via Milton modification by O-GlcNAc transferase. *Cell* 158(1):54-68.

13. Taylor EW*, et al.* (2014) O-GlcNAcylation of AMPA receptor GluA2 is associated with a novel form of long-term depression at hippocampal synapses. *The Journal of neuroscience : the official journal of the Society for Neuroscience* 34(1):10-21.

14. Skorobogatko Y*, et al.* (2014) O-linked beta-N-acetylglucosamine (O-GlcNAc) site thr-87 regulates synapsin I localization to synapses and size of the reserve pool of synaptic vesicles. *The Journal of biological chemistry* 289(6):3602-3612.

15. Griffith LS, Mathes M, & Schmitz B (1995) Beta-amyloid precursor protein is modified with O-linked N-acetylglucosamine. *J Neurosci Res* 41(2):270-278.

16. Yao PJ & Coleman PD (1998) Reduced O-glycosylated clathrin assembly protein AP180: implication for synaptic vesicle recycling dysfunction in Alzheimer's disease. *Neuroscience letters* 252(1):33-36.

17. Ludemann N*, et al.* (2005) O-glycosylation of the tail domain of neurofilament protein M in human neurons and in spinal cord tissue of a rat model of amyotrophic lateral sclerosis (ALS). *The Journal of biological chemistry* 280(36):31648-31658.

18. Arnold CS*, et al.* (1996) The microtubule-associated protein tau is extensively modified with O-linked N-acetylglucosamine. *The Journal of biological chemistry* 271(46):28741-28744.

19. Smet-Nocca C*, et al.* (2011) Identification of O-GlcNAc sites within peptides of the Tau protein and their impact on phosphorylation. *Mol Biosyst* 7(5):1420-1429.

20. Liu F, Iqbal K, Grundke-Iqbal I, Hart GW, & Gong CX (2004) O-GlcNAcylation regulates phosphorylation of tau: a mechanism involved in

Alzheimer's disease. *Proceedings of the National Academy of Sciences of the United States of America* 101(29):10804-10809.

21. Kim C*, et al.* (2013) O-linked beta-N-acetylglucosaminidase inhibitor attenuates beta-amyloid plaque and rescues memory impairment. *Neurobiology of aging* 34(1):275-285.
22. Jacobsen KT & Iverfeldt K (2011) O-GlcNAcylation increases non-amyloidogenic processing of the amyloid-beta precursor protein (APP). *Biochemical and biophysical research communications* 404(3):882-886.
23. Yuzwa SA*, et al.* (2012) Increasing O-GlcNAc slows neurodegeneration and stabilizes tau against aggregation. *Nat Chem Biol.* 8(4):393-399.
24. Borghgraef P*, et al.* (2013) Increasing brain protein O-GlcNAc-ylation mitigates breathing defects and mortality of Tau.P301L mice. *PloS one* 8(12):e84442.
25. Guo B*, et al.* (2014) O-GlcNAc-modification of SNAP-29 regulates autophagosome maturation. *Nature cell biology* 16(12):1215-1226.
26. Wang P*, et al.* (2012) O-GlcNAc cycling mutants modulate proteotoxicity in Caenorhabditis elegans models of human neurodegenerative diseases. *Proceedings of the National Academy of Sciences* 109(43):17669-17674.
27. Kumar A*, et al.* (2014) Decreased O-linked GlcNAcylation protects from cytotoxicity mediated by huntingtin exon1 protein fragment. *Journal of Biological Chemistry*.

28. O'Donnell N ZN, Hart GW, Marth JD. (2004) Ogt-dependent X-chromosome-linked protein glycosylation is a requisite modification in somatic cell function and embryo viability. *Mol Cell Biol.* 24(4):1680-1690.

29. Shafi R IS, Ellies LG, O'Donnell N, Marek KW, Chui D, Hart GW, Marth JD. (2000) The O-GlcNAc transferase gene resides on the X chromosome and is essential for embryonic stem cell viability and mouse ontogeny. *Proc Natl Acad Sci U S A.* 97(11):5735-5739.

30. Sauer B & Henderson N (1988) Site-specific DNA recombination in mammalian cells by the Cre recombinase of bacteriophage P1. *Proceedings of the National Academy of Sciences* 85(14):5166-5170.

31. O'Donnell N, Zachara NE, Hart GW, & Marth JD (2004) Ogt-dependent X-chromosome-linked protein glycosylation is a requisite modification in somatic cell function and embryo viability. *Molecular and cellular biology* 24(4):1680-1690.

32. Schweizer C BS, Bluethmann H, Mansuy IM, Fritschy JM, Mohler H, Lüscher B. (2003) The gamma 2 subunit of GABA(A) receptors is required for maintenance of receptors at mature synapses. *Mol Cell Neurosci.* 24(2):442-450.

33. Welch JM LJ, Rodriguiz RM, Trotta NC, Peca J, Ding JD, Feliciano C, Chen M, Adams JP, Luo J, Dudek SM, Weinberg RJ, Calakos N, Wetsel WC, Feng G. (2007) Cortico-striatal synaptic defects and OCD-like behaviours in Sapap3-mutant mice. *Nature.* 448(7156):894-900.

34. Chen SK TP, Peden E, Cho S, Wu S, Spangrude G, Capecchi MR. (2010) Hematopoietic origin of pathological grooming in Hoxb8 mutant mice. *Cell.* 141(5):775-785.

35. Wu ZL CJ, Flood DG, O'Kane TM, Bozyczko-Coyne D, Savage MJ. (2006) Comparative analysis of cortical gene expression in mouse models of Alzheimer's disease. *Neurobiol Aging.* 27(3):377-386.

36. Dickey CA LJ, Montgomery J, Gordon MN, Eastman PS, Morgan D. (2003) Selectively reduced expression of synaptic plasticity-related genes in amyloid precursor protein + presenilin-1 transgenic mice. *J Neurosci.* 23(12):5219-5226.

37. Beglopoulos V SX, Saura CA, Lemere CA, Kim RD, Shen J. (2004) Reduced beta-amyloid production and increased inflammatory responses in presenilin conditional knock-out mice. *J Biol Chem.* 279(45):46907-46914.

38. Langfelder P HS (2008) WGCNA: an R package for weighted correlation network analysis. *BMC Bioinformatics.* 9:559.

39. Zhang B HS (2005) A general framework for weighted gene co-expression network analysis. *Stat Appl Genet Mol Biol.* 4:17.

40. Huang da W SB, Lempicki RA. (2009) Systematic and integrative analysis of large gene lists using DAVID bioinformatics resources. *Nat Protoc.* 4(1):44-57.

41. Hu Z HJ, Wang Y, Chang YC, Huang CL, Huyck M, DeLisi C. (2009) VisANT 3.5: multi-scale network visualization, analysis and inference based on the gene ontology. *Nucleic Acids Res.* 37:115-121.

42. Hu Z MJ, Wu J, DeLisi C. (2004) VisANT: an online visualization and analysis tool for biological interaction data. *BMC Bioinformatics.* 5(17).

43. Hu Z SE, DeLisi C. (2008) VisANT: an integrative framework for networks in systems biology. *Brief Bioinform.* 9(4):317-325.

44. Yuzwa SA SX, Macauley MS, Clark T, Skorobogatko Y, Vosseller K, Vocadlo DJ. (2012) Increasing O-GlcNAc slows neurodegeneration and stabilizes tau against aggregation. *Nat Chem Biol.* 8(4):393-399.

45. Bramblett GT GM, Jakes R, Merrick SE, Trojanowski JQ, Lee VM. (1993) Abnormal tau phosphorylation at Ser396 in Alzheimer's disease recapitulates development and contributes to reduced microtubule binding. *Neuron.* 10(6):1089-1099.

46. Goedert M JR, Vanmechelen E. (1995) Monoclonal antibody AT8 recognises tau protein phosphorylated at both serine 202 and threonine 205. *Neurosci Lett.* 189(3):167-169.

47. Spillantini MG*, et al.* (1997) Familial multiple system tauopathy with presenile dementia: a disease with abundant neuronal and glial tau filaments. *Proceedings of the National Academy of Sciences* 94(8):4113-4118.

48. Noble W*, et al.* (2003) Cdk5 is a key factor in tau aggregation and tangle formation in vivo. *Neuron* 38(4):555-565.

49. Götz J, Chen F, Van Dorpe J, & Nitsch R (2001) Formation of neurofibrillary tangles in P301L tau transgenic mice induced by Aβ42 fibrils. *Science (New York, N.Y.)* 293(5534):1491-1495.

50. de Silva R*, et al.* (2006) An immunohistochemical study of cases of sporadic and inherited frontotemporal lobar degeneration using 3R-and 4R-specific tau monoclonal antibodies. *Acta neuropathologica* 111(4):329-340.

51. D'Souza I & Schellenberg GD (2005) Regulation of tau isoform expression and dementia. *Biochimica et Biophysica Acta (BBA)-Molecular Basis of Disease* 1739(2):104-115.

52. Jacobsen KT IK (2011) O-GlcNAcylation increases non-amyloidogenic processing of the amyloid-β precursor protein (APP). *Biochem Biophys Res Commun.* 404(3):882-886.

53. Jarrett JT BE, Lansbury PT Jr. (1993) The C-terminus of the beta protein is critical in amyloidogenesis. *Ann N Y Acad Sci.* 695:144-148.

54. Liu F*, et al.* (2009) Reduced O-GlcNAcylation links lower brain glucose metabolism and tau pathology in Alzheimer's disease. *Brain*:awp099.

55. Forster S*, et al.* (2014) Increased O-GlcNAc levels correlate with decreased O-GlcNAcase levels in Alzheimer disease brain. *Biochimica et biophysica acta* 1842(9):1333-1339.

56. Champattanachai V, Marchase RB, & Chatham JC (2008) Glucosamine protects neonatal cardiomyocytes from ischemia-reperfusion injury via

increased protein O-GlcNAc and increased mitochondrial Bcl-2. *American journal of physiology. Cell physiology* 294(6):C1509-1520.

57. Hwang SY*, et al.* (2010) Glucosamine exerts a neuroprotective effect via suppression of inflammation in rat brain ischemia/reperfusion injury. *Glia* 58(15):1881-1892.

58. Ngoh GA, Watson LJ, Facundo HT, & Jones SP (2011) Augmented O-GlcNAc signaling attenuates oxidative stress and calcium overload in cardiomyocytes. *Amino acids* 40(3):895-911.

59. Frost B & Diamond MI (2010) Prion-like mechanisms in neurodegenerative diseases. *Nature Reviews Neuroscience* 11(3):155-159.

60. Clavaguera F*, et al.* (2009) Transmission and spreading of tauopathy in transgenic mouse brain. *Nature cell biology* 11(7):909-913.

61. Oddo S CA, Kitazawa M, Tseng BP, LaFerla FM. (2003) Amyloid deposition precedes tangle formation in a triple transgenic model of Alzheimer's disease. *Neurobiol Aging.* 24(8):1063-1070.

62. Oakley H CS, Logan S, Maus E, Shao P, Craft J, Guillozet-Bongaarts A, Ohno M, Disterhoft J, Van Eldik L, Berry R, Vassar R. (2006) Intraneuronal β-amyloid aggregates, neurodegeneration, and neuron loss in transgenic mice with five familial Alzheimer's disease mutations: potential factors in amyloid plaque formation. *J Neurosci.* 26(40):10129-10140.

63. Kim C ND, Park SY, Song H, Hong HS, Boo JH, Jung ES, Kim Y, Baek JY, Kim KS, Cho JW, Mook-Jung I. (2013) O-linked β-N-acetylglucosaminidase inhibitor attenuates β-amyloid plaque and rescues memory impairment. *Neurobiol Aging.* 34(1):275-285.

64. Griffith LS MM, Schmitz B. (1995) Beta-amyloid precursor protein is modified with O-linked N-acetylglucosamine. *J Neurosci Res.* 41(2):270-278.

65. Hansson O ZH, Buchhave P, Andreasson U, Londos E, Minthon L, Blennow K. (2007) Prediction of Alzheimer's disease using the CSF Abeta42/Abeta40 ratio in patients with mild cognitive impairment. *Dement Geriatr Cogn Disord.* 23(5):316-320.

66. Kazemi Z CH, Haserodt S, McKen C, Zachara NE. (2010) O-linked beta-N-acetylglucosamine (O-GlcNAc) regulates stress-induced heat shock protein expression in a GSK-3beta-dependent manner. *J Biol Chem.* 285(50):39096-39107.

67. Liu F IK, Grundke-Iqbal I, Hart GW, Gong CX. (2004) O-GlcNAcylation regulates phosphorylation of tau: A mechanism involved in Alzheimer's disease. *Proc Natl Acad Sci U S A.* 101(29):10804-10809.

68. Yang X OP, Miles PD, Havstad JC, Zhang F, So WV, Kudlow JE, Michell RH, Olefsky JM, Field SJ, Evans RM. (2008) Phosphoinositide signalling links O-GlcNAc transferase to insulin resistance. *Nature.* 451(7181):964-969.

69. Sakabe K HG (2010) O-GlcNAc transferase regulates mitotic chromatin dynamics. *J Biol Chem.* 285(45):34460-34468.

70. Drougat L O-VSS, Mortuaire M, Foulquier F, Lacoste AS, Michalski JC, Lefebvre T, Vercoutter-Edouart AS. (2012) Characterization of O-GlcNAc cycling and proteomic identification of differentially O-GlcNAcylated proteins during G1/S transition. *Biochim Biophys Acta.* 1820(12):1839-1848.

71. Capotosti F GS, Lammers F, Waridel P, Cai Y, Jin J, Conaway JW, Conaway RC, Herr W. (2011) O-GlcNAc transferase catalyzes site-specific proteolysis of HCF-1. *Cell.* 144(3):376-388.

72. Yang Y GD, Herrup K. (2001) DNA replication precedes neuronal cell death in Alzheimer's disease. *J Neurosci.* 21(8):2661-2668.

73. Yang Y ME, Herrup K. (2003) Neuronal cell death is preceded by cell cycle events at all stages of Alzheimer's disease. *J Neurosci.* 23(7):2557-2563.

74. Varvel NH BK, Patil AR, Pimplikar SW, Herrup K, Lamb BT. (2008) Aβ Oligomers Induce Neuronal Cell Cycle Events in Alzheimer’s Disease. *J Neurosci.* 28(43):10786-10793.

75. Andorfer C AC, Kress Y, Hof PR, Duff K, Davies P. (2005) Cell-Cycle Reentry and Cell Death in Transgenic Mice Expressing Nonmutant Human Tau Isoforms. *J Neurosci.* 25(22):5446-5454.

76. Yang Y VN, Lamb BT, Herrup K. (2006) Ectopic Cell Cycle Events Link Human Alzheimer's Disease and Amyloid Precursor Protein Transgenic Mouse Models. *J Neurosci.* 26(3):775-784.

77. Yu Y ZL, Li X, Run X, Liang Z, Li Y, Liu Y, Lee MH, Grundke-Iqbal I, Iqbal K, Vocadlo DJ, Liu F, Gong CX. (2012) Differential effects of an O-GlcNAcase inhibitor on tau phosphorylation. *PLoS One.* 7(4):35277.

78. Yuzwa SA*, et al.* (2012) Increasing O-GlcNAc slows neurodegeneration and stabilizes tau against aggregation. *Nature chemical biology* 8(4):393-399.

79. Southwell A KJ, Patterson P. (2009) Intrabody Gene Therapy Ameliorates Motor, Cognitive, and Neuropathological Symptoms in Multiple Mouse Models of Huntinton's Disease. *J. Neurosci.* 29(43):13589-13602.

80. Haubensak W KP, Cai H, Ciocchi S, Wall NR, Ponnusamy R, Biag J, Dong HW, Deisseroth K, Callaway EM, Fanselow MS, Lüthi A, Anderson DJ. (2010) Genetic dissection of an amygdala microcircuit that gates conditioned fear. *Nature.* 468(7321):270-276.

81. Dudoit S YY, Callow MH, and Speed TP. (2002) Statistical Methods for Identifying Differentially Expressed Genes in Replicated cDNA Microarray Experiments. *Statistica Sinica* (12):111-139.

82. Clark PM DJ, Mason DE, Hart CR, Buck SB, Peters EC, Agnew BJ, Hsieh-Wilson LC. (2008) Direct in-gel fluorescence detection and cellular imaging of O-GlcNAc-modified proteins. *J Am Chem Soc.* 130(35):11576-11577.

Chapter 3: Investigating the regulation of OGT

3.1 Introduction

Understanding the regulation of OGT is an extremely important next step to uncovering how *O*-GlcNAc glycosylation contributes to cellular signaling in healthy and diseased states. Furthermore, as *O*-GlcNAcylation of several disease-related proteins clearly contributes to pathology, controlling such modifications represent a significant area for therapeutic development. Investigations of OGT enzyme activity and specificity have mainly focused on characterizing the TPR domains of OGT, and defining how substrates interact with OGT. As described in the introductory chapter, a few OGT interacting proteins have been characterized, but most substrate-OGT interactions have not been explored.

OGT regulation by post-translational modification is also poorly understood, although it has been shown that OGT is both *O*-GlcNAc modified (1) and phosphorylated (2, 3). Studies have demonstrated that OGT is phosphorylated by CaMKIV and AMPK, and represent the only examples to date that describe the role of post-translational modifications on OGT activity. Specifically, CaMKIV was shown to modify OGT dynamically in response to KCl depolarization in a calcium influx dependent manner in a neuroblastoma cell line (3). This phosphorylation was accompanied by an increase in OGT enzymatic activity, which was demonstrated both *in vitro* with an activity assay and by an increase in *O*-GlcNAc modified protein staining with an *O*-GlcNAc antibody (RL2). Furthermore, a CaMKIV inhibitor, as well as CaMKIV shRNA was used to

show that CaMKIV inhibition or depletion eliminates OGT phosphorylation after KCl. Although the site of CaMKIV phosphorylation of OGT was not identified, this was the first study to characterize a potential mechanism for OGT activation.

A more recent study demonstrated that AMPK phosphorylates OGT at T444 and activation of AMPK alters OGT substrate specificity and induces nuclear localization (2). Furthermore, OGT nuclear localization was shown to increase *O*-GlcNAcylation of nuclear proteins, as well as acetylation of L9 of Histone 3 in myotubes. This suggests that AMPK modification of OGT may play a role in regulating OGT activity on nuclear proteins and may alter epigenetic factors through histone dynamics. AMPK was shown to be activated by *O*-GlcNAc as well, suggesting extensive crosstalk between the two enzymes. Although these two examples provide valuable insight, they are limited in their scope and do not identify the role of these post-translational modifications of OGT in altering *O*-GlcNAcylation of specific substrates, or the functional consequences of these changes.

Given our incomplete understanding of how OGT is regulated, a previous graduate student in our lab, Dr. Jessica Rexach, sought to identify sites of phosphorylation by subjecting OGT overexpressed and purified from SF9 cells, as well as OGT that was phosphorylated *in vitro* by CaMKIV, to mass spectrometry (4). These studies identified several phosphorylation sites, including S993, S994, S481, which are all on or near the C-terminal catalytic domain of OGT. Additional sites near the N-terminus (S151, S298) were also identified. Importantly, phosphorylation of OGT was detected in response to KCl

depolarization in neurons, using radioactive orthophosphate (4). Dr. Rexach further demonstrated that *O*-GlcNAc glycosylation increases upon KCl depolarization in cortical mouse neurons, and that this increase was dependent on calcium influx, and downstream of CaMKII activation. She also showed that overexpression of phosphorylation-deficient S994A and S993A mutant OGT reversed a neurite inhibition phenotype observed when overexpressing wild-type OGT in cortical mouse neurons. This finding suggested that phosphorylation at these sites may alter OGT activity, as it affects neurite outgrowth differently than wild-type OGT overexpression.

In order to better understand this phenomenon, we sought to generate phosphorylation-specific antibodies to facilitate the detection of OGT phosphorylation at these sites and investigate the mechanisms regulating these phosphorylation events. Phosphorylation-specific antibodies have been used extensively to investigate the role of phosphorylation on proteins in response to cellular signaling (5). For instance, phosphorylation-state specific antibodies for amyloid precursor protein (T654, S655) have shown that phosphorylation at specific sites are regulated in a cell-cycle dependent manner (6). Furthermore, phospho-specific antibodies were used to demonstrate that synapsin I is dynamically phosphorylated in response to brain-derived neurotrophic factor and nerve growth factor stimulation through a MAP kinase signaling pathway (7). This phosphorylation of synapsin I results in reduced G-actin polymerization and may modulate synaptic plasticity in response to neurotrophin signaling. These studies

illustrate the utility of developing phosphorylation-specific antibodies to facilitate mechanistic studies of OGT regulation.

Furthermore, to evaluate whether phosphorylation-deficient mutants S994A and S993A exhibit changes in their catalytic activity, we apply several OGT activity assays that were previously developed. A tried and true radioactive assay has been used in the past to evaluate OGT in a variety of contexts, from complex lysates to purified enzyme (3, 8). The assay relies on tritiated UDP-GlcNAc as a substrate donor for OGT and incorporation of tritiated GlcNAc onto a model casein kinase II peptide substrate is quantified by scintillation counting. Furthermore, a small molecule Thorson sensor was previously shown to be sensitive to UDP concentrations, so we reasoned that this sensor could be used to monitor the liberation of UDP as a proxy for OGT enzymatic activity (9, 10). This small molecule sensor relies on zinc-mediated coordination of UDP to induce a change in fluorescence intensity. Finally, a previously developed FRET probe was used to assess changes in OGT activity in live cells in response to cellular stimuli (11, 12). The FRET probe consists of a construct with the following components: fluorescent protein, casein kinase II peptide substrate, *O*-GlcNAc binding lectin, fluorescent protein. As the casein kinase II substrate becomes *O*-GlcNAcylated, the lectin binds the peptide, bringing the two fluorescent proteins closer together, which increases FRET efficiency. It was shown previously that this process is reversible when OGA removes *O*-GlcNAc from the substrate. The results of these various assays are described in the following sections.

3.2 Results

3.2.1 Neurite Outgrowth

Previously, neurite outgrowth studies demonstrated that S993A and S994A mutant OGT proteins produced longer neurites compared to wild-type OGT overexpression (4). Importantly, this study used different plasmid backbones to express the mutant and wild type OGT proteins. We wanted to use the same backbone for both proteins so that protein expression levels would be the same, thus allowing for a more valid comparison of the effects of S993A, S994A, and WT-OGT overexpression. E15 cortical mouse cultures were dissected and electroporated separately with either D925A OGT (catalytic dead control), WT-OGT, S994A OGT, or S993A OGT expression constructs. The control for our experiments was a catalytic dead form of OGT (D925A), as the GFP construct originally used as a control was potentially toxic to the neurons.

The neurite outgrowth assay shows that WT-OGT overexpression in neurons causes a decrease in total neurite length, compared to a control expressing catalytic dead OGT (Figure 3.1). Importantly, overexpression of either S993A or S994A OGT rescues this phenotype.

3.2.2 Generation of phosphorylation-specific antibodies

After discovering the effect of the S994A mutant on neurite outgrowth, we decided to investigate the site further by generating phosphorylation-specific antibodies which would facilitate *in vitro* studies of OGT phosphorylation in neuronal lysates. One month following the immunization of rabbits with OGT peptides containing phosphorylated S993 or S994 sites, sera were collected and

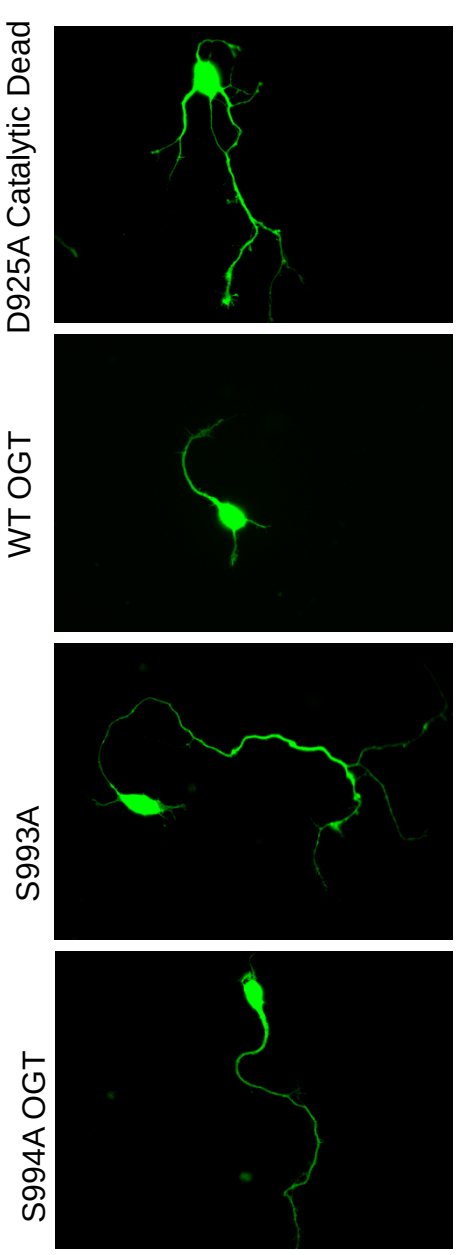

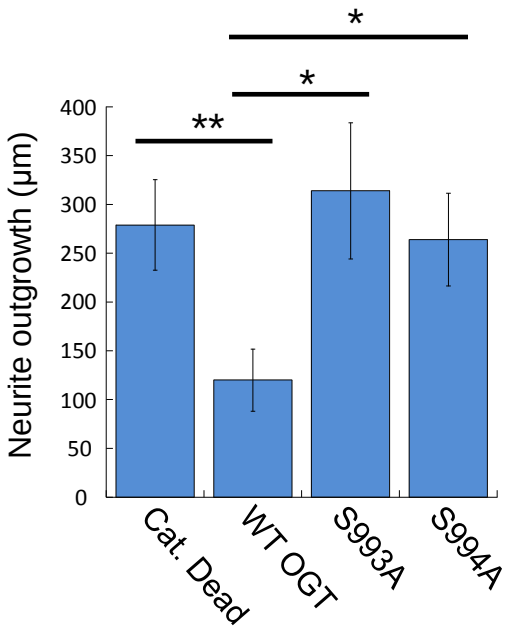

Figure 3.1: OGT overexpression inhibits neurite outgrowth, and mutant OGT expression rescues this phenotype. OGT constructs were electroporated into neurons, and neurite outgrowth was quantified after 3DIV. A catalytic dead form of OGT was used as a control. Expression of wild-type OGT inhibits neurite outgrowth, whereas expression of serine to alanine mutants of phosphorylation sites (S993, S994) has no effect on neurite outgrowth. This finding suggests that phosphorylation of OGT at these sites may regulate its activity.

dot blots were used to evaluate the specificity of the antibodies (Figure 3.2). The dot blots were spotted with 50, 25, or 5ug of the peptide antigens, which contained either phosphorylated serine residues at S993 (PS993), S994 (PS994), or neither (S993/4). Sera demonstrated improved specificity for desired antigens over time. The best samples were taken further, and antibodies were purified with sepharose columns containing the peptide antigen of interest.

After affinity purification, antibody was concentrated and re-evaluated with dot blots, and show specific binding to only the desired peptides (Figure 3.3A). Antibodies were then used to blot cortical lysates. It is evident that these purified antibodies have several non-specific interactions (Figure 3.3B). In order to confirm that the antibodies recognize OGT, an immunoprecipitation (IP) of exogenously expressed FLAG-OGT with FLAG beads was performed and the purified phosphorylation-specific antibodies were evaluated by western blot (Figure 3.3C). None of the phosphorylation-specific antibodies were able to detect FLAG-OGT.

3.2.3 OGT Activity Assays

Demonstrating a significant change in OGT enzyme activity after mutation of a phosphorylation site would strongly suggest that phosphorylation of OGT at these sites regulates its activity. We attempted two different strategies to assess OGT enzymatic activity in vitro. First, a previously developed radioactive activity assay was used to assess OGT activity in vitro after overexpression in 293T cells and purification with FLAG beads (3, 8). Reproducibly, S994A/E mutations in OGT resulted in a significant decrease in OGT activity, comparable to a catalytic

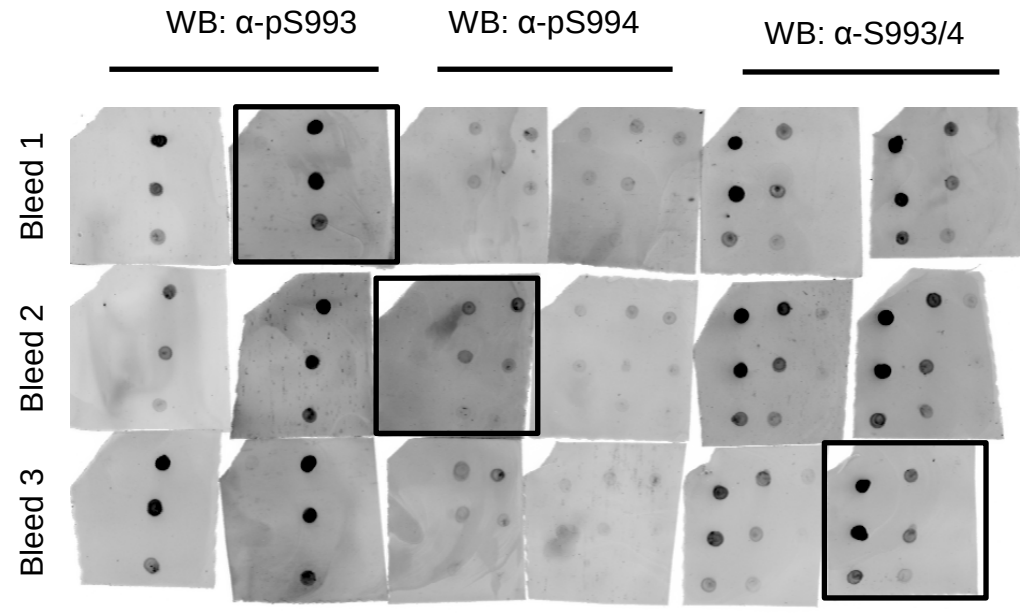

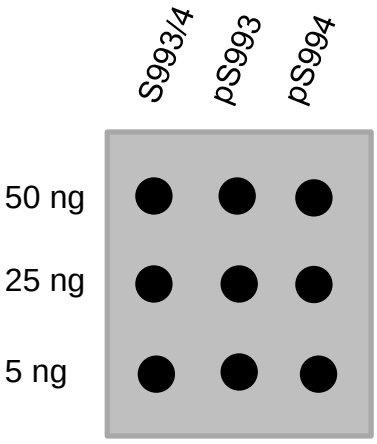

Figure 3.2: Phosphorylation-specific antibodies show changing specificity and affinity depending on sera collection date. Dot blots were used to assess specificity of phosphorylation-specific antibodies. Peptides of either phosphorylated S993, S994, or non-phosphorylated S993&4 were adsorbed to nitrocellulose membranes at 50, 25, and 5 ng per spot. Sera collected from three separate bleeds were used to assess specificity and affinity. The most promising bleeds were purified to isolate phospho-specific antibodies for validation on purified OGT.

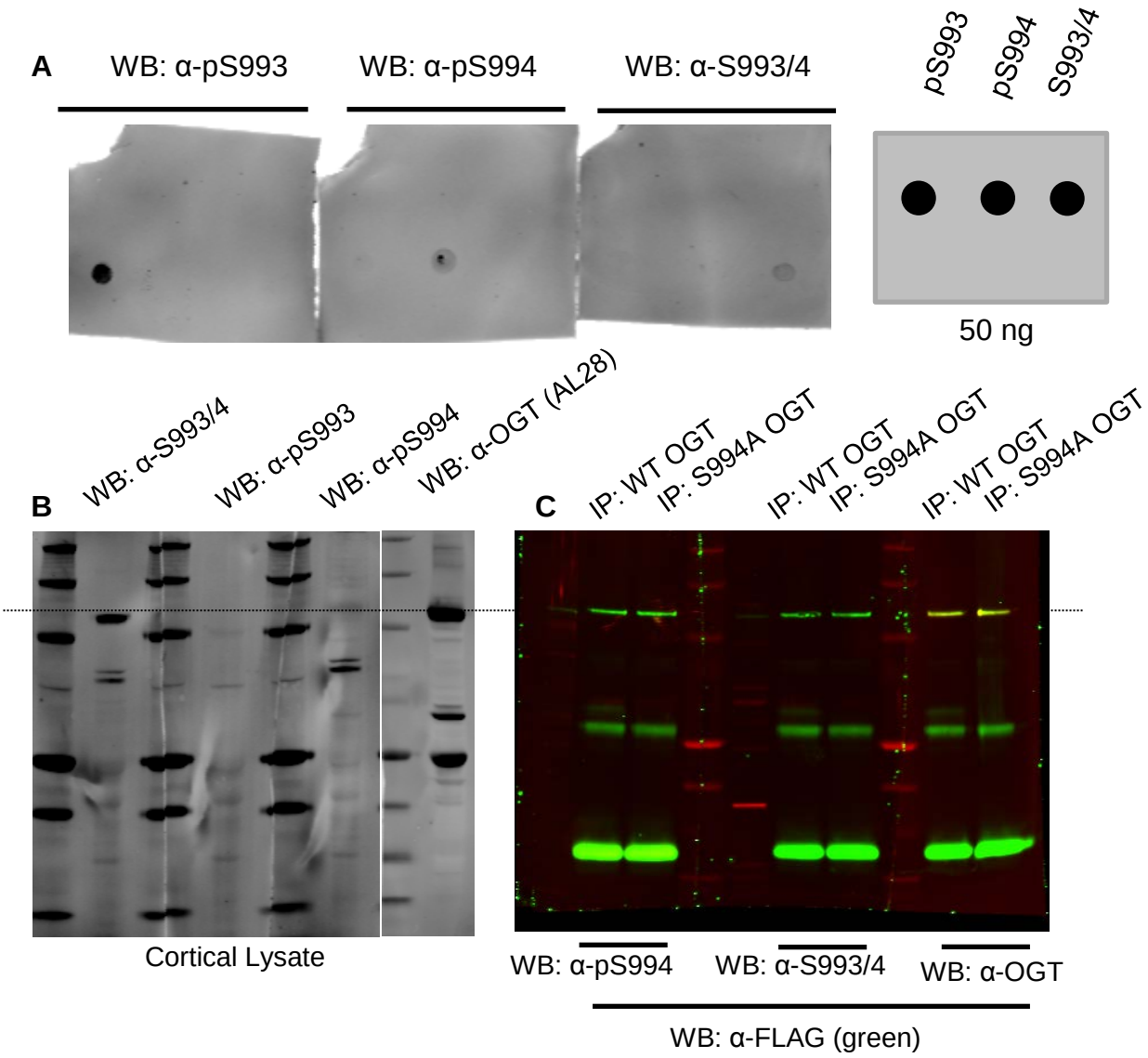

Figure 3.3: Purified phospho-specific OGT antibodies have high specificity for OGT peptides but not full length protein. Dot blots were used to assess specificity of phosphorylation-specific antibodies after affinity purification. (A) Peptides of either phosphorylated S993, S994, or non-phosphorylated S993&4 were adsorbed to nitrocellulose membranes at 50 ng per spot. (B) Purified antibodies were used to probe cortical lysate, and s993/4 antibody bound a protein at the molecular weight of OGT. (C) Immunoprecipitation of WT OGT or S994A OGT with FLAG antibody probed by α-pS994 and α-S993/4 shows no colocalization with FLAG , suggesting that the antibodies may not recognize full length OGT. It is unclear why α-S993/4 antibody recognized OGT out of lysate in B but not IP OGT in C.

dead mutant (D925A) of OGT (Figure 3.4). Because we are most interested in the role of this regulatory modification in response to neuronal depolarization, we moved into neurons to see if KCl depolarization affected OGT activity. In neurons, initial studies have shown that S994A mutant OGT is indistinguishable from wild-type OGT. More replicates are needed to draw conclusions, and optimization of assay conditions would improve signal to noise, which is likely affecting these initial results.

In an effort to improve the throughput of the OGT activity assay, a Thorson probe was used to assess UDP concentration, which is a product of OGT enzymatic activity (9, 10). Optimization of the assay revealed that detergent, DTT, and FLAG beads attenuated Thorson probe signal, and these normal components of the OGT activity assay were omitted. Unfortunately, after multiple rounds of optimization, no response to OGT activity was observed using the Thorson sensor (Figure 3.5).

3.2.4 FRET probe

In order to evaluate changes in OGT activity either in response to cellular signaling or modulation of post-translational modifications, we sought to utilize a FRET assay that would respond to dynamic changes in OGT activity in live cells. A previously developed FRET probe was expressed initially in 293T cells, to confirm efficient expression (11, 12). Distinct fret probes were successfully shown to target to the nucleus and plasma membrane, as well as generally throughout the cell. FRET probe was then extended to N2A cells, and neurons (Figure 3.6).

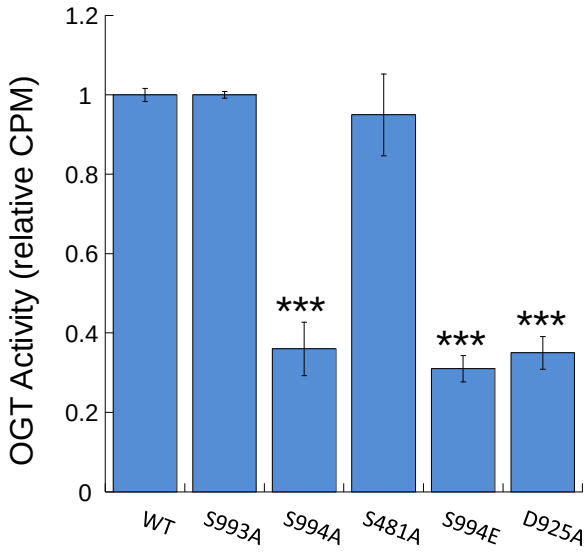

Figure 3.4: In vitro radioactive OGT activity assay shows decrease in S994A mutant activity comparable to a catalytic dead OGT mutant. OGT constructs were transfected into 293T cells and immunoprecipitated with FLAG beads. Activity was measured by incorporation of tritiated GlcNAc onto a casein kinase II peptide. S994A and S994E mutant OGT show decreased activity, comparable to a catalytic dead OGT mutant, D925A. N=3. ***-P<0.00005. Ongoing studies are investigating changes in the activity of OGT and OGT mutants in N2A cells upon neuronal depolarization.

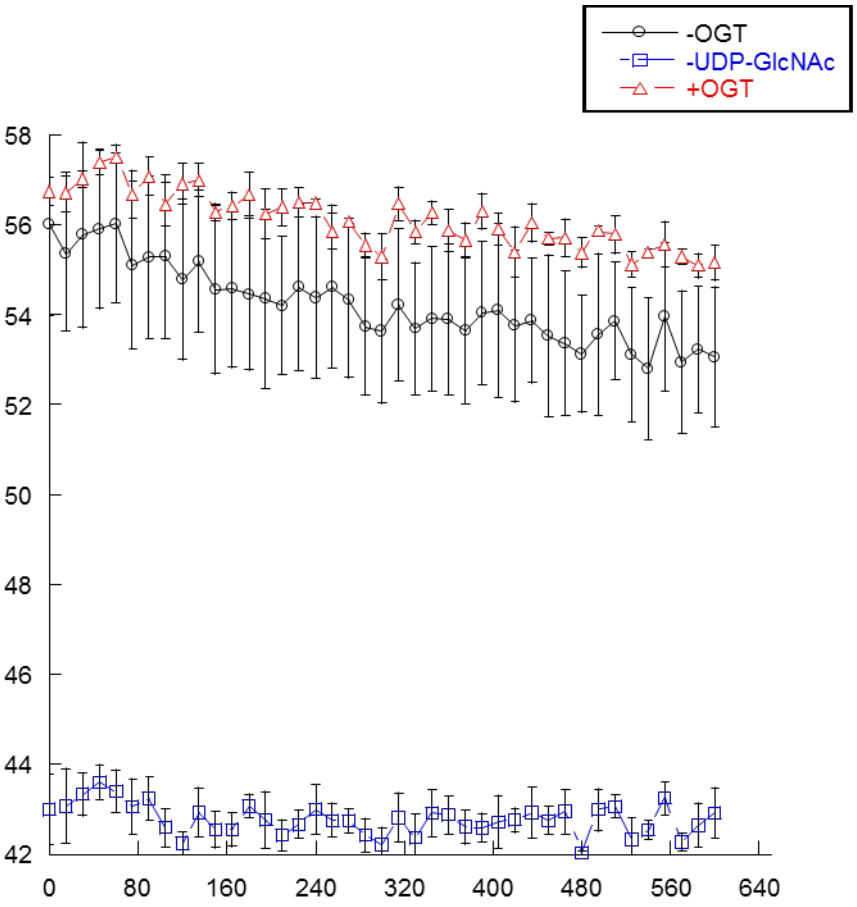

Figure 3.5: Thorson probe does not respond to OGT activity. N2A cells with and without wild-type OGT overexpression were lysed, and FLAG beads were used to immunoprecipitate exogenous OGT. Following elution off beads with 3X FLAG peptide, OGT activity was assessed with the Thorson sensor, which is sensitive to UDP concentration. Compared to non-transfected control, WT OGT samples had no apparent effect on Thorson probe fluorescence. Minus UDP-GlcNAc control had lower overall fluorescence and no change as well.

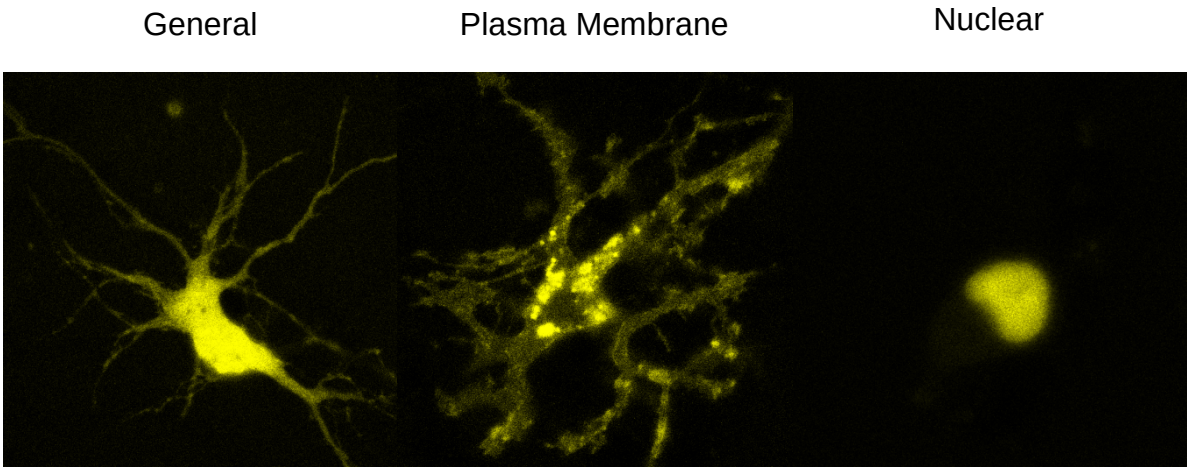

Figure 3.6: FRET probes localize to the plasma membrane and nucleus. General, plasma membrane targeted, and nuclear targetd O-GlcNAc FRET probes show expected distribution after expression in neurons.

After confirming efficient targeting and expression, N2A cells were transfected with the general FRET probe and FRET efficiencies were analyzed in response to KCl depolarization. Previous work established that OGT is activated and *O*-GlcNAcylation increases dynamically in response to KCl depolarization, as quickly as 2-5 minutes after treatment. Upon depolarization, a general increase in fluorescence for both CFP and YFP are observed, and the ratio of YFP to CFP is not significantly changed (Figure 3.7) in the raw signal intensities. Using the RiFRET program to visualize changes in FRET efficiencies, it is apparent that certain areas of the cell display increases in FRET efficiency upon KCl depolarization, but these changes are small and are likely averaged out when quantifying total raw signal intensities. As a control, unglycosylatable FRET probe was shown to be unresponsive to KCl depolarization (Figure 3.8). Furthermore, treatment with PBS instead of KCl also showed no changes in FRET probe fluorescence.

3.3 Discussion

Overexpression of wild-type OGT was shown previously to result in decreased neurite outgrowth, and S994A OGT was shown to rescue this phenotype. In this study, these results were replicated, and S993A was also shown to rescue the wild-type OGT overexpression phenotype. Dr. Rexach had previously shown that glycosylation of CREB represses CREB-regulated gene transcription. Many of these transcriptional changes contribute to neuronal growth, and thus increased *O*-GlcNAcylation could potentially inhibit neuronal growth through a CREB dependent mechanism. Dr. Rexach also showed

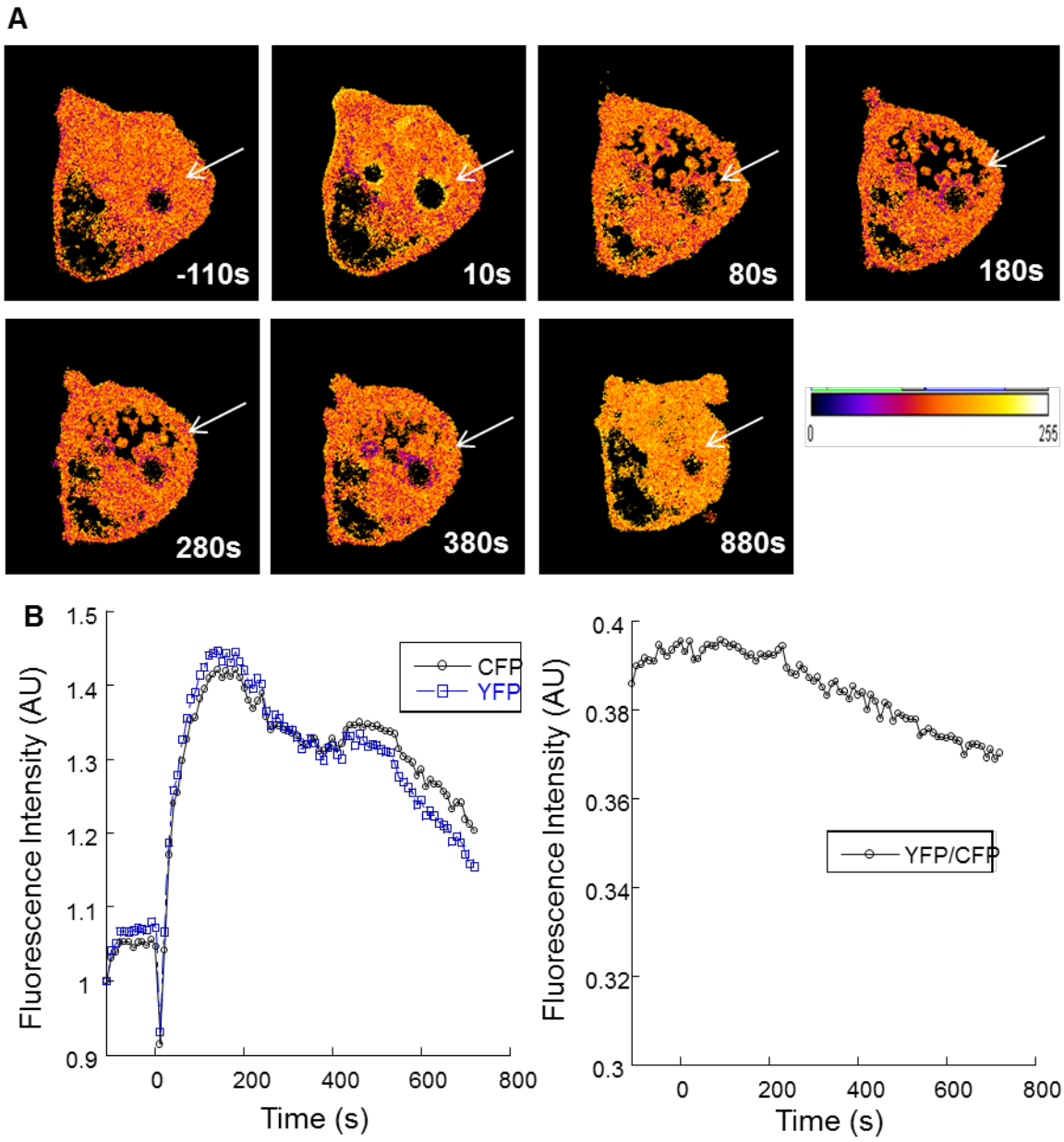

Figure 3.7: FRET probe shows changes in OGT activity after KCl depolarization. (A) Timecourse shows dynamic increases in FRET resulting from increased OGT activity after KCl depolarization (t=0). (B) Quantification of raw CFP and YFP signal, and ratio of YFP to CFP. Overall FRET ratio decreases but certain regions of the cell show increased FRET (arrows).

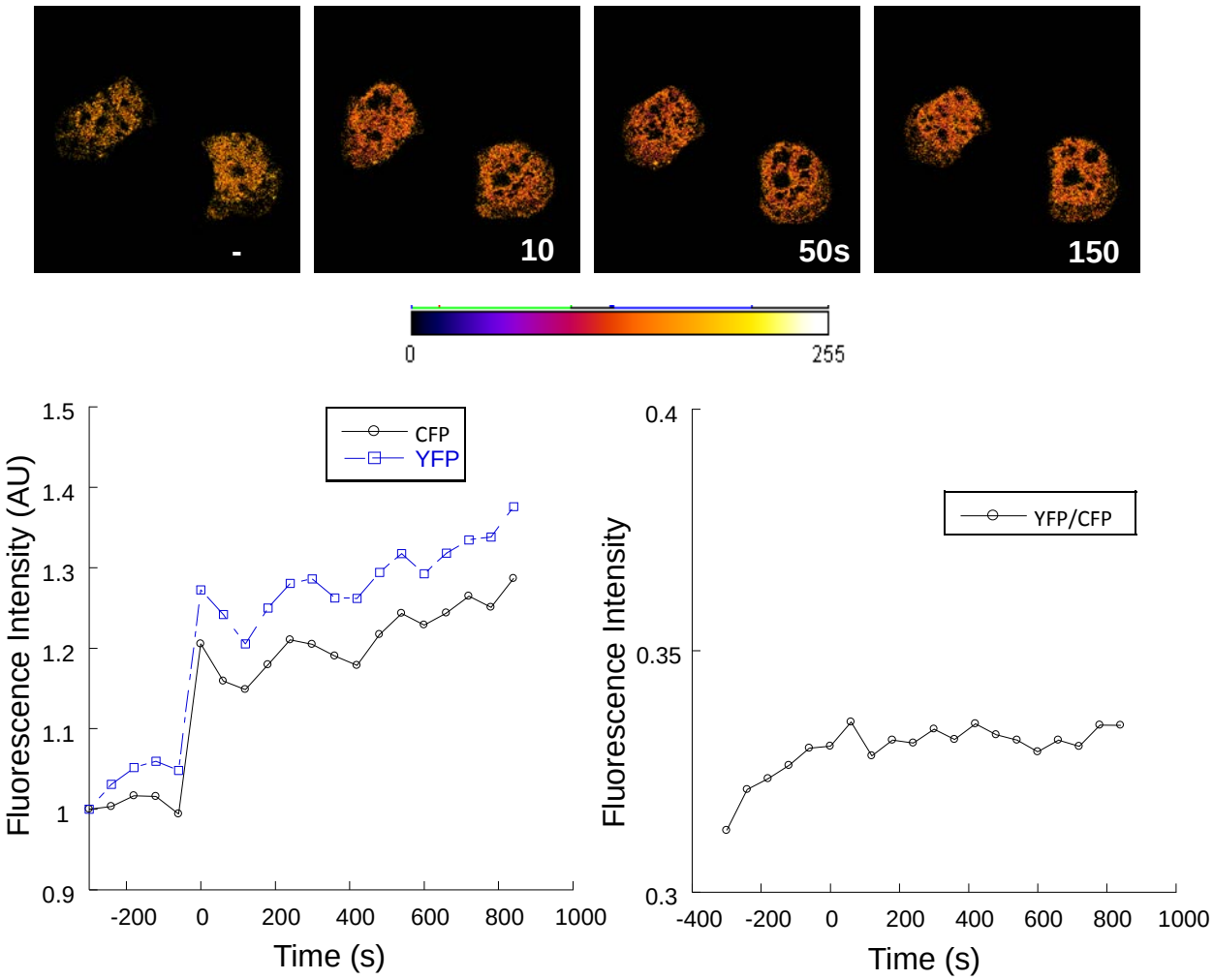

Figure 3.8: Control FRET probe shows no changes in OGT activity after KCl depolarization. Timecourse shows no change in FRET efficiency after KCl depolarization (t=0) with control (unglycosylatable) FRET probe.

that the addition of CREB siRNA eliminated the reduction in neurite outgrowth after wild-type OGT expression. Given these findings, our working hypothesis is that phosphorylation at S993 or S994 activates OGT, and that S993A and S994A constructs are less active, or unable to be activated.

To study these phosphorylation sites further, phosphorylation-specific antibodies were generated, to aid in the detection of these modified forms of OGT in response to specific cellular stimuli. These antibodies would allow for the use of specific kinase inhibitors (such as CaMK inhibitors) to probe for the dependence of kinases for phosphorylation of OGT. Antibody specificity was determined to be excellent with dot blot assays, especially after affinity purification on phospho-peptide sepharose columns. S993/4 antibody appeared to detect OGT in complex cortical lysates; however, none of the antibodies appeared to detect OGT in purified, immunoprecipitated samples. It is possible that some form of cellular induction is required to generate sufficient quantities of phosphorylated OGT to provide enough sample for detection.

As the phosphorylation-specific antibodies continue to be evaluated, a variety of methods to examine OGT activity in vitro were used in an attempt to quantify possible changes in mutant OGT activities. In the most robust OGT activity assay, the radioactivity assay, S994A/E mutants were shown to have significantly reduced activity, comparable to that of catalytic dead (D925A) OGT in 293T cells. Although this cell type is not very relevant to our neurite outgrowth study, it provides promising evidence that these phosphorylation sites have a regulatory role. Attempts to extend this study in neurons were unsuccessful, due

to limitations in the amount of OGT that can be transfected into neurons via electroporation. Isolation of small amounts of OGT via FLAG beads provides many opportunities for experimental error, and represents a significant challenge when assay signal to noise is not ideal. Moving forward, it may be important to optimize the assay conditions, or find strategies to increase the amount of OGT that can be isolated from neuronal samples to yield more reproducible data in neurons.

The Thorson sensor assay clearly showed that with the current assay conditions, no change in UDP concentration is detectable. It is likely that this assay is not sensitive enough to detect OGT activity in this manner, and although it would greatly improve the throughput of OGT activity assessment, this assay does not appear to be a viable option.

Finally, the FRET probe was shown to respond to KCl depolarization, and both treatment with PBS, and KCl depolarization of a non-glycosylatable control probe yielded no response. Despite the observed change in FRET efficiency after KCl depolarization, the dynamic range of the probe is limited in its current state, and likely would require increasing FRET probe expression, or more rigorous data analysis to serve as a useful assessment of OGT activity in live cells. Using the RIFRET program, it appears that certain regions of the cell has significant increases in FRET efficiencies upon KCl depolarization; however, it is unlikely that these changes are large enough to effectively serve as a proxy for OGT activity in live cells. Furthermore, even if these changes increased after optimization, assessment of mutant OGT proteins would only be possible if

endogenous wild-type OGT was eliminated in the cells. A more tractable target would be to treat the cells with specific perturbations, such as calcium chelators or pathway inhibitors, to see whether they have an effect on OGT activity rather than point mutations.

3.4 Conclusion

We have begun to characterize the significance of the S993 and S994 phosphorylation sites of OGT and our results support previously acquired data which show that overexpression of S993A or S994A OGT rescues the inhibition of neurite outgrowth observed after wild-type OGT overexpression. Phosphorylation-specific antibodies were generated but are currently limited in their utility as they specifically recognize their peptide antigens, but not full-length OGT. Evaluating additional production bleeds or optimizing the affinity purification procedure may improve antibody characteristics. Furthermore, it will be important to evaluate the antibodies in response to a cellular stimulus that is expected to enhance OGT phosphorylation, such as KCl depolarization. New antibodies could be generated at Caltech's hybridoma facility, where monoclonal antibodies could be tested for specificity and affinity to full-length phosphorylated protein. A significant challenge would be to obtain pure phospho-OGT for screening purposes, but if possible this may provide a viable strategy moving forward.

The radioactive activity assay shows that S993A and S994A mutant forms of OGT have a significant reduction in OGT activity, compared to wild-type in 293T cells. This study will be pursued in neurons, and enhancing reproducibility

of the assay by increasing the signal to noise ratio is a key first step. Both the Thorson and FRET probe assays do not appear to be sufficiently sensitive to reliably assess OGT activity, and would need to be optimized further to have utility in this capacity. One possibility is to acquire another *O*-GlcNAc fret probe that is based on CaMKII dynamics that has recently been described (13).

If it were possible to demonstrate that mutant (S994A) OGT activity was not changed by KCl depolarization in neurons or neuron-like cells, and that wild-type OGT activity was induced by this stimulus, this would support our hypothesis that phosphorylation of OGT at S994 activates it downstream of KCl depolarization, calcium influx, and CaMKII activation.

3.5 Methods

3.5.1 Neurite outgrowth assay

Cortical neurons were isolated from E15 C56Bl6 mice and electroporated with 10ug of pLEMPRA WTOGT, D925A OGT, S994A OGT, or S993A OGT with the AMAXA nucleofector system (program K009). After electroporation, the neurons were plated on poly-DL-lysine coated coverslips at a density of 25,000 neurons / cm^2 in Neural Basal Medium, 10% FBS, 2 mM Glutamax-l (Invitrogen). Four days later, the cells were fixed with 4% paraformaldehyde 4% sucrose in PBS for 20 min at RT, washed twice with PBS, once with H2O, mounted onto glass slides using Vectashield mounting medium with DAPI, and sealed with clear nail polish. Cells were imaged using a Nikon Eclipse TE2000-S inverted microscope, and images were obtained with Metamorph software using a 40x

objective. Neurite lengths were quantified using NeuronStudio (Version 0.9.92, CNIC, Mount Sinai School of Medicine).

3.5.2 Generation of phosphorylation-specific antibodies

Purchased peptides corresponding to amino acids 989-998 were synthesized with phosphorylated serines at 993 or 994, or non-phosphorylated at both sites (pS993, pS994, S993/4). Peptides were conjugated to thyroglobulin (Pierce) and sent off to Cocalico labs for antibody production. Peptides were injected into rabbits on days 1, 14, 21, and 35 and monthly thereafter. Test bleeds were collected after one month and production bleeds were collected once a month thereafter.

3.5.3 Dot blots and Westerns

Sera were tested by dotting 50, 25, or 5 ng of peptide onto nitrocellulose membrane and sera were blotted with the western protocol in Chapter 2. Sera were purified by anti IgG conjugated to sepharose first, following manufacturer's protocol (Pierce). Then, peptides were conjugated to sepharose beads with a terminal cysteine, following manufacturer's protocol (Pierce). Purified antibodies were concentrated to 1 mg/ml.

3.5.4 KCl depolarization of neurons

Neurons were silenced with 1uM tetrodotoxin (TTX) and 10 uM D-AP5 for 12 hours before addition of 55mM KCl. Cells were then quickly washed in ice cold PBS and lysed on plate in 2% SDS with protease inhibitors and phosphatase inhibitors. Lysates were sonicated twice at 20% power for 10

seconds, and centrifuged at 20kg for 5 min to pellet cellular debris. Protein concentrations were determined by BCA assay (Pierce).

3.5.5 OGT Activity Assays

Radioactive asasys were run essentially as described previously. Briefly, cells were lysed in 20mM Tris 7.5, 10mM MgCl2, 1mM EDTA, PMSF/PIC, 1mM Na2VO4, 10mM NaF, in the presence or absense of 1% NP-40. Lysates were spun down at max G's for 10 min, and supernatants were incubated with FLAG beads for 1 hr at 4C, end over end. FLAG beads were washed 1x in lysis buffer, and then once more in transferase assay buffer (TAB), 20mM Tris 7.5, 10mM MgCl2, 1mM EDTA, 1mM DTT. An aliquot of FLAG beads was reserved for WB to quantify OGT protein levels in each sample. Activity assays were run in 40ul of TAB, with 1mM casein kinase II peptide (genscript, PGGSTPVSSANMM) and 0.2-0.4 uCi tritiated UDP-GlcNAc (Perkin Elmer, NET434050UC). Reactions were run at RT for 2 hours end over end, quenched with 50mM formic acid, 500mM NaCl, and peptides were isolated with C18 spin columns (Pierce 89873). Peptides were eluted into 7mL of aqueous compatible scintillation fluid, and counted. Samples were run in triplicate whenever possible.

3.5.6 FRET Assay

293T, N2A, or neurons grown on glass bottom plates (In Vitro Scientific) were transfected with various FRET probe constructs, allowed to grow for 2-3 days and imaged. At each time point, three images were taken: CFPex, CFPem; CFPex, YFPem; YFPex, YFPem. Generally images were acquired with the 63X objective on a Zeiss LSM 700. Time courses were taken every 10s to 1m and live

cells were imaged for 2-5 min before the addition of KCl (55mM final concentration). Typically, 1mL of the plating medium was taken up into a bulb pipette along with KCl, and expelled into the dish at the appropriate time. Images were analyzed in ImageJ (NIH) and intensities for CFP and YFP (CFPex) were quantified. The RiFRET plugin was used to visualize the changes in FRET efficiencies.

3.5.7 Thorson Assay

FLAG-tagged OGT was expressed and purified as described in OGT activity assays. Following immunoprecipitation, OGT was eluted off FLAG beads with 3X FLAG peptide (Sigma, F4799) at 100 ug/mL with 3 elutions of 10uL each for 30uL of beads. 2uL was saved for a western blot to quantify protein levels. Reaction conditions were as follows: 50mM Hepes 7.5, 6 mM MgCl2, 0.6 mM ZnCl2, 2.5 uM Thorson sensor, 1 mM casein kinase II peptide, 10 uL eluent from OGT IP. When ready to read, UDP-GlcNAc was added to a final concentration of 200 uM and plates were read at 488 nm.

3.6 References

1. Shafi R IS, Ellies LG, O'Donnell N, Marek KW, Chui D, Hart GW, Marth JD. (2000) The O-GlcNAc transferase gene resides on the X chromosome and is essential for embryonic stem cell viability and mouse ontogeny. *Proc Natl Acad Sci U S A.* 97(11):5735-5739.
2. Bullen JW*, et al.* (2014) Cross-talk between two essential nutrient-sensitive enzymes: O-GlcNAc transferase (OGT) and AMP-activated protein kinase (AMPK). *The Journal of biological chemistry* 289(15):10592-10606.
3. Song M KH, Park JM, Kim SH, Kim IH, Ryu SH, Suh PG. (2008) o-GlcNAc transferase is activated by CaMKIV-dependent phosphorylation under potassium chloride-induced depolarization in NG-108-15 cells. *Cell Signal.* 20(1):94-104.
4. Rexach JE (2010) PhD Dissertation.
5. Jczernik A*, et al.* (1991) [23] Production of phosphorylation state-specific antibodies. *Methods in enzymology* 201:264-283.
6. Oishi M*, et al.* (1997) The cytoplasmic domain of Alzheimer's amyloid precursor protein is phosphorylated at Thr654, Ser655, and Thr668 in adult rat brain and cultured cells. *Molecular Medicine* 3(2):111.
7. Jovanovic JN*, et al.* (1996) Neurotrophins stimulate phosphorylation of synapsin I by MAP kinase and regulate synapsin I-actin interactions. *Proceedings of the National Academy of Sciences* 93(8):3679-3683.

8. Kreppel LK & Hart GW (1999) Regulation of a cytosolic and nuclear O-GlcNAc transferase. Role of the tetratricopeptide repeats. *The Journal of biological chemistry* 274(45):32015-32022.

9. Kohira T, Takashima I, Nonaka H, Ojida A, & Hamachi I (2008) Real-time off/on-mode fluorescence assay for enzyme reactions involving nucleoside polyphosphates by use of a xanthene ZnII-Dpa chemosensor. *Chemistry Letters* 37(11):1164-1165.

10. Lee HS & Thorson JS (2011) Development of a universal glycosyltransferase assay amenable to high-throughput formats. *Analytical biochemistry* 418(1):85-88.

11. Carrillo LD, Krishnamoorthy L, & Mahal LK (2006) A cellular FRET-based sensor for beta-O-GlcNAc, a dynamic carbohydrate modification involved in signaling. *J Am Chem Soc* 128(46):14768-14769.

12. Carrillo LD, Froemming JA, & Mahal LK (2011) Targeted in vivo O-GlcNAc sensors reveal discrete compartment-specific dynamics during signal transduction. *The Journal of biological chemistry* 286(8):6650-6658.

13. Erickson JR*, et al.* (2013) Diabetic hyperglycaemia activates CaMKII and arrhythmias by O-linked glycosylation. *Nature* 502(7471):372-376.

Appendix I: Developing Tools to Study OGT

A.1 Introduction

A major goal in the *O*-GlcNAc field is to investigate the role of *O*-GlcNAc transferase (OGT) in cellular signaling events, and to understand the regulation of OGT by TPR mediated interactions or post-translational modifications. This has proven to be quite challenging, because widely used strategies of generating stable knockdown or knockout cell lines for OGT are not possible due to its requirement in proliferating cells (1, 2). As a result, many fundamental questions about OGT biology remain undefined, and the development of new strategies to explore OGT regulation and function is of great importance.

In order to study the significance of the TPR domains in OGT's substrate recognition, it would be useful to develop a system in which endogenous OGT can be completely replaced with exogenously expressed mutant OGT constructs. Ideally, OGT constructs that contain different N-terminal TPR truncations would be expressed in a knockout background. The different enzymatic activities of these mutants would then be evaluated by identifying the proteins that are modified by each mutant. Thus by comparing the *O*-GlcNAc modified proteome between these mutants, we would begin to uncover the role of each TPR domain in the recognition of specific OGT substrates. This study could be further extended to explore other interesting regulatory sites on OGT such as phosphorylation, and to evaluate changes in catalytic activity or substrate specificity resulting from perturbations of regulatory sites.

To develop a model system in which to study OGT, we took advantage of a floxed OGT mouse line that was previously developed (3). These mice have the first exon of OGT flanked with loxP sites, which result in excision of the first exon upon CRE recombinase expression (4, 5). Thus, isolation of cells from these mice and subsequent treatment of the dissociated cultures with CRE expressing lentivirus would allow for the efficient knockout of OGT. With a knockout OGT cell system in hand, we could then express mutant forms of OGT to study the effects of specific domains or PTM's of OGT.

Previously, adenovirus was used to express OGT in cardiomyocytes (6, 7), HeLa cells (2), and HepG2 cells (8). Although adenovirus has been successfully used in many contexts for efficient transfection of primary cells (9-12), it presented challenges to generating OGT mutant constructs that we wished to study. Most importantly, the generation of adenovirus requires several cloning steps with the use of shuttle vectors. As we anticipated the need to produce many mutant forms of OGT to investigate the roles of various TPR domains or post-translational modifications (such as serine to alanine mutants, or serine to aspartate or glutamate), we sought a system that would not require extensive cloning to create each mutant. Furthermore, adenovirus represented a more significant threat for infecting humans, and serious precautions would need to be taken to prevent infections. We turned our attention to the use of lentiviral vectors, which use a single plasmid that can be mutagenized in one step to facilitate the creation of many mutants.

Lentivirus has been used extensively to transfect many different cell types efficiently and with low cytotoxicity (13). This strategy for cellular transfection is especially useful for difficult-to-transfect cell lines such as primary cells and post-mitotic cells such as neurons. Commonly used lentiviral vectors are replication-deficient, which increases their safety tremendously, as they are not able to replicate without the exogenous addition of replication genes in trans (14). Lentiviral vectors have a finite capacity for RNA cargo, although virus has been made successfully with cargo over 18 kb in length (15). Despite this large upper maximum, viral titers decrease semi-logarithmically with increasing vector length, and generating high-titer lentivirus with vectors over 7.5 kb is very challenging in practice (16). Beyond the size of the vector, lentivirus infectivity can be optimized by including a polypurine tract in the transfer vector, harvesting virus at earlier time points, collection in serum-free media, and concentration by ultracentrifugation (17). Thus, although there are size restrictions to lentivirus-mediated transfection, it represents the best option for efficient transfection of neurons.

A.2 Results

A.2.1 Developing a cellular OGT knockout system

We sought to develop an OGT knockout system, to understand the role of the TPR repeats in OGT substrate specificity. Our initial strategy focused on knocking down OGT in human embryonic kidney (HEK293T) cells, because of their overall robust nature. These cells are easily transfected, and thus mutant OGT protein could easily be expressed in this cell type after efficient knockdown.

Previous work in the lab produced a transient OGT knockdown 293T line (OGTkd 293T), which had ~90% knockdown of OGT (Figure 4.1A). This was accomplished by transfecting cells with an shRNA construct that targeted endogenous OGT. Although OGT protein levels were substantially reduced in these cells, global *O*-GlcNAc levels remained significant (Figure 4.1B), as monitored by a chemoenzymatic method that allows visualization of *O*-GlcNAc modified proteins by fluorescence (18). Thus, background *O*-GlcNAc levels were simply too high for this system to be useful.

We then turned our attention to our mouse line that carries a floxed OGT genotype. Transfecting these neurons with CRE recombinase produces true OGT knockout cells, and previous work in the lab showed that these neurons remain viable for weeks. We characterized the time course of OGT knockout in neurons after the addition of CRE recombinase. As shown in Figure 4.2, complete knockout occurs by 10DIV after the addition of CRE recombinase. Two different OGT antibodies, DM17 and AL28, confirmed loss of OGT protein, and anti-*O*-GlcNAc antibody RL2 demonstrated loss of *O*-GlcNAcylated proteins.

In order to efficiently transfect neurons, we attempted to generate OGT expressing lentivirus. Previous attempts in the lab were unable to generate infectious OGT lentivirus, even though production of other lentiviruses expressing proteins such as a CRE was successful. In order to understand why OGT lentivirus was not successful, we generated a catalytic dead form of OGT (D925A) in a lentiviral construct, and were successfully able to infect 293T cells

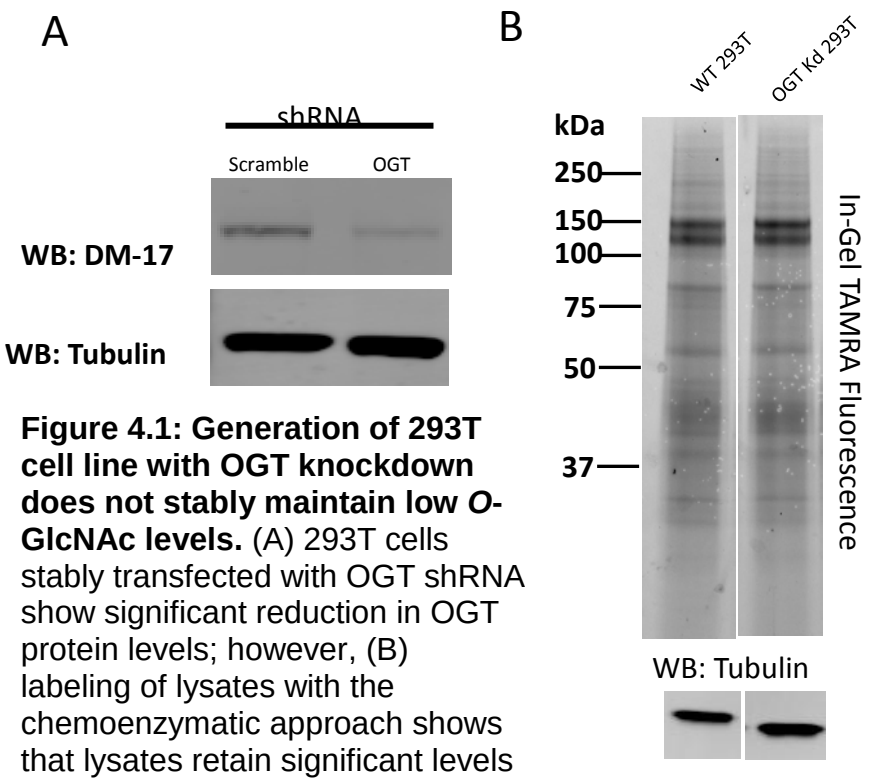

Figure 4.1: Generation of 293T cell line with OGT knockdown does not stably maintain low *O*-GlcNAc levels. (A) 293T cells stably transfected with OGT shRNA show significant reduction in OGT protein levels; however, (B) labeling of lysates with the chemoenzymatic approach shows that lysates retain significant levels of *O*-GlcNAcylated proteins.

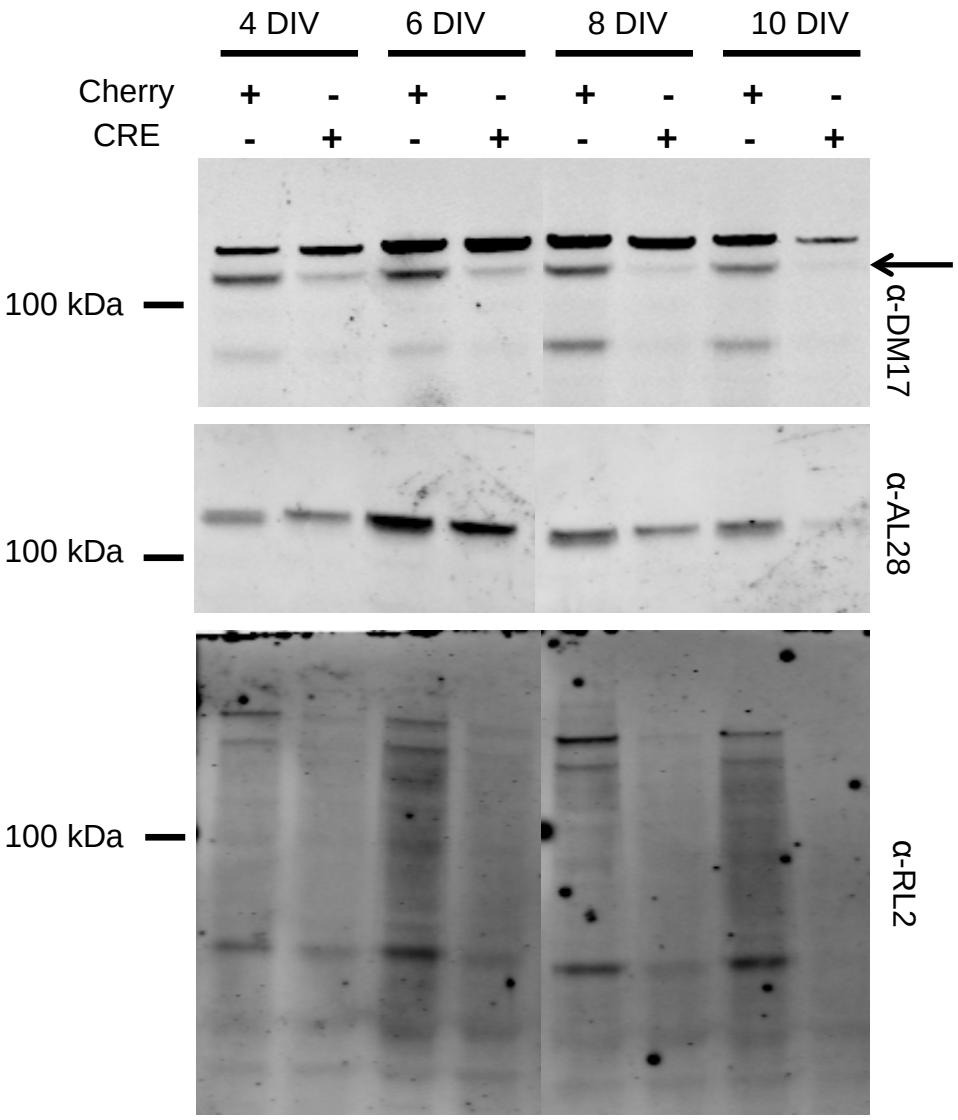

Figure 4.2: OGT knockout with CRE virus in floxed OGT neurons occurs by day 10. Cortical neurons from floxed OGT mice were isolated and treated with either Cherry control or CRE cherry lentivirus. Two different OGT antibodies (DM17, AL28) were used to evaluate OGT protein levels, and shows almost complete loss of OGT protein by 10DIV. Anti-O-GlcNAc antibody RL2 shows loss of O-GlcNAcylated proteins by 10DIV.

(Figure 4.3A). This result suggested that OGT activity during lentivirus generation may contribute to our inability to generate infectious OGT virus.

In an attempt to limit the effects of OGT expression during lentiviral packaging, we transfected virus producing cells with the packaging proteins first, in the absence of the OGT containing lentiviral construct. This was done to allow the packaging proteins to be expressed in the cells before OGT overexpression. Then after 12 hours, the OGT containing lentiviral construct was transfected into the same cells (Figure 4.3B). Some virus was made, and although at very low titer, was able to transfect both 293T cells and a few neurons (Figure 4.3C, D). By optimizing the timing of transfections, it may be possible to produce higher titer virus with this strategy. This was not immediately pursued, because the observed titer was very low.

With the knowledge that OGT catalytic activity was likely repressing virus production, we attempted to develop a strategy to temporarily turn off OGT expression during virus production. We decided to use a CRE-loxP system to introduce a translational stop codon before the OGT gene, which could be excised upon the addition of CRE recombinase (Figure 4.4A).

In this way, the translation of OGT would be off during virus production, but after the virus was produced and used to infect neurons, CRE recombinase could be added to excise the stop codon and allow for OGT expression. A lentiviral construct containing a floxed stop cassette in front of the OGT gene was generated, and it successfully produced virus (Figure 4.4B). Unfortunately, the floxed stop cassette was not efficiently excised from the plasmid by CRE

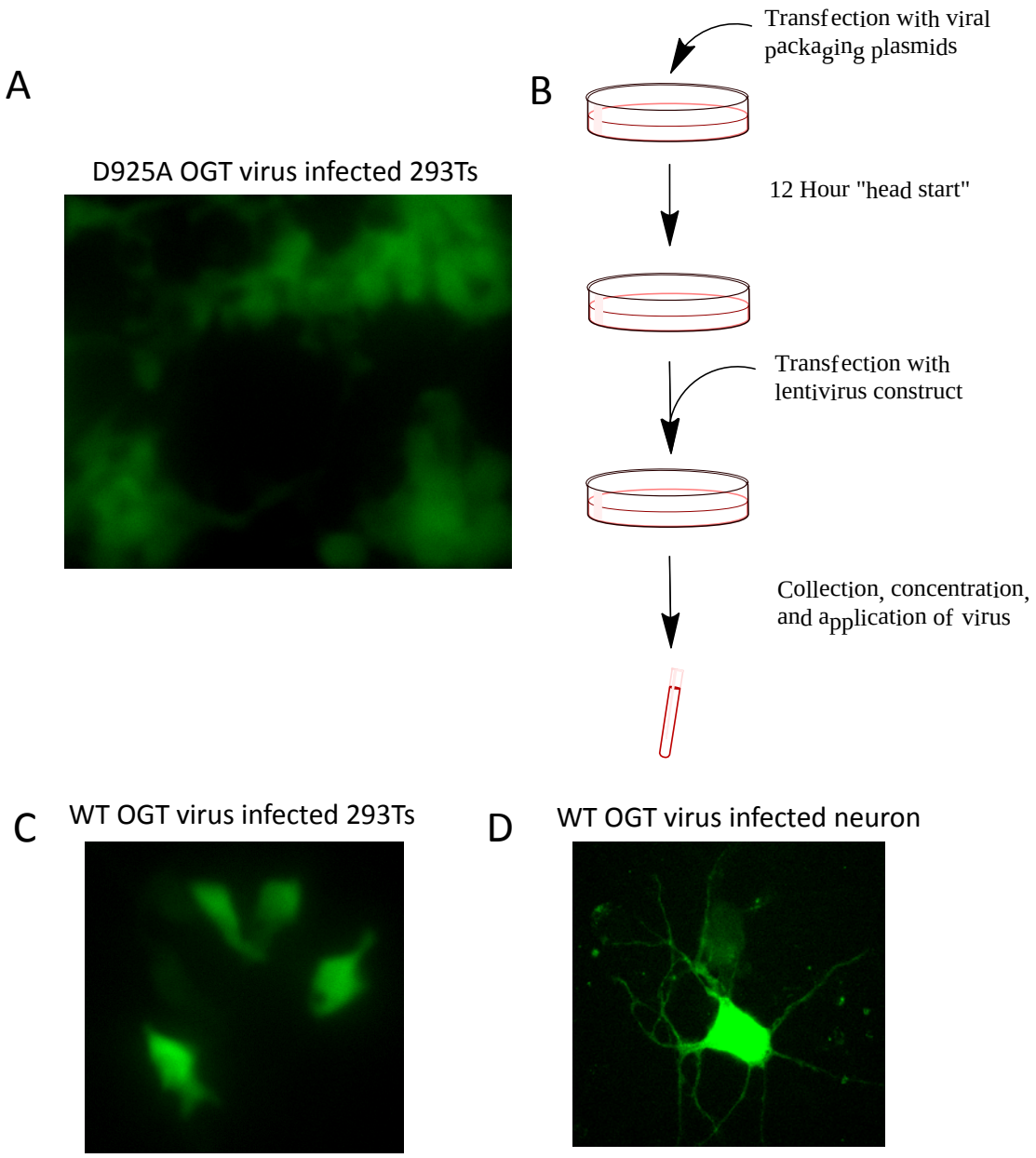

Figure 4.3: Towards generating infectious OGT lentivirus. (A) Successful packaging and transduction of 293T cells with catalytic dead OGT (D925A) suggests that OGT activity during lentivirus packaging inhibits lentivirus production. (B) Strategy to produce lentivirus by allowing viral proteins to be expressed before addition of OGT containing plasmid. (C, D) Wild-type OGT virus successfully transfecting 293T cells and neurons. Unfortunately titers were extremely low.

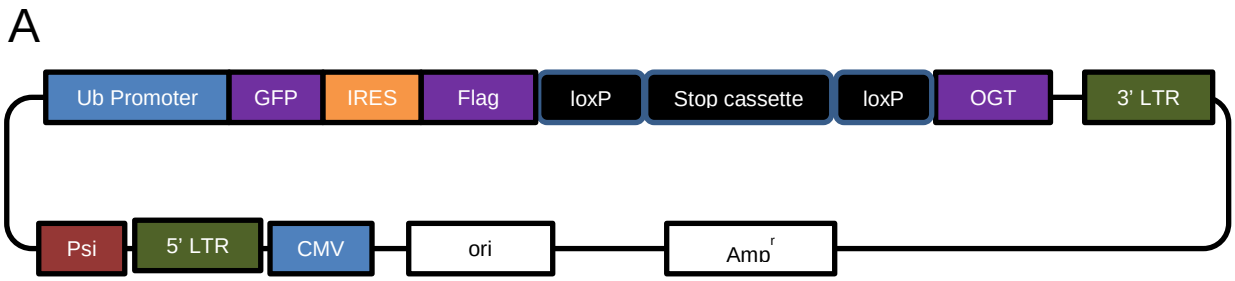

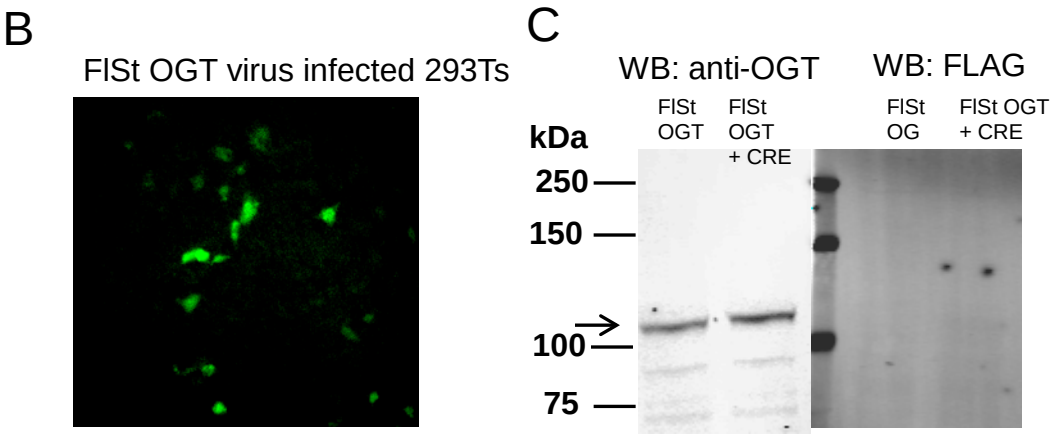

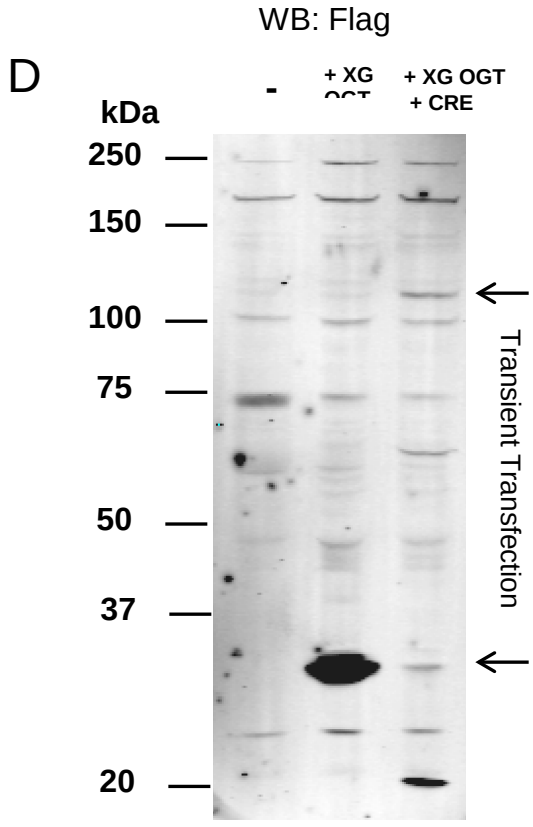

Figure 4.4: Using a floxed stop casette to eliminate OGT expression during virus production . (A) Schematic of floxed stop cassette construct used to turn off OGT expression during virus packaging. OGT is only expressed if CRE recombinase is present to remove the stop cassette. (B) Virus is successfully made from the construct in (A), and infects 293T cells. (C) However, upon the addition of a CRE expressing plasmid, no FLAG tagged OGT is expressed, suggesting a problem with the floxed stop cassette. (D) To avoid possible complications with a stop cassette that is too short to mediate recombination, GFP was inserted between the loxP sites. It was efficiently removed upon addition of CRE, and a species corresponding to FLAG-OGT appeared as well. Unfortunately, this construct never made infectious virus, possibly due to the increased size of the new construct.

recombinase, as no flag-tagged OGT was observed after addition of CRE (Figure 4.4C). We hypothesized that there were not enough intervening base pairs between the two loxP sites to efficiently create the secondary Holliday junction structure necessary. Although it was reported that a minimum of 90 base pairs was required and our stop cassette contained 100 intervening base pairs, the excision did not take place.

Typically, commercially available floxed stop cassettes contain several hundred intervening base pairs, but this was initially avoided because our lentiviral construct was already large and viral titer is known to drop significantly with increased construct size (19). As the small cassette did not work, we then attempted to create a construct with a larger intervening sequence. We generated a construct that contained a floxed GFP with stop codon in front of the OGT gene. When this construct was transiently transfected with or without CRE in 293T cells, we observed the desired products, as visualized by FLAG western analysis (Figure 4.4D), indicating that the stop cassette was efficiently removed by CRE. Unfortunately, this construct did not produce infectious virus, and we suspect this is due to the extra size that the floxed GFP adds to the construct, making it too large.

We also attempted to generate OGT virus by expressing OGT behind a neuronal-specific promoter. We reasoned that if the OGT gene was driven by a neuronal-specific promoter, it would not be expressed in virus producing cells (293FT) and thus expression of virus packaging proteins would not be inhibited. We obtained synapsin and calcium/calmodulin-dependent kinase II (αCamKII)

promoter lentivirus constructs from Dr. Rusty Lansford (Caltech). During initial characterization, these empty virus constructs expressing only GFP efficiently made virus and infected neurons. Unfortunately, we observed GFP expression in our 293FT virus production cells, meaning that these cells must have active transcription of synapsin and αCamKII promoter-regulated genes. This was quite unexpected, but a review of the literature revealed a study that suggested that 293T cells had many characteristics of immature neurons, including expression of neurofilaments L, M and H (12).

A.3 Discussion

The main challenge to generating an OGT knockout cell line is that it is required for cellular proliferation. As a result, efforts to knockdown OGT in 293T cells proved futile, because when colonies that contained greater than 80% knockdown were isolated, after a few passages these cells gradually increased OGT levels. This is believed to occur because OGT expression provides a tremendous growth advantage and thus cells that express more OGT are selected for after each passage. Even in experiments containing cells with over 80% knockdown, *O*-GlcNAc levels seemed to be similar to wild-type cells, and it appears that even 10% of normal OGT protein levels are sufficient to maintain *O*-GlcNAc levels. In order to study the effects of OGT mutations or TPR truncations, a clean background would be needed. As complete knockout is not possible for dividing cells, we turned our attention to post-mitotic neurons.

Floxed OGT mice provide a source of neurons and fibroblasts that have the potential to become OGT knockout. We concentrated on neurons, as they

are post-mitotic and may be less susceptible to toxicity associated with loss of OGT. Cortical neurons were isolated from E15 embryos and were treated with CRE recombinase expressing lentivirus to knock out OGT. Complete loss of OGT protein was show to occur by 10DIV after virus addition, and anti-*O*-GlcNAc antibody showed a loss of *O*-GlcNAc signal by 10DIV as well. This represents a novel strategy to study the effects of OGT loss, which is not normally possible in dividing cells.

Although this system provides a potential source of OGT knockout cells, several challenges needed to be addressed before we could utilize this system experimentally. The largest challenge with using neurons is that they are resistant to most forms of transfection. Typical calcium phosphate or liposomal mediated transfection techniques produce at best 10% transfection efficiencies, and are toxic to the cells. Electroporation of neurons results in transfection efficiencies approaching 30%, but causes extensive cell death (~50%). We sought a transfection technique that would yield high efficiencies, and low cell toxicity. This led us to a lentivirus mediated transfection system, which has been used in many instances to transfect neurons at greater than 95% efficiencies with little cell toxicity (19).

Despite our best efforts, initial attempts to generate OGT lentivirus were unsuccessful. We were able to make high titer lentivirus for CRE recombinase and mCherry, and so we evaluated the differences between the constructs. The only difference was the identity and size of the gene cargo being delivered. Thus, we suspected that inefficiencies in virus generation may be due to the transient

overexpression of OGT during viral production. It has been shown that *O*-GlcNAc modification of the transcription factor SP1 suppresses its activity, which is necessary for expression of lentiviral packaging proteins in certain instances (20). Although SP1 does not regulate the expression of the lentiviral packaging proteins in our system, it is possible that the significant increase in OGT expression during virus production has a similar inhibitory effect on the expression of these proteins, especially in light of the fact that *O*-GlcNAc modification has been identified on many proteins that regulate transcription and translation (21). In order to test this hypothesis, we generated a catalytic dead form of OGT and showed that it was packaged into lentivirus, suggesting that OGT activity during virus production was indeed inhibiting infectious virus production. We attempted to circumvent this issue by transfecting viral packaging proteins 12 hours before OGT construct transfection, to give the viral proteins a 'head start' in the absence of OGT overexpression. This produced some infectious virus that was able to transfect 293T cells and a few neurons, but at incredibly low titers. Optimization of the timing if transfection of each lentiviral construct may improve titers, and should be explored in the future.

Finally, in an attempt to completely turn off OGT expression during virus packaging, a floxed stop cassette was used to introduce a stop codon before the OGT gene, which could be removed upon the addition of CRE recombinase. This construct successfully made OGT virus, but we were unable to remove the stop codon with CRE recombinase. We suspected that this was due to the small distance between the two loxP sites (100bp), and so we introduced a GFP in

front of the stop codon. 293T cells transiently transfected with this construct was shown to only express OGT after the addition of CRE recombinase expressing plasmid. Unfortunately, this construct never made infectious virus, and we propose that the additional 700bp from the GFP inserted may have increased the lentivirus construct to a size that was too large to be incorporated into a virus capsid efficiently. Importantly, cloning lentiviral constructs suffered from frequent unproductive recombination of plasmids and new cloning strategies may facilitate the development of new lentiviral constructs.

A.4 Conclusion

Here we have generated and characterized a neuronal OGT knockout system where efficient knockout of OGT occurs in 10 days and provides a source of OGT-null cells for future studies. Although our initial attempts to produce OGT virus have failed, it remains an important goal because efficient transfection of neurons with OGT mutants would provide us with a strategy to characterize the function of the TPR repeats and other OGT mutants.

Future work will aim to make our floxed GFP construct smaller to facilitate virus production. It may also be possible to find a promoter that expresses in neurons but not in 293T cells, as this would also prevent OGT overexpression during virus production. A tetracycline-inducible OGT could also be used to limit OGT expression in 293T cells, although a fetal bovine serum (FBS) substitute may be necessary as most FBS contain tetracycline. Finally, development of a FLAG-tagged OGT mouse with Cas9 technology is currently being explored in

the lab, and OGT mutants of interest could be introduced into endogenous loci with this technology, in cell lines if not in mice.

A.5 Methods

A.5.1 Production of 293T OGT knockdown cells

OGT shRNA constructs were made as described by manufacturer's protocol (Addgene) and transfected into 293T cells with Lipofectamine 2000 (Invitrogen) using manufacturer's protocol. Cells were then plated at a low density and single colonies were picked, and tested for OGT knockdown. Western analysis was performed as described in Chapter 2, with DM-17 anti-OGT antibody (Sigma).

A.5.2 Chemoenzymatic labeling with GalT

Cells were lysed as described in Chapter 2 in 2% SDS with protease inhibitors, and 200ug of protein was precipitated and labeled at 1 mg/mL as per the Click-It™ *O*-GlcNAc Enzymatic Labeling System instructions (Invitrogen). Briefly, precipitated samples were dissolved to 5 mg/mL in 1% SDS, 20 mM HEPES, pH 7.9 and diluted 5-fold into a buffer with the following final concentrations: 20 mM HEPES, pH 7.9, 50 mM NaCl, 2% NP-40, 5.5 mM MnCl2. UDP-GalNAz **1** (25 µM), and GalT (25 ng/µL) were added, and the samples were incubated at 4 °C for 14-20 h. The samples were subsequently labeled with the TAMRA-alkyne dye **3** as per the Click-It™ TAMRA Glycoprotein Detection Kit instructions (Invitrogen). Samples were then loaded onto Bis-Tris gels and visualized with a Typhoon imager.

A.5.3 Lentiviral constructs

pLEMPRA-FLAG-OGT: OGT shRNA lentivirus vector was constructed by inserting into the pLLX vector (Zhou Neuron 2006) an OGT shRNA DNA hairpin directed against the sequence 5'- GCCTGACAATACTGGTGTT -3'. pLEMPRA FLAG-OGT vector was constructed by removing the MeCP2 sequence and shRNA cassettes from the pLEMPRA-MeCP2 vector (Zhou Neuron 2006) and cloning in the OGT shRNA cassette (from the pLLX vector) and the rat OGT sequence subcloned from pcDNA3.1/HisC-HA3-OGT (a kind gift from Dr. Jeffrey E. Kudlow). To make the pLEMPRA-FLAG-OGT sequence resistant to the shRNA, the five silent mutations were introduced into the CREB sequence indicated in lower case letters: 5'AAGAgCCtGAcAAtACtGGT3'. The different mutants of OGT were created using QuikChange Lightning site-directed mutagenesis kits. The resulting pLEMPRA-FLAGOGT construct expresses FLAG-OGT following an EGFP-IRES sequence. *pLenti-PGK-iCRE-mCherry* and *pLenti-PGK-iCRE-T2a-mCherry*: iCRE-nls from pBOB-CAG-iCRE-SD (Addgene plasmid 12336) was subcloned into a pLenti- PGK-H2B-mCherry vector (a kind gift from Dr. Rusty Lansford, California Institute of Technology) after first removing the H2B sequence. The iCRE was positioned N-terminus to and in-frame with the mCherry to generate a fusion protein. To produce separated CRE and mCherry proteins, pLenti-PGK-iCRE-T2a-mCherry was also generated. CRE-T2a-mCherry was produced by introducing the T2a with GSG linker sequence (GSGEGRGSLLTCGDVEENPGP) into the Xba1 site between the iCRE and mCherry sequence elements of pLenti-PGK-iCRE-cherry. pLEMPRA-

FLAG-floxed stop cassette-OGT: loxP sites were introduced to a PCR product with primers to amplify either a region of 100bp with multiple stop codons in many frames (floxed stop cassette) or a GFP with a stop codon at the end. This insert was cloned behind the FLAG tag and in front of the OGT of pLEMPRA-FLAG-OGT, using an EcoR1 site. pLenti Syn and CamKII constructs were a gift from Dr. Rusty Lansford, Caltech.

A.5.4 Production of lentivirus

Lentivirus was generated using the Invitrogen Virapower kit and corresponding protocol with some modification. 293TF cells were seeded onto tissue culture plates that had been fresh coated with 0.1% gelatin A (Sigma), and grown in DMEM with 10% FBS. At 60% confluence, cells were washed 1x with sterile PBS (Ca/Mg-free) and media was replaced with 5 ml of DMEM media with no additives. At this time, cells were transfected with the lentivirus packaging plasmids pLp1, pLp2, VSV-G and lentivirus vector (1:1:1:1 by weight) according to the Lipofectamine2000 (Invitrogen) instructions but with only half the recommended total DNA used per transfection. After 6h incubation, the cell media was replaced with Complete DMEM solution (DMEM high glucose, 10% FBS, 1 mM Na pyruvate, 1 % nonessential amino acids (GIBCO 1140), penicillin (100 U ml-1), streptomycin (100 mg ml-1, 10 mM Hepes). From this point on, media was collected and replaced every 12 hours for 3 days, filtered through a 0.8 μm syringe filter, tested, and stored frozen at -20 °C.

A.6 References

1. O'Donnell N, Zachara NE, Hart GW, & Marth JD (2004) Ogt-dependent X-chromosome-linked protein glycosylation is a requisite modification in somatic cell function and embryo viability. *Molecular and cellular biology* 24(4):1680-1690.
2. Slawson C*, et al.* (2005) Perturbations in O-linked β-N-acetylglucosamine protein modification cause severe defects in mitotic progression and cytokinesis. *Journal of Biological Chemistry* 280(38):32944-32956.
3. O'Donnell N ZN, Hart GW, Marth JD. (2004) Ogt-dependent X-chromosome-linked protein glycosylation is a requisite modification in somatic cell function and embryo viability. *Mol Cell Biol.* 24(4):1680-1690.
4. Smith AJ*, et al.* (1995) A site–directed chromosomal translocation induced in embryonic stem cells by Cre-loxP recombination. *Nature genetics* 9(4):376-385.
5. Sauer B & Henderson N (1988) Site-specific DNA recombination in mammalian cells by the Cre recombinase of bacteriophage P1. *Proceedings of the National Academy of Sciences* 85(14):5166-5170.
6. Facundo HT*, et al.* (2012) O-GlcNAc signaling is essential for NFAT-mediated transcriptional reprogramming during cardiomyocyte hypertrophy. *American Journal of Physiology-Heart and Circulatory Physiology* 302(10):H2122-H2130.

7. Sujith D*, et al.* (2015) High glucose induces mitochondrial dysfunction independently of protein O-GlcNAcylation. *Biochemical Journal* 467(1):115-126.

8. Perez-Cervera Y*, et al.* (2013) Insulin signaling controls the expression of O-GlcNAc transferase and its interaction with lipid microdomains. *The FASEB Journal* 27(9):3478-3486.

9. Danthinne X & Imperiale M (2000) Production of first generation adenovirus vectors: a review. *Gene therapy* 7(20):1707-1714.

10. Kass-Eisler A*, et al.* (1993) Quantitative determination of adenovirus-mediated gene delivery to rat cardiac myocytes in vitro and in vivo. *Proceedings of the National Academy of Sciences* 90(24):11498-11502.

11. Ruley HE (1982) Adenovirus early region 1A enables viral and cellular transforming genes to transform primary cells in culture. *Nature* 304(5927):602-606.

12. Shaw G, Morse S, Ararat M, & Graham FL (2002) Preferential transformation of human neuronal cells by human adenoviruses and the origin of HEK 293 cells. *FASEB J* 16(8):869-871.

13. Vigna E & Naldini L (2000) Lentiviral vectors: excellent tools for experimental gene transfer and promising candidates for gene therapy. *The journal of gene medicine* 2(5):308-316.

14. Kay MA, Glorioso JC, & Naldini L (2001) Viral vectors for gene therapy: the art of turning infectious agents into vehicles of therapeutics. *Nature medicine* 7(1):33-40.

15. Kumar M, Keller B, Makalou N, & Sutton RE (2001) Systematic determination of the packaging limit of lentiviral vectors. *Human gene therapy* 12(15):1893-1905.

16. Yacoub Na, Romanowska M, Haritonova N, & Foerster J (2007) Optimized production and concentration of lentiviral vectors containing large inserts. *The journal of gene medicine* 9(7):579-584.

17. Logan AC*, et al.* (2004) Factors influencing the titer and infectivity of lentiviral vectors. *Human gene therapy* 15(10):976-988.

18. Clark PM DJ, Mason DE, Hart CR, Buck SB, Peters EC, Agnew BJ, Hsieh-Wilson LC. (2008) Direct in-gel fluorescence detection and cellular imaging of O-GlcNAc-modified proteins. *J Am Chem Soc.* 130(35):11576-11577.

19. Logan AC, Lutzko C, & Kohn DB (2002) Advances in lentiviral vector design for gene-modification of hematopoietic stem cells. *Curr Opin Biotechnol* 13(5):429-436.

20. Jochmann R*, et al.* (2009) O-linked N-acetylglucosaminylation of Sp1 inhibits the human immunodeficiency virus type 1 promoter. *J Virol* 83(8):3704-3718.

21. Khidekel N, Ficarro SB, Peters EC, & Hsieh-Wilson LC (2004) Exploring the O-GlcNAc proteome: direct identification of O-GlcNAc-modified proteins from the brain. *Proceedings of the National Academy of Sciences of the United States of America* 101(36):13132-13137.